MASTER OF SCIENCE

The integrated stress response kinase general control non-derepressible 2 (GCN2) is a novel prognostic biomarker and therapeutic target in malignant pleural mesothelioma

Gold, Lyssa Talia

Award date:
2023

University of Dundee

School of Medicine

‘The integrated stress response kinase general control non-derepressible 2 (GCN2) is a novel prognostic biomarker and therapeutic target in malignant pleural mesothelioma’

By

Lyssa Talia Gold

Supervised by: Dr Glenn Masson and Professor Russell Petty

A thesis is submitted as part of the requirements for the degree of MSc by Research in Medicine

June 2023

Declaration

I, Lyssa Talia Gold, hereby certify that this thesis, which is approximately 20,000 words in length, has been written by me, that all references cited have been consulted by me, that the work of which this work is a record has been carried out by me, or principally by myself in collaboration with others as acknowledged, and that it has not been submitted in any previous application for a higher degree.

I was admitted as a research student at the University of Dundee as a candidate for the degree of MSc (Res) in September 2021.

Date: 27th February 2023

Signature:

Acknowledgments

This work has come about in no small part because of the good will and support of many excellent people, both in my personal and professional life. I would like to express my deepest appreciation to the GRM lab for many countless acts of assistance, guidance, and moral support. Of my lab members, Vanesa deserves special mention for being both an excellent colleague and friend and for providing distraction and laughter when called for (thus preserving my sanity). I would also like to acknowledge the help I received from Dr Susan Bray and Dr Neil Kernohan, both in dealing with the immunohistochemical side of things and in guiding me through the fascinating world of histology: without their combined efforts I would not have had any slides to analyse, nor the ability to do so. My thesis committee have been a constant source of valuable advice and helped to keep me on track throughout this process. My friends, who have patiently listened to gripes, despair, and scientific rabbit holes with good humour and offered me a little bit of reality when needed, have all been wonderful. Becky and Rory especially must be thanked by name for their continuous love, support, and faith, which constantly inspired and buoyed me. Finally, I am equally indebted to my family, who have also been patient ears and sources of reflection and offered boundless care and support.

Table of contents

Abstract

Malignant pleural mesothelioma (MPM) is a cancer of the mesothelial cells of the pleural cavity, with a five-year survival rate of five percent and extremely limited treatment options with poor response rates. Previous work identified the transcription factor C/EBP homologous protein (CHOP) as a prognostic biomarker in MPM. CHOP levels are also associated with the amino acid response (AAR) arm of the integrated stress response (ISR), mediated by nutrient stress sensing kinase general control non-derepressible 2 (GCN2). GCN2 activity is hijacked in multiple cancers to overcome nutrient starvation associated with tumorigenesis, and both inhibiting and activating compounds have shown promising results as potential new therapeutics. This work immunohistochemically stained MPM tumour samples for GCN2 and determined whether levels were associated with patient prognosis. GCN2 levels were associated with worse patient prognoses and was also a predictive factor for one-year outcomes. GCN2 may therefore prove a useful staining target to determine prognosis in MPM patients. Additionally, the correlation between high GCN2 levels and worse patient prognoses suggests that GCN2 levels are associated with more aggressive cancer and identifies a potential weakness in MPM tumours that could be exploited therapeutically.

Abbreviations

AAR: Amino acid response

ALL: Acute lymphoblastic leukaemia

ASNase: Asparaginase

ASNS: Asparagine synthetase

ASS1: Arginosuccinate synthetase

ATF4: Activating transcription factor 4

AUC: Area under curve

BMM: Biphasic malignant mesothelioma

BRCA1: Breast cancer type 1 susceptibility protein

CHAC1: ChaC glutathione-specific gamma-glutamylcyclotransferase 1

CHOP: C/EBP homologous protein

EAA: Essential amino acids

EMM: Epithelioid malignant mesothelioma

GCN2: General control non-derepressible 2

GSH: Glutathione

HRI: heme-regulated eIF2α kinase

ISR: Integrated stress response

KM: Kaplan-Meier

LR: Log-rank

MTORC1: Mammalian target of rapamycin complex 1

MM: Malignant mesothelioma

MPM: Malignant pleural mesothelioma

NEAA: Non-essential amino acid

NEDD4L: neural precursor cell-expressed, developmentally down-regulated 4-like

PERK: PKR-like ER kinase

PIC: Preinitiation complex

PKR: Double-stranded RNA-dependent protein kinase

ROC: Receiver operator characteristic

SMM: Sarcomatoid malignant mesothelioma

TMA: Tissue microarray

TME: Tumour microenvironment

TNM: Tumour, node, metastasis

UPR: Unfolded protein response

VEGF: Vascular endothelial growth factor

Chapter one: The integrated stress response and the role of GCN2 in tumorigenesis

Adapted from https://doi.org/10.1042/BST20211252, of which LTG is an author

1.1 The Integrated stress response and GCN2

The integrated stress response (ISR) is a eukaryotic intracellular signalling pathway comprised of four serine-threonine stress-sensing kinases that converge on the same target of phosphorylation, serine 51 of the eukaryotic initiation factor subunit eIF2α. Each kinase is devoted to a certain stress: double-stranded RNA-dependent protein kinase (PKR) responds to viral infection; PKR-like ER kinase (PERK) senses stress in the endoplasmic reticulum (ER) related to protein misfolding and is located in the ER-Lumen; heme-regulated eIF2α kinase (HRI) senses heme deficiency and is expressed predominantly in erythroid cells; and general control non-derepressible 2 (GCN2) senses amino acid deficiency [1].

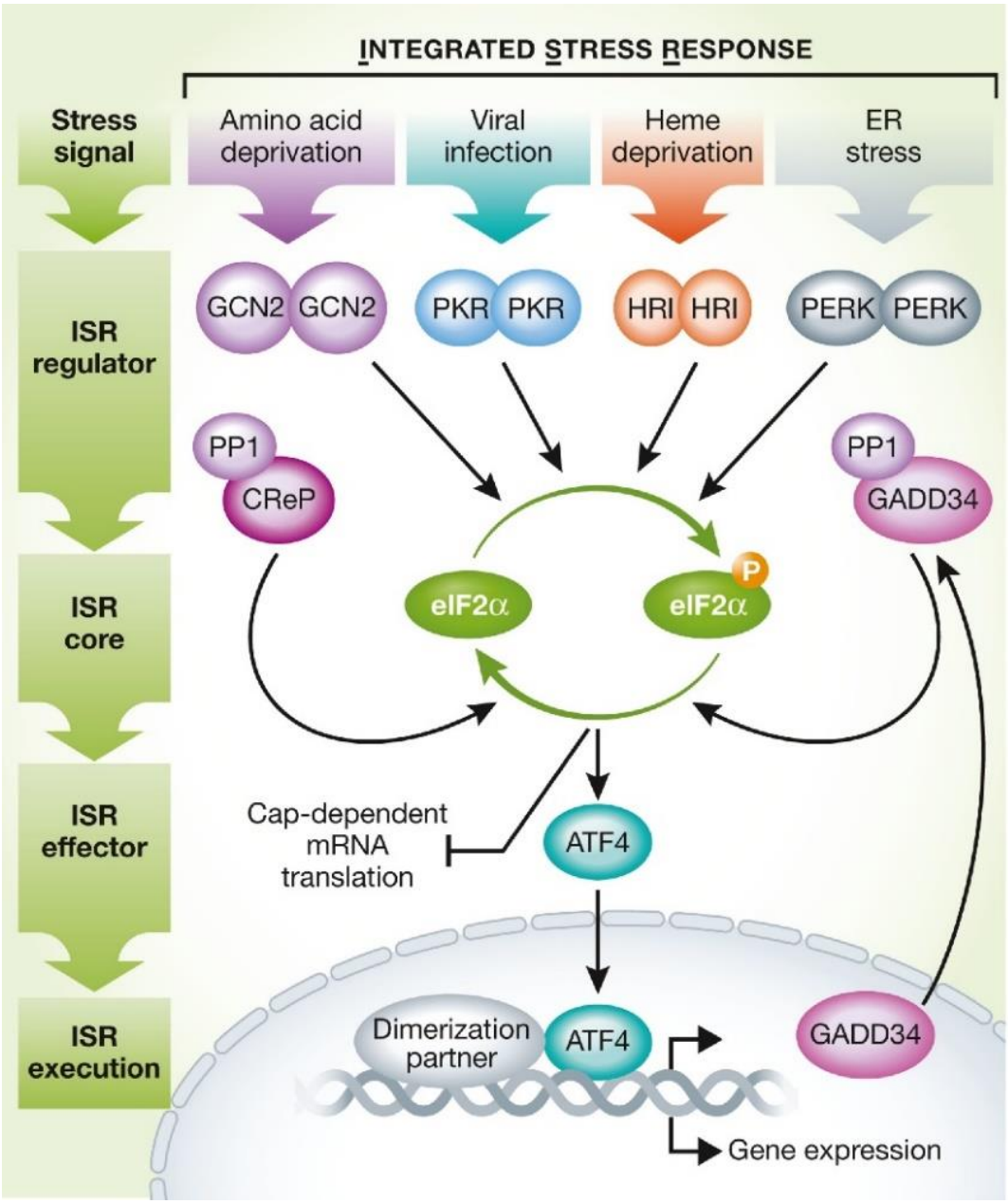

Figure 1a. The integrated stress response. Internal (i.e., ER stress) or external (i.e. viral infection, amino acid deprivation) activates one of four stress sensing kinases (PERK, PKR, HRI, GCN2), all of which phosphorylate eIF2α at serine 51. This supresses preinitiation complex (PIC) formation and subsequently translation and protein synthesis. Genes related to relieving stress are preferentially translated, most notably, the transcription factor ATF4, the main effector of the ISR, which regulates the expression of adaptive genes. The ISR is regulated by two phosphatases which both dephosphorylate eIF2, the constitutively expressed CReP[2], and the inducible GADD34[3]. Figure taken from Pakos-Zebrucka et al., 2016[1].

Stresses may be intrinsic (i.e., protein misfolding, proteotoxicity) or extrinsic (i.e., amino acid or oxygen deprivation) in origin[4], but share the common feature of destabilising cellular homeostasis. Stress is ameliorated by eIF2α

phosphorylation at serine 51 (fig. 1a), which (1) supresses global protein synthesis, and (2) promotes the expression of certain key genes, with the end result of either restoring homeostasis or inducing apoptosis[1]

The S51 phosphorylation state on eIF2α is key to the ISR response, as it suppresses recycling of the ternary complex (TC) required for translation initiation. The TC (fig. 3b) is comprised of eIF2 (in three sub-units, eIF2α, β and γ), GTP, and an initiator Met-tRNAi, which the TC carries to the start codon for translation initiation[5]. The TC first associates with the 40S ribosomal subunit, and with other binding partners eIF1, eIF1A, and eIF3, forms the 43S pre-initiation complex (PIC)[5,6]. Upon successful recognition of the initiation codon, the ternary complex's GTP is hydrolysed, reducing its affinity for the initiator Met-tRNAi; subsequent association of the 60S ribosomal subunit forms the 80S ribosome and displaces eIF2-GDP, leaving the Met-tRNAi behind[7].

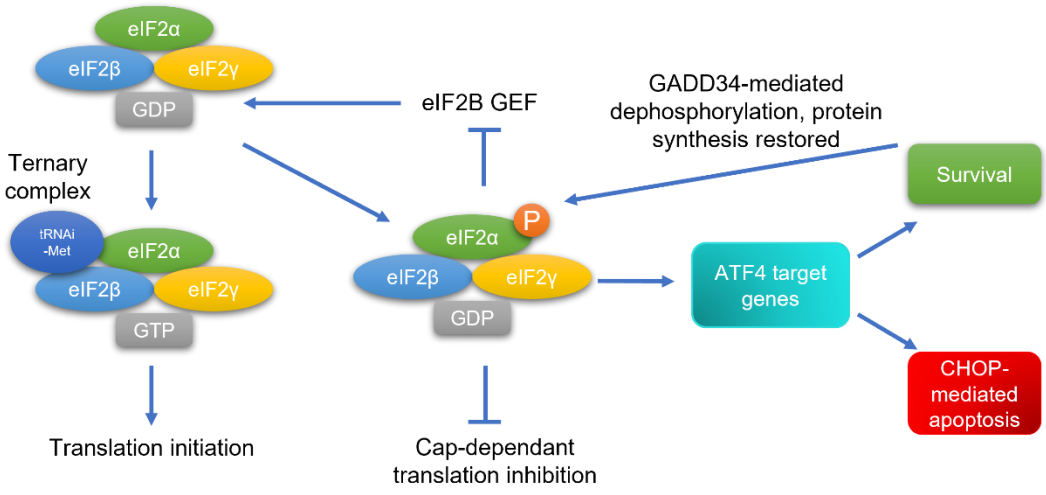

Figure 1b. The phosphorylation state of ternary complex (TC) component eIF2α mediates suppression of protein translation during the integrated stress response: TC is required for initiator Met-tRNAi delivery to the pre-initiation complex. After each initiation cycle, TC-GDP must be recycled to TC-GTP by guanine nucleotide exchange factor eIF2B, facilitating binding to a new Met-tRNAi. eIF2α phosphorylation increases its affinity for eIF2B, halting TC recycling and suppressing translation initiation. Certain stress-related genes, including the transcription factor ATF4, possess upstream open reading frames that facilitate preferential translation during the stress response (fig. x). This translational control either restores cellular homeostasis or induces CHOP-mediated apoptosis if stress is prolonged.

Recycling of the TC is necessary for the next translation initiation event and relies upon the guanine nucleotide exchange factor (GEF, fig. 1b) eIF2B[8], which converts eIF2-GDP to eIF2-GTP and facilitates Met-tRNAi recruitment[9] and another round in translation. Phosphorylation of eIF2α by any of the four ISR kinases increases the affinity between eiF2 and eIF2B, which prevents eIF2-GDP: GTP recycling, and decreases TC concentration[5]. This decreases the concentration of TC in the cell and limits the rate of translation initiation, supressing global cap-dependent protein synthesis. However, certain stress-related genes are preferentially expressed due to the presence of 5' upstream open reading frames (uORF's) in their mRNA, facilitating either a return to homeostasis or triggering apoptosis if stress is prolonged and unresolved[1].

ATF4 and translation reinitiation

The most notable of these is activating transcription factor 4 (ATF4), a basic leucine zipper (bZIP) and the primary transcription factor of the ISR[1,10]. As a bZIP, ATF4 can form homo- and heterodimers with other transcription factors to deliver a tailored stress response[1]. The stress profile (i.e., stress type, intensity, and length), strongly influences whether the response is pro-survival, driving a return to homeostasis[11] or autophagy[12], or instead apoptosis is initiated when homeostasis is unattainable. As can be seen in fig. 1e, because the eIF2α-ATF4 pathway has multiple genes under its control, a single stressor is likely to trigger multiple processes simultaneously to deliver a truly targeted response.

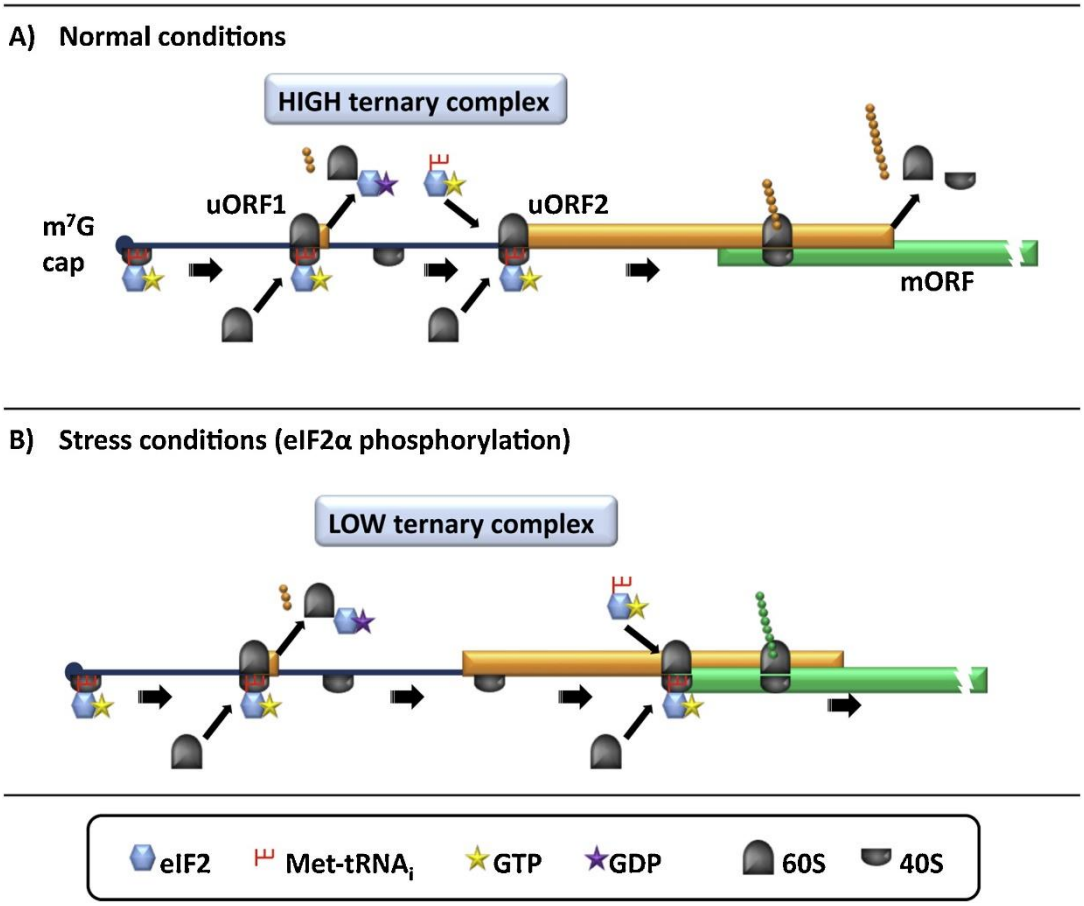

Figure 1c. ATF4 mRNA translation suppression (A) or reinitiation (B) in response to integrated stress response activation and eIF2α phosphorylation. The ATF4 mRNA possesses two upstream open reading frames (uORF 1 and 2). During normal conditions, levels of phosphorylated eIF2α are low and ternary complex (TC) supply is high. The ribosome successfully translates uORF1 and TC is rapidly recycled for reinitiation at uORF2, which overlaps with, and therefore represses, the ATF4 mRNA. Under ISR activation and high eIF2α phosphorylation, the TC availability is far lower, and cannot be recycled before the processing 40S subunit reaches uORF2. the ATF4 mORF is derepressed and preferentially translated, mediating further translational changes in its role as a transcription factor that either ameliorate stress or trigger apoptosis. Taken from Somers et al., 2013[5].

Under ISR activation, selective translation reinitiation of stress-related genes is managed by the presence of upstream open reading frames (uORF's) in their mRNA, with human ATF4 being the best elucidated example. The 5' untranslated region (UTR) of its mRNA contain two uORF's (fig. 1c). uORF1 codes for 3 amino acids, whilst uORF2 codes for a longer 59-residue transcript, which critically overlaps with the ATF4 mORF and results in its repression[10].

When eIF2α is unphosphorylated under unstressed conditions, a high concentration of TC is available (fig. 1c, A), and it is not limiting to translation

initiation. As a result, when uORF1 translation has finished, the 40S subunit continues to process along the mRNA and a new TC can quickly reassociate before the uORF2 is reached. This second transcript is successfully translated, causing repression of ATF4. However, when eIF2α is phosphorylated, available TC concentration decreases and becomes limiting (fig. 1c, B). uORF1 would again be successfully translated, however, TC supply would not be high enough to facilitate reassociation in time to translate uORF2. The 40S subunit therefore continues to scan past this, with successful reassociation of the TC at the ATF4 mORF, upregulating translation[5].

Homeostasis or apoptosis?

The eIF2α-ATF4 pathway can either promote a return to homeostasis, or trigger apoptosis, and the phosphorylation state of eIF2α is the hinge upon which these diverging fates hang. If phosphorylation, and by extension the ISR, persist, then CHOP-mediated apoptosis results[1]. Alternatively, eIF2α may be dephosphorylated, restoring protein synthesis, and allowing cellular recovery from the stress response. eIF2α is subject to two phosphatase complexes with a catalytic core in common; the constitutively expressed protein phosphatase 1 (PP1)[2] and the inducible GADD34 (fig. 1a), the expression of which is upregulated during the ISR via ATF4[13]. Like ATF4, GADD34 contains 5' uORF's in its mRNA untranslated region, further contributing to its elevated expression during the ISR[14]. GADD34-mediated eIF2α dephosphorylation therefore operates as a negative feedback loop as the ISR progresses (fig. 1a), winding down the response as stress is ameliorated by the pro-survival transcriptional changes effected by the eIF2α-ATF4 pathway.

However, if stress persistent and cannot be resolved, apoptosis can result, with the most well-understood mediator of this component of the ISR being CHOP. As a transcription factor, it is capable of upregulating pro-apoptotic members of the BCL-2 family, which form mitochondrial protein channels that allow cytochrome-c release and downstream caspase activation and cell

death[15]. This family of proteins includes the pro-apoptotic proteins BAK and BAX, which oligomerise to form the necessary mitochondrial channels for permeabilization and subsequent apoptosis, and these are upregulated by CHOP. However, this family also contains anti-apoptotic proteins that are supressed by CHOP as part of this response[15]. There is further evidence that CHOP contributes to cell death activation by upregulating transcription of death receptor 5 (DR5)[1], which downstream has been shown to upregulate caspase-8 levels[16], further contributing to mitochondrial insults and cytochrome-c release also being mediated by BAK-BAX oligomers. Finally, CHOP can upregulate levels of the oxidase ERO1α, which elevates H_2O_2 levels in the ER by oxidising protein disulphide isomerase (PDI). Subsequent leakage into the cytoplasm creates a damaging, oxidative and inflammatory, environment that further contributes to apoptosis[1,15].

The rapid proliferation of cancer cells in the tumour microenvironment (TME) is associated with uncontrolled growth and avoidance of cell death. It creates an area of low pH, hypoxia, metabolite deficiency and proteotoxicity[17], and these tumours fail to ensure adequate vascularisation, limiting their access to oxygen and metabolites[18]: to achieve successful, prolonged tumorigenesis, this stress state must be overcome, and apoptosis avoided. Given this state, it is unsurprising that the ISR is dysregulated in cancer. Firstly, because it is able to sense amino acid starvation (GCN2) and protein misfolding (PERK) stress caused by this proliferation and supress protein synthesis to temporarily reduce the processing load, and secondly, because ATF4 and CHOP lie under its control, the two transcriptional effectors of survival and apoptosis, respectively. ATF4, through downstream pathways, is able to facilitate adaptation to biological stress beyond the canonical stress sensed by the upstream kinase: the GCN2-ATF4 pathway regulates ROS homeostasis, angiogenesis, and cell proliferation, as will be discussed later.

The ISR is one of the pro-survival pathways that may be hijacked in cancer, with PKR, PERK, and GCN2 all implicated in cancer[13], and has been demonstrated not only to facilitate adaption to biological stresses, but also as key methods for the acquisition of drug resistance in multiple solid-state

cancers. Gemcitabine resistance in pancreatic cancer relies upon the wider ISR[19], whilst cisplatin resistance in gastric cancer is conferred by the GCN2-ATF4-xCT pathway[20] (discussed later). As a key nutrient sensor, GCN2 is already of interest in tumour development. However, our current understanding of the GCN2-eIF2α-ATF4 pathway, as evidenced in fig. 1e, indicates that it plays a far wider role in processes relevant to tumorigenesis, underlining the need for better understanding of (1) how GCN2 supports tumorigenesis, and (2) how this can be targeted therapeutically.

1.2 GCN2 activation in cancer

GCN2 is the only pan-conserved eukaryotic ISR kinase, with the yeast homolog (Gcn2) controlling the whole ISR in that context[21]. Mammalian GCN2 autophosphorylates at least two residues (T899 & T904) upon activation[22,23] by deacylated tRNA, an intracellular accumulation of which signals amino acid starvation, which is also sensed by Gcn2 in yeast. It is likely that tRNA interact with the HisRS-like domain of GCN2, which engages the kinase domain in an autoinhibitory interaction that is disrupted upon activation[24]. More recent work also implicates the ribosomal P-stalk[25,26] and ribosome stalling[27] as potential activation events, but whether these occur in concert with deacylated tRNA or perhaps indicate a hierarchical difference between yeast and higher eukaryotes is still unclear.

GCN2 phosphorylation is a functional indicator of GCN2 activation and also a potential biomarker in cancer. Ye *et al*.[12] showed that in comparison to non-cancerous tissue, both phosphorylated and unphosphorylated GCN2 levels are elevated in multiple cancers, including, breast, lung, and colon (fig. 1d).

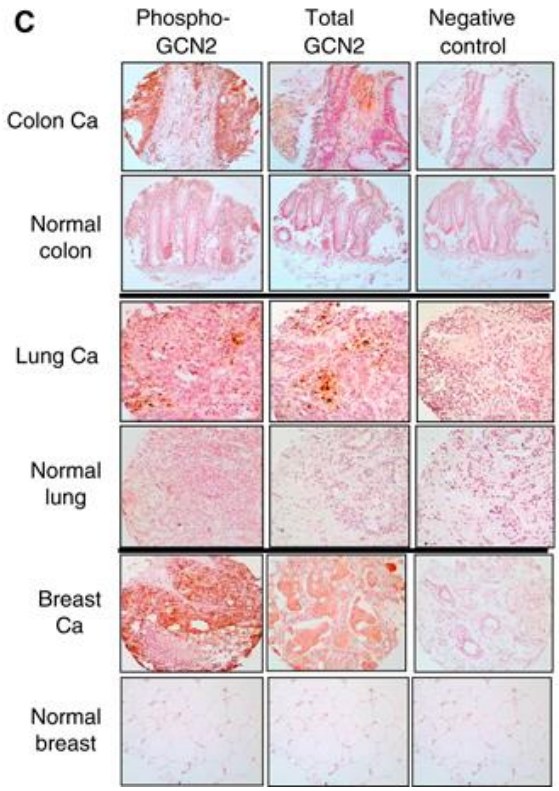

Figure 1d. Tumour biopsy and control tissue stained with antibodies for phospho-GCN2 and non-phospho-GCN2: This work by Ye et al. in 2010[12] demonstrated that in colon, lung, and breast cancer tissue, levels of active (phospho-GCN2) and total GCN2 were elevated in comparison to healthy control tissue. The elevated GCN2 activity observed indicates a potential role in promoting tumour fitness.

These trends have been observed in human oral squamous cell carcinoma[28] and most recently, in prostate cancer[29]. Translating these high levels to patient prognoses, work around human papillary renal cell carcinoma patients by Ge *et al*.[30] found higher GCN2 levels to be predictive of worse patient outcomes, identifying this as a potential biomarker to tailor treatment plans. These experimental data are further supported by extensive bioinformatic work by Saavedra-García *et al*.[31] using data from The Cancer Dependency Map (DepMap) and The Cancer Genome Atlas (TCGA) to identify cancers dependant on GCN2. In a study that also probed dependency on the three other ISR kinases, they found that GCN2 had significantly more cancers reliant upon it (~13%), compared to HRI (0.1%), PKR (0%), or even PERK (0.7%). In agreement with the prognostic indications surrounding GCN2 levels found by Ge *et al*.[30] in glioblastoma and multiple myeloma, they found that patients with

a transcriptional profile indicating GCN2 reliance, those patients' cancer was markedly more aggressive, and required radio and chemotherapy earlier and for longer than other patients without this dependency. Their work also demonstrated that across the GCN2-dependant cancers, transforming growth factor β (TGF-β) signalling genes were enriched, a potential auxiliary biomarker in these tumours.

Despite plentiful evidence that GCN2 levels are elevated in cancers, the underlying mechanism that enables these greater levels of GCN2 to be maintained is not clear. GCN2 has a short half-life, and work by Wei *et al*. in 2015 posited that GCN2 levels are, in healthy cells, maintained at a low cytoplasmic concentration by efficacious use of the proteasomal degradation pathway, thereby also avoiding GCN2's apoptotic effects. Cellular β-arrestin1/2 associates with GCN2 and recruits the E3 ligase NEDD4L (neural precursor cell-expressed, developmentally down-regulated 4-like) to form a ternary complex that mediates GCN2 degradation. Crucially, GCN2-T899 phosphorylation, post-activation, disrupts the formation of this complex and protects from degradation: rather than elevated translation, they suggest that it is this that drives increasing GCN2 levels, which after prolonged elevation initiates (C/EBP Homologous Protein) CHOP-mediated apoptosis[32].

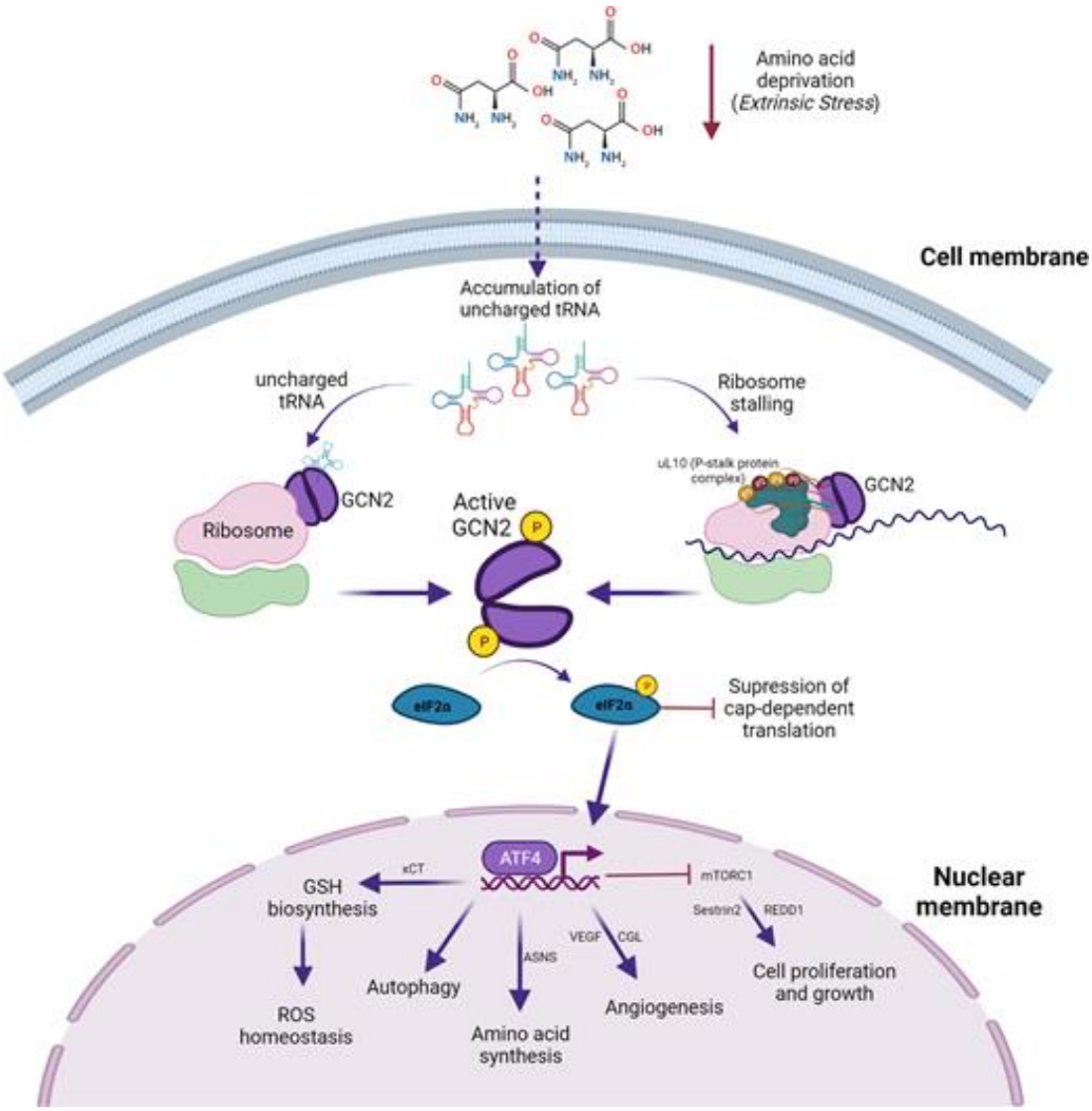

Figure 1e. The amino acid response (AAR) arm of the integrated stress response (ISR), showing the different pathways under GCN2-eIF2α-ATF4 control. Amino acid starvation triggers GCN2 activation, either by direct interaction between GCN2 and deacylated tRNA, or by triggering ribosome stalling events that facilitate GCN2 recruitment to the ribosome and interaction with the p-stalk protein complex. Both would result in eIF2a phosphorylation, suppression of global protein synthesis, preferential upregulation of certain stress-related genes via ATF4. Multiple processes downstream of the GCN2-ATF4 pathway are potentially relevant to cancer stress, including ROS homeostasis, angiogenesis, amino acid synthesis and transport, and cell proliferation. Taken from Gold & Masson., 2022[33].

Another aspect of the ISR that must be considered when regulating specific stress-sensing kinases therapeutically, is the significant overlap in functionality, especially between PERK and GCN2. This is unsurprising, given the commonalities in the stresses they respond to. Both initiate the eIF2α-

ATF4 pathway in glucose starved MEF cells[12]: for PERK this is likely because glucose starvation impairs protein synthesis. As cancer cells often harness amino acids such as glutamine as an alternate carbon source via glutaminolysis[34], this is likely why GCN2 is part of this response. This compensatory relationship can also be seen in soft tissue sarcoma mice models where ATF4 signalling is upheld in GCN2 KO mice by PERK activity[35], requiring that both kinases' activity be targeted to effectively supress eIF2α activation.

1.3 The amino acid response and therapeutic starvation regimes

The amino acid response (AAR), a part of the wider ISR, is controlled by GCN2. To respond to amino acid depletion effectively, the GCN2-ATF4 pathway controls both amino acid synthesis and transporter genes. Therapeutically depriving cancers of targeted metabolites, including amino acids, is already a robust treatment strategy (reviewed in Fung *et al*., 2017[36]) with obvious relevance to GCN2: despite current limited work detailing the role GCN2 plays in these therapeutic strategies, we know that the GCN2-ATF4 pathway is the key to survival for many solid-state tumours experiencing non-essential amino acid (NEAA) starvation. This weakness has been exploited and effectively characterised in the case of asparagine synthetase (ASNS), which lies under GCN2-ATF4 control[12,37], and where amino acid starvation was successfully coupled to GCN2 inhibition. ASNS catalyses the glutamine-dependant conversion of aspartate to asparagine to support protein synthesis and cell growth in tumour cells[12].

Multiple cancers, including acute lymphoblastic lymphoma (ALL), are ASNS depleted, making them dependent on exogenous asparagine[38], and current treatment utilises the ASNS inhibitor L-asparaginase (ASNase) to induce starvation of this essential amino acid. Treatment of CREF-CRM ALL cells, and also of acute myelogenous leukaemia and pancreatic cancer cells, with a GCN2 inhibitor sensitises them to ASNase (fig. 1f) by halting GCN2-mediated ASNS induction, augmenting treatment and inducing MAPK-mediated apoptosis[39]. This demonstrates GCN2's potential as a synergistic target to

improve the efficacy of other therapeutics or amino acid starvation approaches. In mouse xenograft studies[12], GCN2 or ATF4 silencing alone dramatically reduces tumour volume, demonstrating the contribution of this axis to successful metastasis even without amino acid challenge. This result may also hint at the ISR'S role in promoting vascularisation (see below).

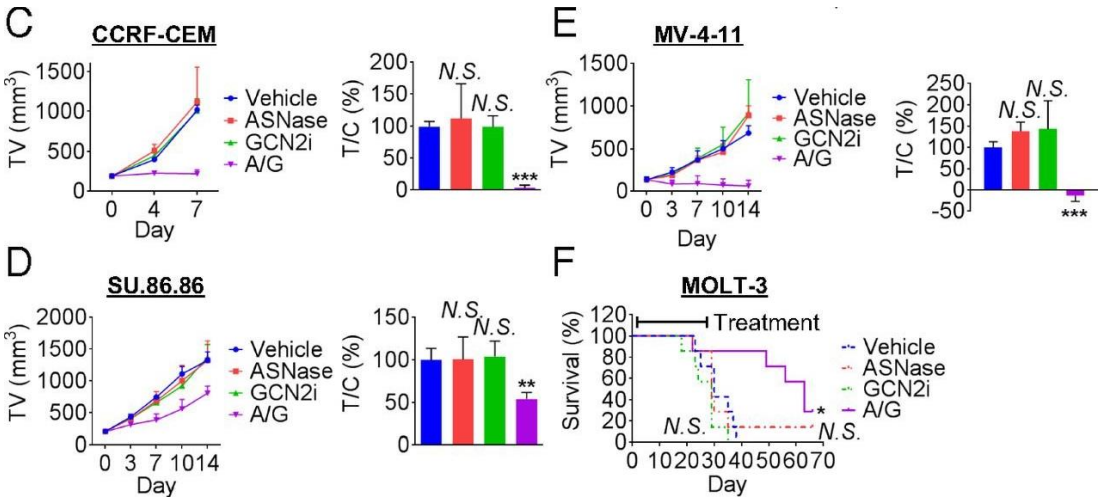

Figure 1f. [C-E]: Treatment of mice xenografted with acute lymphoblastic leukaemia (ALL) tumours, with control vehicle (Vehicle), ASNase (A; 1000U/g, once daily), GCN2i (G; 10mg/kg, twice daily), or ASNase + GCN2i (A/G). CCRF-CEM (C) and MV-4-11 (E) cell lines treated with ASNase and GCN2i show no increase in tumour volume at day 7 and 14 respectively, and no increase in cancer cell survival ratio (T/C). SU.86.86 (D) cell line shows steady increase in tumour volume and cell survival from day 0 to 14, but with values around 50% of the control or either of the single treatments, indicating combined efficacy. [F] MOLT-3 ALL cells inoculated into SCID mice treated 3 days/week with control vehicle, ASNase (A; 1000U/g, once daily), GCN2i (G; 10mg/kg, twice daily), or ASNase + GCN2i (A/G), over 28 days. Survival analysis carried out over 70 days. (* P<0.05; ** P<0.005; ***P<0.0005). Significant survival difference in mice treated with A/G when compared with the vehicle control. Taken from Nakamura et al., 2018[39].

Another aspect of tumour amino acid reliance, in addition to reliance for protein synthesis, is the use of amino acids as alternate bioenergetic sources. Glutaminolysis, for example, via mitochondrial ATP production, supplies tumours with an alternate source of carbon and nitrogen for subsequent nucleic acid, lipid, and amino acid synthesis[34], facilitating large biomolecule synthesis and biomass accumulation. Gln starvation therefore limits not only its own amino acid supply in tumours, but also those synthesised downstream from it via glutaminolysis, activating the GCN2-ATF4 pathway. In MYC-mediated neuroblastoma, Gln starvation activates the AAR and induces

apoptosis and tumorigenesis[40], demonstrating tumour reliance upon these alternate metabolic pathways, which could feasibly be targeted via GCN2.

As mentioned previously, the GCN2-eIF2α-ATF4 axis is also able to exercise transcriptional control over multiple other stress-relieving pathways beyond amino acid synthesis and transport, but which still play an important role in relieving this stress. This includes, ROS homeostasis arising from cysteine starvation; proteotoxicity by regulating MYC, promoting vascularisation via VEGF, and regulation of mTORC1 and thus regulating cell proliferation. As will be discussed more comprehensively in the next chapter, some of these processes have already been targeted in malignant pleural mesothelioma (MPM) targeted therapy development, namely vascular endothelial growth factor (VEGF).

1.4 Angiogenesis

GCN2 primarily promotes an increase in intracellular amino acid levels, either by synthesis of non-essential amino acids (NEAA) or uptake of extracellular essential amino acids (EAA's). Another action of the GCN2-ATF4 pathway is to promote angiogenesis by regulating vascular endothelial growth factor (VEGF) in response to amino acid starvation[28,41,42]. VEGF secretion is primarily triggered in response to hypoxic conditions[43], but is also secreted independently of hypoxia, for example, when healthy cells respond to amino acid stress, they secrete VEGF to increase nutrient-rich blood flow. Cancer cells, due to the extreme nutrient demands of rapid tumour growth, outpace blood and nutrient supply and also take advantage of this pathway[28]. This has been demonstrated *in vivo,* using mouse xenografts of GCN2 knockdown (KD) squamous cell carcinoma (UM-SCC-22B, fig. 1g). GCN2 KD supressed VEGF expression levels and resulted in smaller tumours with reduced vascular density[28], indicating that this relationship could be used to reduce solid-state tumour size.

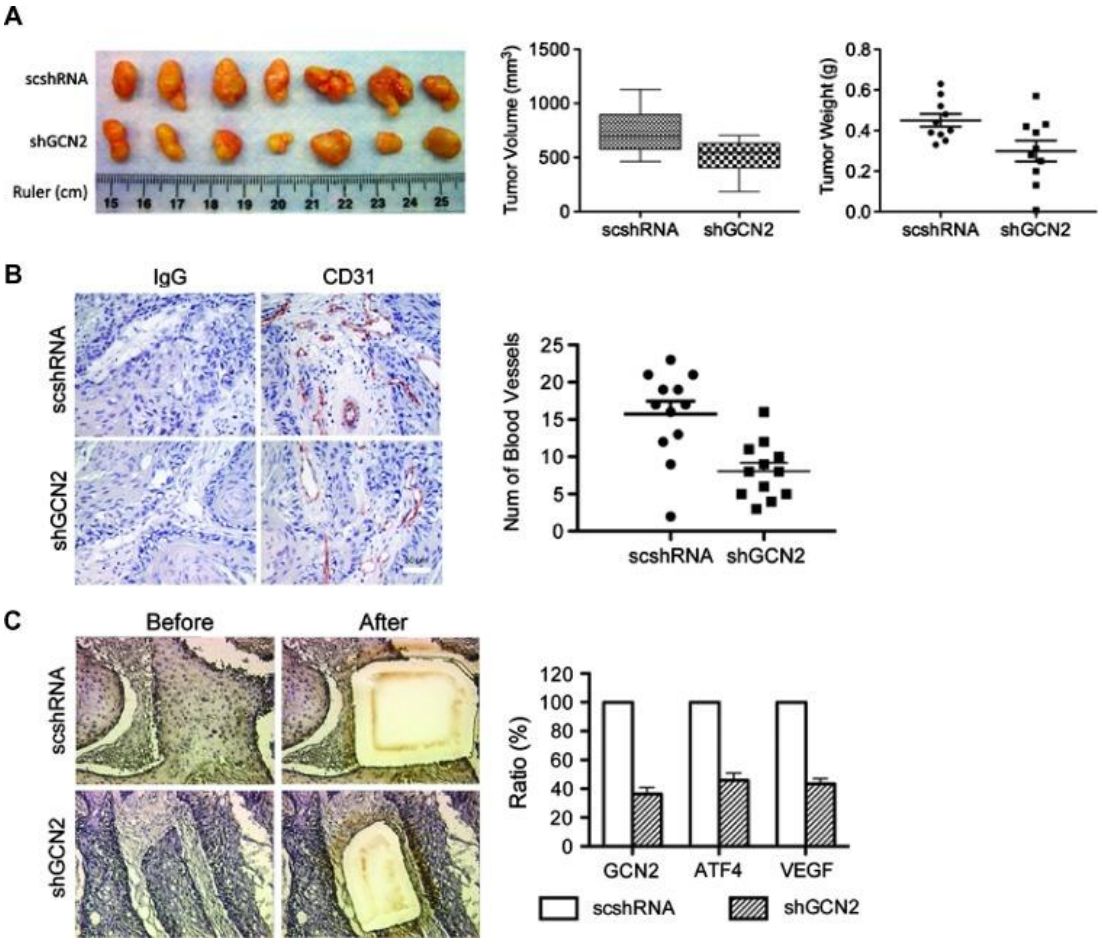

Figure 1g. scshRNA (control) and scshGCN2 UM-SCC-22B cell lines were used to generate xenograft tumours in SCID mice: (A) tumour volume and mass were both lower in the scshGCN2 condition when compared to the scshRNA control mice (B) Tumour micro-vessel density was assessed to determine relative vascularisation between the two conditions, using immunohistochemical staining for endothelial cell marker CD31 (left), and then quantified (right). IgG = negative staining control. scshGCN2 xenograft tumours were less vascularised and had fewer blood vessels. (C) qPCR was used to determine expression levels of GCN2, ATF4, and VEGF; all three were shown to decrease by ~60% in response to shGCN2 treatment. Taken from Wang et al., 2013[28]

1.5 ROS and protein homeostasis

Whilst reactive oxygen species (ROS) play an important role across cellular functions[44], they can also cause significant cellular damage if unregulated, including lipid peroxidation or protein oxidation. This induces a state of oxidative stress that requires cellular antioxidants, such as glutathione (GSH) to reverse[45]. Perturbed levels of multiple amino acid levels have been demonstrated to induce oxidative stress in this manner, with a GCN2-eIF2α-ATF4 response being crucial to restore oxidative balance [45,46]. In work carried out in triple-negative breast cancer cells by Chen *et al*. in 2017[47], it was

demonstrated that cysteine starvation leads to necroptosis by inducing mitochondrial fragmentation, resulting in the release of ROS, such as superoxide (O^{-}_{2})[47]. The GCN2-eIF2α-ATF4 pathway activates with two possible transcriptional targets: ChaC glutathione-specific gamma-glutamylcyclotransferase 1 (CHAC1), which degrades GSH for its cysteine, resulting in oxidative stress and cell death[47]; and the light subunit of the Xc- cysteine/glutamate antiporter (xCT, or SLC7A11), which exchanges intracellular glutamate for extracellular cysteine, subsequently allowing GSH synthesis and ROS mitigation[48].

This pathway allows healthy cells to respond to natural fluctuations in ROS levels: issues arise when it is exploited by cancer cells to gain drug resistance, as for cisplatin and gastric cancer.

Cisplatin primarily operates by interacting with chromosomal DNA, specifically by forming crosslinked adducts with purine residues. This induces DNA damage and inhibits DNA replication, preventing cell division and inducing apoptosis (Dasari & Tchounwou., 2014). In addition to this, it also induces oxidative stress in cells, which causes intracellular damage to lipids, proteins, and DNA. Most importantly in the context of cisplatin, it also delivers mitochondrial insults that result in a loss of membrane potential, increase in permeability, and activation of pro-apoptotic factors, most notably caspase 9, which activates so-called ‘executioner’ caspases 3 and 7, which mediate downstream apoptosis (Dasari & Tchounwou., 2014). However, in gastric cancer the subsequent mitochondrial dysfunction and ROS augment drug resistance by activating the GCN2-eIF2α-xCT pathway. The xCT cysteine-glutamate antiporter is crucial for the import of cysteine necessary for glutathione biosynthesis (fig. 1h). It is the antioxidant activity of this molecule that opposes this aspect of cisplatin activity, and therefore GCN2 confers a drug-resistant phenotype: in these cancers xCT indicates a negative prognosis[20,48].

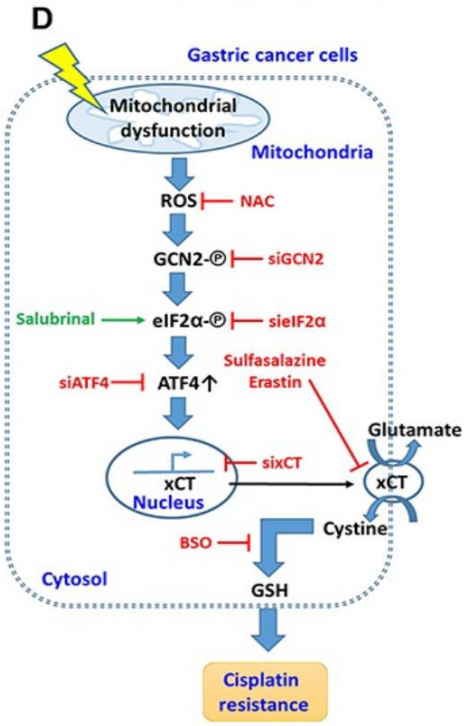

Figure 1h. GCN2's role in glutathione (GSH) synthesis contributes to a cisplatin resistant phenotype in gastric cancer cells. The xCT (SLC7A11) subunit of the cysteine-glutamate antiporter lies under control of the GCN2-ATF4 pathway. In response to elevated ROS levels under cisplatin treatment, GCN2 upregulates levels of this transporter to facilitate GSH biosynthesis. ROS-mediated apoptosis is opposed by GSH antioxidant activity, resulting in a drug resistant phenotype. Taken from Wang et al., 2016[48].

This conferred chemoresistance may extend beyond cisplatin, with work in 2021 by Saavedra-García *et al*.[31] demonstrating a central role for GCN2 in recovery from proteotoxic stress induced in multiple myeloma (MM) cells. Proteosome inhibitors are an important class of chemotherapeutics that also induce oxidative stress by proteosome inhibition, allowing proapoptotic proteins to accumulate, which cause mitochondrial insults and elevate cytoplasmic ROS levels[49,50]. By pairing multiomics with the GCN2 inhibitor GCN2iB[39], Saavedra-García *et al*. observed that MM cells recovering from proteotoxicity were sensitised to GCN2 inhibition. In these cells, GCN2 supported a return from proteotoxicity firstly by ensuring amino acid supply for translation, and by contributing to wider oxidative recovery post-treatment, indicated by decreased levels of GSH, cysteine, and N-acetyl cysteine under GCN2iB treatment[31].

Mitochondria are essential organelles which, beyond ATP synthesis, play important roles in signalling and regulating cell fate: when damaged, aberrant oxidative phosphorylation can lead to an accumulation of ROS, which is harmful to the wider cell[51]. Mitophagy, the process by which damaged mitochondria are removed from the cell, supports tumorigenesis by ensuring metabolic needs are not impaired by these afunctional mitochondria[52], and also protects cancer cells from chemotherapeutically induced cell death[53]. In pancreatic cancer cells, GCN2 has been implicated in this process[54]. In these cancer cells, depleted levels of the mitochondrial structural protein Mic60 (aka “Mitofilin”) initiates extreme mitochondrial stress, evidenced by increased outer membrane permeability and inner membrane depolarisation, decreasing oxidative phosphorylation, and increasing cellular oxidative stress. In an adaptive response to this depletion the ISR was activated, demonstrated by upregulation, transcriptional activation, and nuclear translocation of ATF4. GCN2-Akt survival signalling ensured these cells avoided death and metastasis was promoted[54].

1.6 Proteotoxicity

As well as helping cancer cells to recover from therapeutically induced proteotoxicity, GCN2 has also been demonstrated to bestow tolerance to proteotoxicity[55] arising from the increased metabolic demands of tumorigenesis, which can result in the accumulation of misfolded, toxic protein, and cellular stress. This is exemplified in colorectal cancers (CRC), which almost universally accumulate loss-of-function mutations in the tumour suppressor APC (adenomatous polyposis coli), releasing the proto-oncogene MYC from its regulation, and facilitating an increase in mRNA levels[55]. MYC is oncogenic in many cancers, with its activation linked to multiple pro-growth and proliferative pathways that contribute to an increase in cellular biomass[56]. This pro-growth activity stimulates protein synthesis, draining amino acid and metabolic resources, and resulting in: (1) a state of proteotoxic stress as proteins are misfolded, which would typically result in cell death; and (2) the triggering of the ISR via GCN2. In work by Schmidt *et al*. in 2019[55], a negative

feedback loop enacted by GCN2-eIF2α activation was identified, where survival is promoted by suppression of MYC translation, conserving metabolites and halting proteotoxic accumulation (fig. 1i).

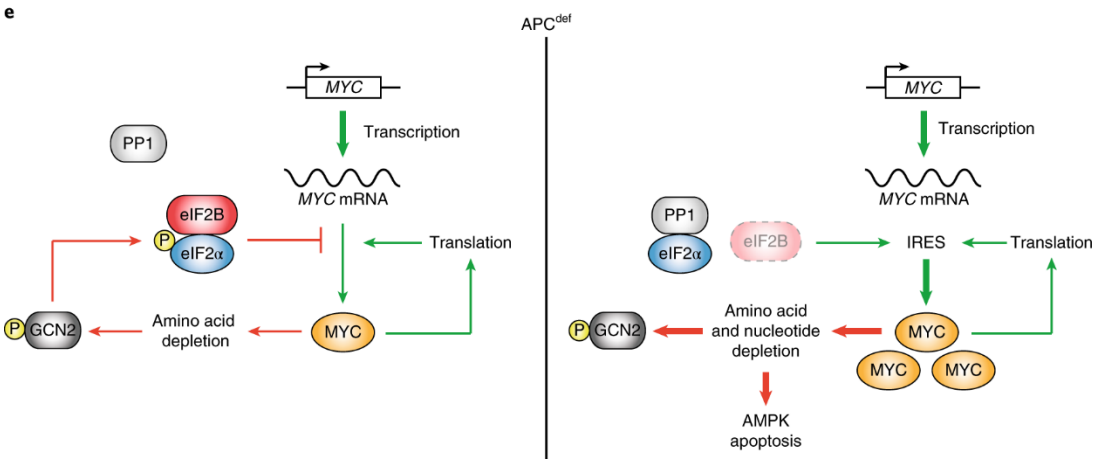

Figure 1i. APC-deficient colorectal cancer (CRC) cells demonstrate an MYC-GCN2-eIF2α negative feedback loop, limiting protein synthesis to avoid apoptosis (left): In APC-proficient cells (right), APC's anti-tumour activity represses MYC, and it cannot drive proliferatory translation that would induce apoptosis. Taken from Schmidt et al., 2019[55].

APC is a well-known CRC biomarker, and this work went on to explore the therapeutic benefits of targeting GCN2 in this cancer. Inhibiting GCN2 with the compound A-92 induced apoptosis dose-dependently; furthermore, this was accompanied by a reduction in MYC and elevation of eIF2α mRNA levels, substantiating the conceptualised pathway and validating GCN2 as a viable therapeutic target.

1.7 Cell proliferation and MTORC1

MYC is not the only proliferative nexus that GCN2 exercises control over; it can also regulate mammalian target of rapamycin complex 1 (mTORC1), another 'master' sensor of amino acid availability[11]. Under amino acid replete conditions, mTORC1 is derepressed and an anabolic cellular state of synthesis and growth is promoted, allowing the cell to respond dynamically to metabolite and energy supply[57]. In healthy cells experiencing amino-acid related stress, mTORC1 would be repressed by multiple amino acid-

responsive regulatory proteins (i.e., Sesn2, CASTOR1, SAMTOR)[57]. In solid state cancers, whilst MTOR mutations are not frequent, there is growing evidence that multiple cancers have non-oncogene addiction to mTOR function, with deletion inhibiting prostate cancer formation in mice[58,59]. Under amino acid stress, GCN2 regulates mTORC1 to stop it activity, suggesting a regulatory relationship between these two kinases and their respective pathways. Work in 2018 by Nikonorova *et al*.[11] demonstrated this relationship by treating GCN2$^{-/-}$ mice with asparaginase (ASNase), a drug typically used in ALL treatment that converts asparagine to aspartic acid to induce asparagine starvation, which should repress mTORC1 activity. Instead, a rapid increase in hepatic mTORC1 activity (fig. 1j) was observed[11], with the same trend also observed in separate experiments in pancreatic mTORC1[60].

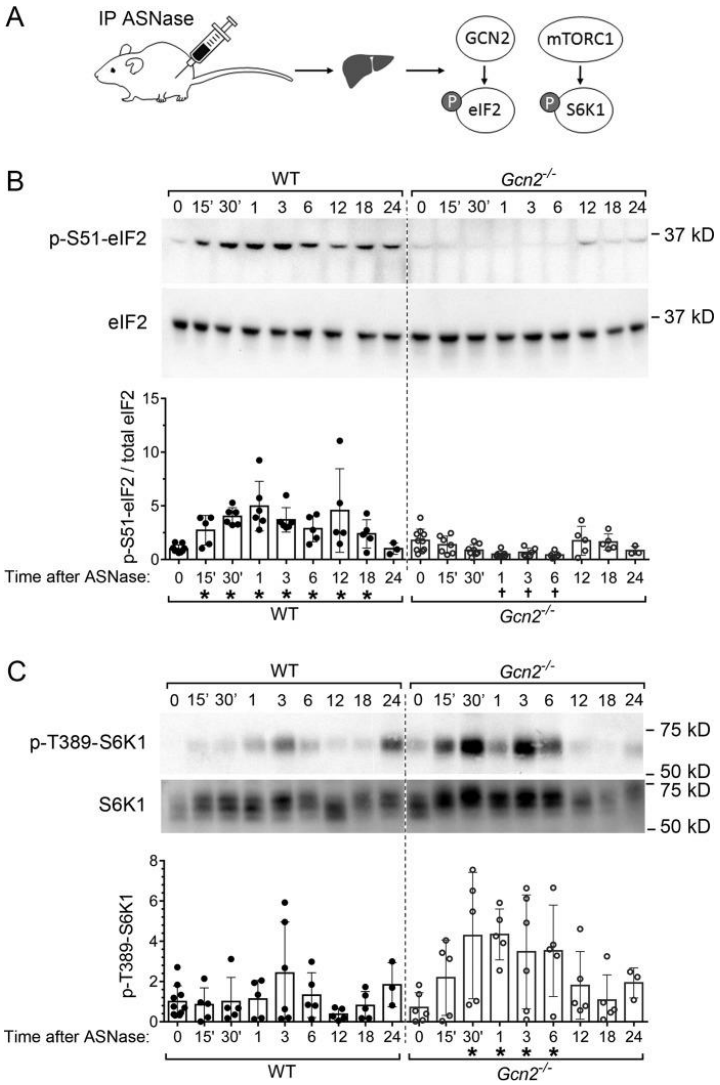

Figure 1j. GCN2 status decides eIF2 and mTORC1 activation under ASNase treatment in mice: (A) diagram showing treatment plan, with ASNase injected intraperitoneally and mice killed at timepoints for liver harvesting to determine hepatic GCN2 and mTORC1 activation levels. (B) Mice were treated with ASNase and livers harvested over 24hrs to determine hepatic eIF2α/ eIF2α-p-S51 levels. As expected, Gcn2 -/- mice showed no increase in eIF2α activation compared to WT, in response to amino acid starvation. (C) Hepatic mTORC1 activation was determined similarly using p-T389-S6K1. In contrast to hepatic GCN2, the GCN2-/- condition showed strong hepatic mTORC1 activation versus WT control. This indicates that GCN2 deletion facilitates hepatic mTORC1 activation under amino acid starvation conditions, and that under starvation conditions, GCN2 may supress mTORC1 as part of the amino acid response. Taken from NIkonorova et al., 2018[11].

This activation is supressed by eIF2α, which reinforces that it is the GCN2-eIF2α pathway regulating mTORC1 in this context, thereby promoting cell survival by supressing untenable protein synthesis. Removing this regulation is therefore potentially a way to trigger stress-induced cell death in cancers,

especially those demonstrating MTOR addiction that may be even more vulnerable.

1.8 GCN2 mutations associated with disease

Interestingly, human patients with GCN2 mutations resulting in disease typically present with pulmonary disease and possess loss-of-function mutations that lead to pulmonary arterial hypertension (PAH)[61], and its two subtypes, pulmonary veno-occlusive disease (PVOD)[62] and or pulmonary capillary haemangiomatosis (PCH)[61,63], as can be seen in fig. 1k.

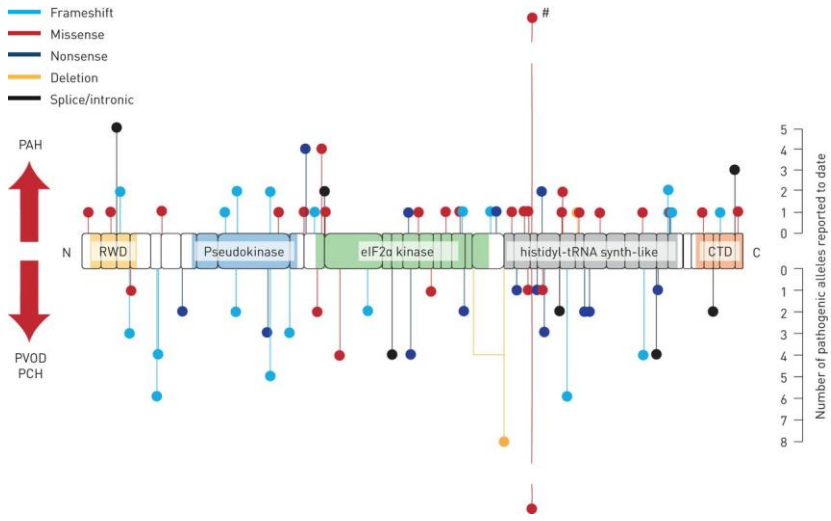

Figure 1k. Mutations in EIF2AK4, the gene coding for GCN2, are linked to pulmonary arterial hypertension- (PAH): PAH, and its two subtypes, , pulmonary veno-occlusive disease (PVOD)) and or pulmonary capillary haemangiomatosis (PCH) are the result of vascular remodelling and resultant heart failure. Mutations are present across all domains. RWD (RING-finger proteins, WD repeat-containing proteins, yeast DEAD-like helicase), pseudokinase, eukaryotic initiation factor (eIF)2α kinase, histidyl-tRNA synthetase-like and carboxy-terminal domain (CTD). Length of lines indicates the number of reported alleles in each region, amassed from the literature. There are potentially 48 alleles across all reports, however this may be lower due to replicates. Taken from Emanuelli et al., 2020[64].

PAH is a rare and lethal disease, with the majority of patients being young adults. It results in vascular remodelling that elevates pulmonary vascular resistance and causes lethal right-side heart failure[64]. PVOD and PCH are more lethal that PAH, and recently have been linked to a biallelic mutation in EIF2AK4 (the gene coding for GCN2) with a strong familial component, but which is also present in 25% of non-familial PVOD cases, suggesting that

GCN2 mutations may have a further role in pulmonary disease[64]. The lungs are frequently exposed to stress by exposure to inhaled chemical toxins, bacteria, or viruses[65]. Therefore, ISR activity is unsurprising and may contribute to resistance to these insults. In a non-disease context, GCN2's ability to enact vascular remodelling could facilitate access by immune cells to aid in this defence.

1.9 Current progress targeting GCN2 therapeutically in cancer

Targeting oncogenic kinases is a key strategy in pharmacology. It is evident from the experimental work surrounding GCN2 in cancer that both inhibiting and activating GCN2, depending upon the disease context, has therapeutic promise. To-date, small inhibitors[66,67] and activators[68] have been explored with some promise, however, the lack of a full structure for GCN2 currently limits structure-led approaches. This limitation has not stopped the first phase 1a/b GCN2 clinical trial[69] beginning in 2022 (NCT05121948) for the GCN2 modulator HC-7366 in patients with multiple kinds of solid-state tumours. When developing these compounds, a key concern is ensuring that the compound has good kinase selectivity and a preferential pharmacokinetic profile to ensure good binding and potency.

Fujimoto *et al*. developed and screened a number of GCN2 inhibitory compounds from modified sulfonamides, building on previous work that demonstrated binding primarily to B-raf, but also to GCN2 as a secondary target[66,70], with the aim of improving specificity and binding from the initial GCN2 IC_{50} of 720 nM. Although a fully resolved GCN2 structure has not yet been achieved, they utilised a structural homology model to then utilise structure-based drug design focusing on the kinase domain (residues 576-1012) and yielding seven compounds. *In vitro* kinase and *in vivo* cell (U20S) assays were used in initial screening to assess the inhibitory activity against GCN2. Five of these seven compounds had 'good' inhibitory activity in the low nanomolar range for both assays (<24.0 nM), and two had good selectivity over PERK (PERK IC_{50}, 230 nM and 9000 nM). These were brought forward for further cell assays in ALL cells treated with ASNase (GCN2 inducer) and

showed binding to the DFG motif, between the two lobes of the kinase domain. Both had uninspiring antiproliferative effects (cell viability: 65% to 75%). Finally, a CCRF-CEM xenograft model experiment in mice treated with asparaginase showed a dose-dependent reduction in p-GCN2 and ATF4 levels for the single compound brought forward, indicating bioavailability and successful targeting of the GCN2-ATF4 pathway, although this was a short-term experiment and did not yield data on off-target effects or and therapeutic benefits to tumour size.

Work in 2022 by Tang *et al*.[68] identified that GCN2 was bound and activated by the cancer drug neratinib (NRB), a tyrosine kinase inhibitor (TKI) that competitively binds to the ATP binding domain of epidermal growth factor receptors (EGFR)[68,71]. NRB bound at higher concentrations to GCN2 (K_d = ~100 nM) than EGFR and resulted in GCN2 and eIF2α phosphorylation, and upregulation of ATF4 and downstream SLC transporters xCT (SLC7A11) and ASCT2 (SLC1A5), independent of NRB's primary mode of EGFR binding[68]. This led them to explore other ATP-competitive kinase inhibitor compounds as potential GCN2 activators. Screening of other EGFR inhibitors identified one compound, Erlotinib, that bound to and activated GCN2, although with a lower K_d for GCN2 (~4000 nM) than NRB. Wider screening of ATP-competitive inhibitors identified two further binding compounds that also activated GCN2 and resulted in eIF2α phosphorylation: Sunitinib, with a K_d of ~150 nM, and Dovitinib, with a K_d of ~175 nM. Although all four identified compounds require higher concentrations to activate GCN2, this consistent activation event in response to several different tyrosine kinase inhibitors identifies a promising avenue towards developing more effective activating compounds. Hyperactivation of the ISR results in apoptosis[72], therefore, developing a more targeted compound to harness this activity has real therapeutic potential.

In what may be the most promising advance with regards to GCN2 therapeutic manipulation, HiberCell last year announced a phase 1a/b clinical trial of a "novel, highly selective" GCN2 modulator as an antitumour compound to be trialled in patients with multiple types of solid tumours, including head and neck squamous cell carcinoma, non-small cell lung cancer, colorectal cancer, and transitional cell carcinoma of the bladder[69]. This trial is restricted to North

America and is currently still in the recruitment phase, but, if successful in establishing compound safety and a maximum tolerated dose for a subsequent phase 2 trial, a larger, more geographically diverse, cohort is likely to be required.

Together, this plots the first attempts to target GCN2 in cancer, with approaches harnessing the contradictory role of GCN2 in cancer to both activate and inhibit depending on the disease context. Inhibition may be beneficial in some cases to limit chemotherapeutic resistance, such as for gemcitabine and cisplatin, or to block angiogenesis and therefore metabolically starve proliferating cancer cells. However, induced prolonged activation is also an attractive route as it results in apoptosis. It is clear that the complexity of the AAR, and its ability to respond to stress in a dynamic and nuanced way, requires far better understanding than we currently possess if we are to utilise this weakness in cancer to its highest potential.

Chapter two: Malignant pleural mesothelioma, the current treatment landscape, and a role for GCN2

Malignant mesothelioma (MM) is an incurable and treatment-limited cancer with a very poor patient prognosis (<1 year). MM affects the serous membranes lining the internal organs and cavities and is caused predominantly by asbestos exposure. Disease latency, combined with continued asbestos use worldwide and a lack of a cure or any effective treatments, pose an imminent and prolonged public health issue. Greater understanding of the cellular processes underpinning MM pathogenesis is required to develop more effective, targeted, therapies and improve patient outlook.

2.1 Malignant mesothelioma (MM)

Mesothelial cells, from which MM tumours arise, comprise the surface level of cells that form a protective, serous membrane coating internal organs such as the lungs (pleura) and cavities (peritoneum)[73]. 90% of MM cases occur in the pleura, whilst cases in the peritoneum lining the abdominopelvic cavity contribute 7%-10% of MM cases[74]. Asbestos exposure can be linked to 95% of all MM cases[73]: occupational exposure introduces a 10% likelihood of an individual developing the disease over their lifetime[75]. Prognosis is incredibly poor, as MM is essentially incurable - without treatment, median survival is 7-10 months, which increases to a maximum of 22 months with treatment[76], and the 5-year survival rate is ~5%[77].

Although reporting quality varies by country, for the 59 countries with quality data, 15,000 annual deaths were reported for 2014-2017, which the Asbestos Disease Research Institute found extrapolated to a global annual death rate of 38,400[78]. A malignant mesothelioma diagnosis is treated as a near-fatal one, for which treatment is used palliatively and to slow progression.

2.2 Asbestos and mesothelioma

Asbestos is a naturally occurring hydrated magnesium-silicate mineral[75] that forms fibres that are insulative against heat, electricity, and water. These properties were extensively utilised during the industrial revolution, and have resulted in a massive, global industry surrounding its mining and manufacturing that persist today[79]. It was not until 1955[80] that its carcinogenic properties were concretely established, and 1965[81] that exposure was linked to mesothelioma specifically. This new understanding led to the slow introduction of laws restricting asbestos mining and use, with over 60 countries having implemented national bans to-date[82], and the UK banning asbestos in 1999[83].

However, these legislative restrictions are not yet universal, and have not eliminated existing asbestos, which is vulnerable to mechanical stress and therefore poses a continuing risk in older or poorly maintained buildings. The World Health Organisation (WHO) estimates that 125 million people are still exposed to asbestos in their workplaces[84]. This is further exacerbated by the fact that, despite current epidemiological understanding, the mining, export, and manufacturing of asbestos is still prevalent in multiple countries globally, most notably Brazil, China, Canada, India, Russia, and South Africa[73], with cumulative populations of over 3.27 billion. Additionally, MM has a median latency period of 40 years separating exposure and symptom presentation[73], and the disease typically presents in the fifth or sixth decade[75]. Therefore, even with efforts to reduce the burden of asbestos, we are likely faced with a global, prolonged healthcare burden, with further waves arising in countries that currently lack restrictions to be expected.

The majority of MM cases are in men aged 50-60 years old with links to asbestos mining or production[79], but cases are not restricted to this population: women and children who are family members of these workers are at a 10-fold risk of developing MM through secondary exposure, and so are those living in proximity to industrial asbestos sites[73,79]. Asbestos exposure, either historic or contemporary, is not going anywhere; we therefore need to turn our focus to the unavoidable approaching pandemic of malignant mesothelioma.

2.3 Asbestos and carcinogenicity

Asbestos fibres, when inhaled, become trapped and aggregate in the alveoli of the lower lung[75], accruing primarily in the pleura, and minorly in the peritoneum[85]. Asbestos subtype, as well as crystal structure, chemical composition, surface reactivity, transition metal presence, and fibre length[86] all contribute to toxicity.

The cascade of cellular events linking asbestos exposure to MM presentation, which may be separated by a latency period of 40 years or more, is not fully understood. Current work suggests that larger asbestos particles trigger chronic inflammation that alters the cellular microenvironment and predisposes mesothelial cells to mutagenesis[87]. A key feature of MM pathogenesis is asbestos-induced iron accumulation, resulting in ferroptosis resistance[88], with “asbestos bodies” of a core asbestos fibre associated with iron-containing elements being key to histological diagnosis[87].

Asbestos particle size is a deciding factor in whether the prolonged inflammation that leads to mesothelioma is triggered. Macrophages, as part of the innate immune system, phagocytose asbestos[89], but fibres over 10 µM result in “frustrated phagocytosis”[90], which damages the macrophage and triggers chronic inflammation leading to carcinogenesis. All phagocytosed asbestos triggers the NOD-like receptor family pyrin domain containing 3 (NLRP3) inflammasome, which promotes maturation and release of cytokine -1β into the extracellular space[91], but this process persists for fibres >10 µM. Other inflammatory proteins, including high-mobility group box-1 protein (HMGB1), are released, and promote an inflammatory environment defined by macrophage accumulation and NLRP3 activation, leading to TNF-α secretion. These inflammatory cells are able to induce DNA damage in nearby mesothelial cells by releasing reactive oxygen and nitrogen species, promoting DNA damage mutagenesis[87,92].

There is a strong genetic factor determining MM development, with certain key genes contributing to mesothelial carcinogenesis. Genomic analysis in MM has identified mutations in 5 genes: NF2, LATS2, SETD2, CDKN2A (P16), and

TP53[87]. Further work in mouse mutant models identified the latter two genes, Cdkn2a and Trp53, as key to mesothelioma development in two separate pathways[93].

This mutagenic environment is further complicated by the high prevalence of BAP1 mutations[94] in mesothelioma (60%), which is associated with early onset and less aggressive disease[95], especially in comparison with other cancers where mutations occur, most notably breast cancer. BAP1 binds to breast cancer type 1 susceptibility protein (BRCA1) and acts as a tumour suppressor[96]. As a nuclear deubiquitylase, it has control over genes relating to DNA replication, repair, and apoptosis[87,97,98] after asbestos-induced DNA damage. Additionally, cancer-associated BAP1-mutants supress ferroptosis by loss of SLC7A11 (xCT) regulation that would usually trigger ferroptosis by inducing cysteine depletion[99]. BAP1 may therefore contribute to the extended latency period of MM by offsetting DNA damage accumulation caused by reactive oxygen and nitrogen species and also helping mesothelial cells experiencing chronic inflammation to avoid ferroptosis.

2.4 Histological subtypes in malignant mesothelioma

MM can be divided into three main histological subtypes with differing prognoses and treatment strategies. They are separated based on cell morphology, with cells having either an epithelioid or sarcomatoid appearance[100]. Prognosis and treatment approach are determined by combining histological appearance with mesothelioma staging according to the Tumour-Node-Metastasis (TNM) system designed by the International Mesothelioma Interest Group, which splits disease progression into one of four stages, with more advanced disease classified as unresectable[101]. Due to its morphological heterogeneity, MM can often be visually indistinguishable from benign proliferations, and so diagnosis relies upon additional techniques to improve the probability of a correct diagnosis, including immunohistochemical staining[102].

2.4.1 Epithelioid malignant mesothelioma (EMM)

EMM is a diffuse malignancy that occurs in 80% of all MM patients and is also associated with a better prognosis than the other main subtypes. Tumours arise in the airways from invading epithelial-shaped mesothelial cells from the pleural surface, which form distinct, more solid structures than other MM subtypes. This may result in tubulopapillary, glandular, or micropapillary substructures that can aid histological diagnosis. Additionally, the typical epithelioid appearance can make differential diagnosis against adenocarcinoma difficult, requiring (immuno)histochemical stains to differentiate[73].

2.4.2 Sarcomatoid malignant mesothelioma (SMM)

SMM tumours are defined by either spindle-shaped mesothelial cells or mesenchymal-appearing cells that have infiltrated from the pleura. It is far rarer than its epithelioid variant, comprising ~10% of cases, and is associated with a far worse prognosis of 5-6 months if untreated. A sub-variant of SMM, desmoplastic malignant mesothelioma (DMM), is even rarer (~2%). With a similar prognosis to SMM, it is typified by dense, collagenous, stroma in at least 50% of the tumour[100].

2.4.3 Biphasic malignant mesothelioma (BMM)

BMM has a mixed histology of at least 10% of both epithelioid and sarcomatoid, and prognosis typically lies between these two subtypes[100]. This diverse composition makes this subtype the easiest to diagnose[73]. Some work has suggested that survival is positively impacted by a greater proportion of epithelioid within the tumour: <50% epithelioid was associated with a median survival of 6.62 months, increasing to 11.8 months at >50% epithelioid, versus 20.1 months for pure epithelioid[103].

2.5 Current treatment strategies

Whilst all cases of mesothelioma are deemed untreatable in the curative sense, there are still treatments available to extend or improve the remainder of life, and approaches differ by mesothelioma subtype and staging.

2.5.1 Surgery

Surgery is offered to patients with stage one to three of the disease without sarcomatoid histology. However, patients with comorbidities or who are deemed unfit for surgery are excluded, which given the late onset of MM, significantly restricts the number of patients for whom this is an option. Additionally, the surgery performed is typically an extrapleural pneumonectomy (EPP), which removes the entire lung alongside the pleura, pericardium, and diaphragm, with the aim of removing the entire tumour[75]. This approach is accompanied by high mortality (4-9%) and morbidity (complications arise in 60% of patients)[104], making it only beneficial in very limited cases. Less invasive lung-sparing surgeries such as pleurectomy may increase median survival to 15.8 months[75], and can be combined with radiation and chemotherapy as part of a trimodal approach, but is not curative as it does not achieve full tumour resection[104]

2.5.2 Chemotherapy

Despite surgery being a limited treatment option for MM patients, accompanied by not insignificant dangers, the chemotherapeutic arsenal is also limited, in part due to the relative resistance MM shows. Single-agent therapies, such as anthracyclines, platinum analogues, and antimetabolites show limited response rates (~10%-20%[105]) and fail to achieve a complete response, as do most combinatorial treatment regimens[106–108]. One of the few exceptions to this is the platinum-based cisplatin, which is the most bioactive single-agent therapy in MM[109], and is now relied upon as the core of dual-agent MM therapy.

Although cisplatin captures the highest single-agent response rate (16.7%), this is increased significantly in combination with the antimetabolite pemetrexed to 41.3%[110]. This now comprises both the frontline and multimodal approach to MM treatment, often alongside surgery and radiotherapy. However, despite this improved response rate, 60% of patients' disease do not respond, and disease continues to progress. Even on cisplatin-pemetrexed, median time to disease progression is only 5.7 months, versus 3.9 months for cisplatin, and survival period is 12.1 months, versus 9.3 months on cisplatin alone[75]

Other combinatorial approaches exist, such as cisplatin with gemcitabine or vinorelbine, but neither of these show a vast improvement in either response rate (12%-48%; 30%) or median survival (9.4 -13 months; 16.8 months) over cisplatin-pemetrexed[75,111].

There is currently no curative chemotherapeutic approach available for MM. Current agents may relieve symptoms, extend life expectancy, and push back disease progression, making it a useful palliative approach, but response rate for even these objectives is low, and new approaches are evidently desperately needed if MM diagnosis is not going to continue to be a death sentence.

2.5.3 Radiotherapy

Radiotherapy is a strictly palliative treatment approach in MM: although it can have limited effects in the transient reduction of tumour volume, therefore offering pain relief. The large area of chest cavity requires an excessive field of radiation, incurring second hand organ toxicity. Used by itself, response rates are low and survival period is not improved, restricting this technique to use supportively in combination with other approaches[105].

2.6 Development of Targeted Therapies

The uninspiring traditional treatment landscape of malignant mesothelioma has led to research in targeted therapies. Two aspects of malignant mesothelioma cancer biology implicate the GCN2-eIF2α-ATF4 pathway and have been the subject of clinical trials. Vascular endothelial growth factor (VEGF) is relevant to tumour angiogenesis, but also has a role as both a growth factor and mitogen in mesothelial cells[112]. Secondly, a majority (63%) of pleural malignant mesothelioma tumours are arginosuccinate synthetase (ASS1) negative[113], making it highly sensitive to arginine auxotrophy, a sensitivity that has also been explored in acute lymphoblastic leukaemia.

2.6.1 VEGF

VEGF plays a well-known role in tumour development as an inducer of angiogenesis, ensuring blood and nutrient supply[114], and, under amino acid starvation conditions, its angiogenic activity is upregulated by GCN2-ATF4[28]. However, VEGF activity also contributes to the abnormality of tumour vasculature, resulting in inconsistent blood flow that increases interstitial pressure and compression of blood vessels. This opposes the homogenous penetration of chemotherapeutic agents and introduces areas of hypoxia[112] that further upregulates angiogenesis and VEGF. A hypoxic environment has been shown to cause changes in gene expression that supress apoptosis and drive autophagy[115], whilst also promoting genomic instability and metastatic potential[116,117].

In the context of mesothelioma, VEGF is of special interest due to its role as an autocrine growth factor in MM, and a mitogen in mesothelial cells. Cell proliferation increases dose dependently with VEGF concentration in malignant mesothelioma cells, and serum levels are elevated over normal mesothelial cells, correlating negatively with patient survival[118]. In this context, VEGF exposure has been demonstrated to increase cell viability by as much as 100%[119].

This scientific basis has led to multiple attempts at developing antiangiogenic strategies to treat malignant mesothelioma, but this has had limited success. Small-molecule inhibitors[120], tyrosine kinase inhibitors[121–123], and anti-VEGF antibodies[124] have all been trialled. With the exception of the anti-VEGF antibody bevacizumab, none of these have shown effectiveness in treating malignant mesothelioma. Bevacizumab is a recombinant humanised IgG1 antibody, derived from a murine monoclonal antibody, which successfully nullifies the ability of all VEGF variants to bind to their receptors, either mesothelial or endothelial cells, supressing this mitogen's proliferative effects[124]. The phase 2/3 mesothelioma avastin cisplatin pemetrexed study (MAPS) compared the effects of bevacizumab addition to the standard chemotherapeutic pairing of pemetrexed-cisplatin (PCB), versus pemetrexed-cisplatin (PC) alone. The study's primary outcome of overall survival (OS) showed an improvement in the PCB condition (median 18.8 months; 95% CI 15.9–22.6; 164 (74%) of 223 died) over the PC condition (median 16.1 months; 95% CI 14.0–17.9; 179 (79%) of 225 died). The secondary outcome of progression-free survival (PFS), after a median follow-up period of 39.4 months also improved in the PCB condition (median 9.2 months) versus PC alone (median 7.3 months)[125]. Despite the potential of incorporating bevacizumab into MM treatment, incorporation into standard treatment plans has been patchy and varies significantly by region, largely due to cost. Similarly, the company behind the MAPS trial have not filed this therapy for mesothelioma specifically[112]. What this trial has reinforced, is that malignant mesothelioma therapies are most effective in combination, and that harnessing understanding of the underlying cellular processes allows us to target the disease more effectively.

2.6.2 ASS1

Around 50% of malignant pleural mesothelioma tumours (making up 90% of all MM) do not express asparagine synthetase (ASS1), as a result of aberrant CpG methylation in the gene's 5' regulatory sequence[113]. ASS1 is responsible for catalysing the rate limiting step in arginine biosynthesis, but is silenced in

malignant mesothelioma, in almost all prostate cancers, and in 40%-60% of all small cell lung cancers and breast cancers, making these cancers reliant upon extracellular arginine to survive[126]. Therefore, although arginine is not typically an essential amino acid, in these cancers it is limiting.

Asparagine synthetase (ASNS), which is under the control of GCN2 via ATF4, the central transcription factor of the integrated stress response, is induced by arginine starvation. In 2018, Cheng *et al*.[127] demonstrated extracellular arginine depletion in ASS1-low BT-549 breast cancer cells resulted in ASNS-mediated cell death. Arginine starvation induces ASNS, which funnels aspartate to asparagine production: this drop in aspartate disrupts mitochondrial oxidative phosphorylation by supressing the aspartate-malate shuttle required for electron transfer and proper mitochondrial function, resulting in acetyl Co-A and ROS dysregulation, and ultimately inducing a cytotoxic state.

They also demonstrated that ASNS knockdown allowed these cells to survive arginine starvation by halting aspartate metabolism by ASNS. Although this work was carried out in breast cancer cells, ASS1-deficiency, and subsequent arginine auxotrophy, is observed in multiple cancers, including MM. ASNS is one of multiple amino acid synthesis genes under GCN2-ATF4 control. As discussed previously in this thesis, targeting ASNS in acute lymphoblastic leukaemia (ALL) cells, another ASS1-deficient cancer[128], combinatorially with the inhibitor asparaginase (ASNase) and a GCN2 inhibitor reduced proliferation and induced apoptosis.

Phase 2 clinical trials have been carried out in malignant mesothelioma using a pegylated form of the enzyme arginine deiminase as a targeted therapy to determine the efficacy of this treatment as both a single and multi-agent therapy. The enzyme catalyses the deamination of arginine to citrulline, so may enhance arginine starvation in ASS1-deficient tumours. The Arginine Deiminase and Mesothelioma (ADAM) phase 2 study[129] (NCT01279967) trialled ADI-PEG20 against a multimodal, best supportive care (BSC), approach. With a cohort of 68, it demonstrated that ADI-PEG20 with arginine starvation, when compared to BSC, showed improvements in median

progression-free survival (3.2 months versus 2.0 months) and in life expectancy (15.7 months versus 12.1 months).

The mechanistic basis of the ADI-PEG20 treatment has been explicitly demonstrated to involve the GCN2-eIF2α-ATF4 pathway in invasive bladder cancer, another cancer with ASS1 loss[130]. ASS1-deficient bladder cancer cells were shown to be ADI-PEG20 sensitive, activating the GCN2-eIF2α-ATF4 pathway and inducing C/EBP homologous protein (CHOP), which they found mediated apoptosis in the ASS1-deficient bladder cancer cells.

A second phase 2/3 trial (NCT02709512) is specifically investigating ADI-PEG20 in combination with the already established cisplatin-pemetrexed chemotherapy in malignant pleural mesothelioma patients. No results have yet been published, but, in light of the ADAM trial, and that the most effective MM treatments appear to be multi-agent ones, this could establish a new component in MM therapy.

With the glimmers of hope provided from targeted therapies to better treat what is still an incurable disease, improved understanding of the underlying cellular processes in malignant mesothelioma is vital to developing effective therapies, either as a stand-alone, or, given current trends, to augment the current arsenal.

2.7 GCN2 and malignant mesothelioma

Mesothelial cells, as part of their role forming the serous lining of the internal organs and cavities, synthesise large volumes of glycoproteins, introducing ER-related stress. Malignant cells already experience ER-related stress; hypoxia-induced protein modifications in the ER induce protein misfolding[131] and overwhelming unfolded protein content quickly overwhelms the secretory pathway[132]. The addition of further ER-related stress as a result of malignancy in these mesothelial cells results in the activation of the unfolded protein response (UPR) arm of the integrated stress response (ISR), via three signal transducers: stress-sensing kinase protein kinase R (PKR)-like endoplasmic reticulum kinase (PERK, or EIF2AK3), IRE1, and ATF6[132]. Work carried out

by Dalton *et al*. in 2013[133] investigated whether upregulation of certain biomarkers associated with UPR activation could be used prognostically in MM patients[133]. Tissue microarrays (TMA's) taken from 135 malignant mesothelioma patients were stained immunohistochemically with antibodies targeting markers of ER-stress, specifically the HSP70 chaperone BiP, the transcription factor C/EBP Homologous Protein (CHOP), and growth arrest and DNA damage-inducible protein GADD34. They found that expression levels of CHOP correlated with patient survival and may therefore be used as a biomarker to determine tumour aggression.

CHOP is one of the mRNA's preferentially translated in response to ISR activation by ATF4 activity, containing an upstream open reading frame (uORF) in the 5' untranslated region that exempts it from requiring cap recognition by the eIF4F complex[1,10]. As a target of ATF4, it is upregulated by the ISR, making it an indirect indicator of multiple stressors. Under ER-related stress, a CHOP-ATF4 heterodimer can bind to C/EBP-ATF response element (CARE) sequences to regulate expression of genes relevant to ER-stress resolution, including the transcription factor *atf3*, *ppp1r15a* (GADD34), and the tryptophanyl-tRNA synthetase *Wars*[134]. This dimer is also highly relevant to GCN2-related stress resolution, as PERK and GCN2 have significant overlap functionally in the context tumour microenvironment stresses, which activate both kinases. The CHOP-ATF4 dimer, in response to ER-stress, regulates genes at the nexus of PERK and GCN2 control, including amino acid metabolism, translation, and the unfolded protein response[134]. During amino acid stress, the C/EBP-ATF4 heterodimer also regulates expression in genes related to autophagy by binding to CARE sequences, which act as amino acid response elements (AARE) in this context.

2.8 Aims

This work will build upon that by Dalton *et al*., which determined a prognostic role for CHOP in malignant mesothelioma tumour microarrays (TMA's). Given that CHOP levels are also linked to the GCN2 arm of the ISR, this work investigated whether GCN2 levels in malignant pleural mesothelioma (MPM)

were associated with patient prognosis and its potential as a novel biomarker. As covered in chapter one, Cancer Dependency Map analysis (DepMap) of GCN2 has already shown a dependant relationship in 13% of cancers[31]. GCN2 knockdown experiments in xenograft mouse tumours have been demonstrated to decrease tumour volume significantly, which occurs by supressing GCN2's upregulation of VEGF and subsequent angiogenesis[28], which is already a target of therapeutic interest in malignant mesothelioma. The central aim of this work is therefore to determine whether GCN2 levels correlate with poorer patient prognosis, and therefore its potential as a novel prognostic biomarker and therapeutic target in malignant pleural mesothelioma.

Chapter three: Methods

3.1 Tissue microarrays

Tissue microarrays (TMA's) were obtained from Mesobank tissue bank based at the NHS Royal Papworth Hospital, the largest UK pleural mesothelioma biobank[135]. TMA's were prepared by the biobank for 204 patients with cores of 0.6 mm diameter, with between four and five replicates for each patient included on concurrent locations within the set. Demographic data was provided for each patient, including age at diagnosis, time to death, gender, TNM classification, and histopathology (table 1). Normal kidney, heart, and liver tissue was dispersed throughout the slide sets for the purpose of microscope orientation, and these also underwent staining. Consistency in staining was observed for these tissues within and between slides, indicating that staining conditions were consistent and not a source of error.

3.2 Ethics

This work was carried out in partnership with the Tayside Biorepository and under their existing approval from the Local Research Ethics Committee.

3.3 Immunohistochemistry

The Invitrogen MA5-32704 anti-GCN2 rabbit monoclonal antibody was used to detect non-phosphorylated GCN2. Initially, a phospho-GCN2 antibody targeting T899 (Abcam, ab75836) was to be used to stain a second set of TMA slides also obtained from the MesobanK as a direct measure of GCN2 activity, however this antibody did not pass protocol refinement.

Protocol optimisation and immunohistochemistry was carried out by Dr Susan Bray at the Tayside Biorepository.

No mesothelioma or TMA offcut tissue was available for optimisation. A range of other cancerous tissues (B-cell lymphoma, breast metastasis in bone, head and neck squamous cell carcinoma, placenta, colon, liver, cervix, prostate, lymph node, and a composite NHS block) were used instead. This allowed confirmation of (1) the appropriate antibody dilution to observe staining of 1:100 (2) that staining was occurring *specifically* in the cytoplasm and not in the nucleus, in line with our expectation for GCN2.

Prior to staining, sections were placed in an oven at 60°C for one hour to melt residual wax. Deparaffinisation and antigen retrieval were performed in a DAKO PT Link for 20 minutes at 97°C, using DAKO EnVision™ FLEX Target Retrieval Solution (high pH) buffer (50x concentration, K8004). Immunostaining using the DAKO EnVision™ FLEX system was performed in a DAKO Link Autostainer. Sections were initially washed in Flex Wash Buffer (K8006) for five minutes at room temperature, prior to manual application of the Flex-Peroxidase-Blocking Reagent (SM801) for five minutes at room temperature, followed by incubation with anti-GCN2 rabbit monoclonal antibody (Invitrogen MA5-32704) at 1-100 dilution overnight at 4°C.

The automated platform was then used (DAKO Link Autostainer) for the following incubation steps: 20 minutes in Flex/HRP labelled polymer (SM802), 15 minutes in Flex Envision Mouse Link (SM804), five minutes in Flex DAB+ working solution (SM803), twice, five minutes in Copper Sulphate solution, and five minutes in Flex Haematoxylin. Between each incubation step, sections were rinsed with Flex Wash Buffer, with a final wash in dH_2O.

Sections known to stain positively were included in each batch of staining, and negative controls were prepared by replacing the primary antibody with DAKO antibody diluent. Slides were manually washed in tap water before being rinsed in graded concentrations of alcohol, with three final rinses in xylene. Glass coverslips were applied.

Prior to scoring, TMA's were viewed to confirm that staining was localised to the cytoplasm, which is where GCN2 is located. As can be seen in fig. 3a,

staining is limited to the cytoplasm in both epithelioid and biphasic TMA sections, and the nuclear counterstain haematoxylin (blue) can be clearly observed, indicating that no non-specific staining in the nucleus is occurring.

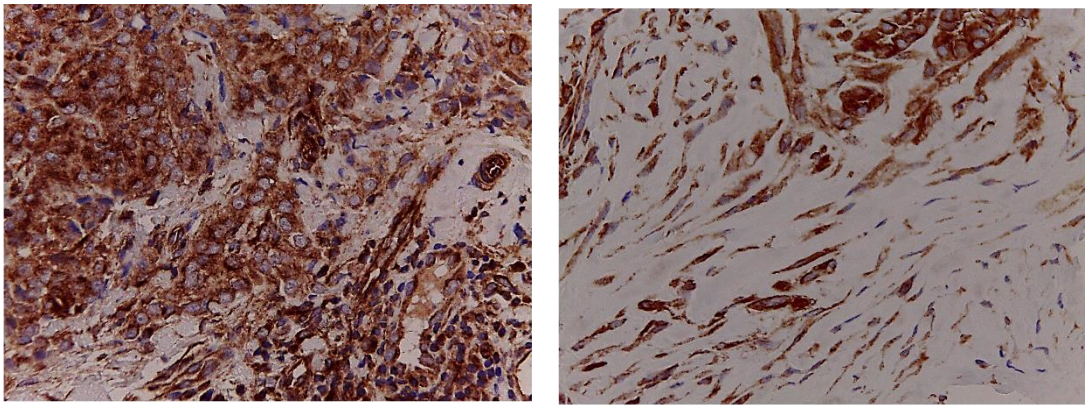

Figure 3a. GCN2 staining localisation to the cytoplasm in epithelioid and biphasic MPM TMA tissue samples. GCN2 is a cytoplasmic protein, and staining (brown) was restricted to this cellular region, supporting the specificity of the GCN2 antibody. The nuclear region is stained only by the haematoxylin counterstain (blue), further indicating antibody specificity. Image brightness and contrast has been increased to improve staining visibility.

3.4 Scoring

To quantify GCN2 levels, an image library compiling each tumour section was captured using LEICA ICC50 HD microscope at 10x magnification, using the Leica LAS EZ Application Suite Version 3.4.0. Individual sections were then scored on two scales.

First, staining intensity scores from 0 to 5 (fig. 5b) were assigned independently by LTG and two undergraduate students (MN and NH). Secondly, a proportion staining score from 0 to 100, representing the percentage of all cells in the section stained, was assigned. These scores were combined for each section to give a value from 0 to 500 and an average of all replicates calculated for each patient. Due to time constraints, only slide 1 was assessed by the two additional scorers (appendix).

To determine variation in scores assigned by LTG compared to MN and NH, the ratio between the 0-500 score assigned by LTG and MN or NH was calculated, which indicated the percentage difference (appendix) between the two scores for that patient. These values were then averaged for all patients (LTG vs MN; LTG vs NH), to determine the average variation. This generated an average difference of +4.3% (LTG vs MN) and -3.8% (LTG vs NH), indicating a strong agreement in scoring.

3.5 Statistical analysis

Statistical analysis was carried out using GraphPad Prism 9 (GraphPad Prism version 9.5.1 for Windows, San Diego, California USA) and RStudio[136]. Survival was assessed from date of histological diagnosis to death. Patients that were still alive were excluded from the survival analysis. Univariate survival analysis for demographic data and GCN2 scores used the log-rank (LR) test and was visualised as Kaplan-Meier (KM) survival curves, both in GraphPad Prism.

The pROC package[137] in RStudio was used to generate receiver operator characteristic (ROC) curves to determine whether GCN2 was a prognostic marker in malignant pleural mesothelioma (MPM) patients. An ROC curve is a classification model that plots the relationship between a binary outcome variable (i.e., whether death has occurred at a certain timepoint or not) and a continuous predictor variable (i.e., a diagnostic score), determining how well the predictor is able to discriminate on whether an event has actually occurred at any point along the curve, and this therefore indicates whether there is a predictive relationship between the two variables.

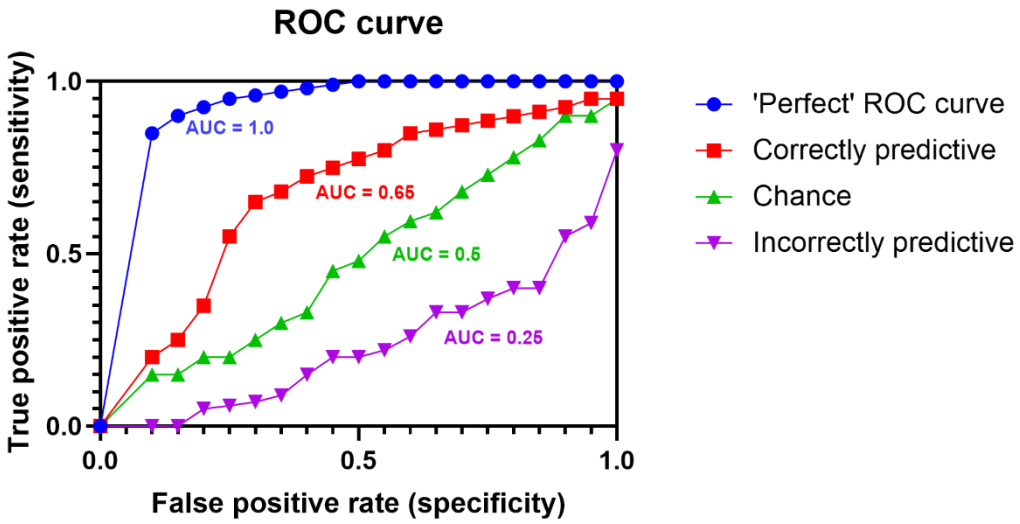

Figure 3b. Example ROC curves generated from data with different predictive relationships: a (blue, AUC = 1.0) perfectly predictive relationship, a (red, AUC=0.65) positively predictive relationship, a (green) non-predictive relationship solely governed by chance, and finally, an (purple, AUC=0.25) incorrectly predictive relationship. The AUC is also referred to as a C-statistic in this context. Figure adapted from Carter et al., 2016.[138] Acronyms: ROC: receiver operating characteristic | AUC: area under curve.

The true positive rate, or specificity (i.e., the rate at which the continuous variable correctly predicts the outcome, x-axis) is plotted against the false positive rate, or sensitivity (y-axis)[138]. If the relationship between the two is truly predictive, the true positive rate will exceed the false positive rate. The area under curve (AUC), also referred to as the C-statistic[139], is the output from this analysis, and indicates whether the two variables have a predictive relationship. A perfect, correctly predictive relationship generates an AUC value of 1.0 (blue line, fig. 3b), wherein the entire plot lies under the curve. Conversely, a model that indicates a non-predictive relationship no different from chance would plot a linear line with an AUC value of 0.5 (green line, fig. 3b). Finally, an incorrectly predictive model (purple line., fig. 3b), where the false positive rate exceeds the true positive rate, would generate a plot with an AUC <0.5[138]. Statistical analysis and figures were generated in RStudio. Based on previous work in MPM[133,140], a significance cut-off of 0.65 for the C-statistic was used.

To test individual variables for prognostic significance, ROC curves were generated using the pROC package in R-studio[136]. Survival was treated as the binary outcome in each comparison, with each variable tested on its

ability to predict one-year survival outcomes. To facilitate this, the continuous survival classification was converted to a binary good (<365.0 days) or bad (>365.0 days) classification.

Differences in GCN2 scores between histological subtypes (epithelioid, biphasic, sarcomatoid) were determined in GraphPad Prism using an ordinary one-way ANOVA with Bonferroni *post hoc* test to correct for family-wise error.

Section 4.1. Patient cohort characteristics

Five tissue microarray (TMA) slides were obtained from the MesobanK[135] tissue bank (Royal Papworth Hospital, Cambridgeshire) containing malignant pleural mesothelioma (MPM) samples from a total of 204 patients. Samples were biopsied at Royal Papworth Hospital, Cambridge, and between four and five replicates per patient included sequentially within the TMA set. Accompanying patient characteristic data is summarised in table 1 and is in line with wider patterns in malignant mesothelioma patients. The majority of patients were males (184 of 204; 90.2%) with a median age of 69. Epithelioid histology was the most prevalent (126 of 204, 61.8%), followed by biphasic (47 of 204, 23.0%), and sarcomatoid histologies (sarcomatoid | 29 of 204, 14.2%; desmoplastic | 2 of 204, 1.0%). TNM (tumour, node, metastasis) data was provided partially or entirely for 65 of 204 patients. For patients with this data available, 56.9% (T3-T4, 37 of 65) had more extensive tumours that covered all pleural surfaces in one side of the body. 41.3% showed some degree of lymph node involvement (N1-N3, 26 of 63), and 35.5% of cancers showed evidence of distant metastasis (M1/1a, 22 of 62). Ten patients were excluded from the analysis. Four were still alive and so could not be included. Living status data was missing for three patients (1.5%), and a further three were excluded because no tissue sections were present for these patients within the slide set. Time to death was provided for 194 of 204 patients. This value measured length of time from histological diagnosis to death in days and was used in survival analyses against GCN2 scores and other demographic data held for the cohort.

Table 1: Patient Characteristics

	Number of patients	Total number of patients	Percentage of patients
Gender		204	
Female	20		9.8%
Male	184		90.2%
Histologic type		204	
Epithelioid	126		61.8%

Biphasic	47		23.0%
Sarcomatoid	29		14.2%
Desmoplastic	2		1.0%
Alive		204	
Yes	4		2.0%
No	197		96.6%
No data	3		1.5%
Tumour Extent (T)		204	
0	1		0.5%
1/1b	8		3.9%
2	19		9.3%
3	20		9.8%
4	17		8.3%
No data	139		68.1%
Node spread (N)		204	
0	37		18.4%
1	8		3.92%
2	16		7.8%
3	2		1.0%
-	141		69.1%
Metastasis (M)		204	
0	40		19.6%
1/1a	22		10.8%
-	141		69.1%
Reasons for exclusion:		10	30.0%
Missing survival and time to death data	3		30.0%
No tissue sections present	3		40.0%
Alive at time of analysis	4		

Section 4.2. Univariate survival analysis of demographic data: Kaplan-Meier curves and Log-Rank test

A univariate survival analysis using a log-rank (LR) test was used to determine whether the demographic data in table 1 was prognostically significant for this patient population. The same analysis was then carried out for the GCN2 staining scores generated as part of this work (section 4.3). Survival over time was visualised as Kaplan-Meier (KM) survival curves, prior to LR analysis.

The KM survival curves calculate the probability of an event (here, death) happening at any point along the curve for each group included in the analysis, which is then plotted as a probability of survival over time[141]. The log-rank test is then used to determine whether a significant difference exists between the curves plotted, providing a p-value. The LR test is functionally a chi-square test with a large sample that tests the null hypothesis that there is no difference

between the KM curves plotted. This is determined by summing the differences between the observed and expected values for all points on one of the curves. The cumulative observed-expected value generated is used to determine the hazard ratio, 95% CI, and p-value for the test[141]. If the p-value is significant ($p<0.05$) the null hypothesis is rejected, and it can be assumed that the variable under investigation, i.e., gender, GCN2 score, is affecting survival and is therefore prognostically significant. The hazard-ratio indicates the strength of the effect between the first group in the analysis and the comparison group and is only generated for a two-curve analysis. A value of 1 is a 'baseline': a value below 1 indicates a reduced likelihood of death in the first group compared to the second. Conversely, a value over 1 indicates an increased likelihood of death in the first group. This can be used as a more tangible indicator for the differences in survival present beyond the p-value[141].

4.2.1: Gender

Malignant mesothelioma in the UK is the highest in the world and is more prevalent in men than women (2.9 per 100,000; 0.6 per 100,000, or 82.9%: 17.1%). Females also have a significantly higher survival rate, with a hazard ratio of 0.85 (95% CI: 0.81-0.90) (Alpert et al., 2020). In our cohort, we would therefore expect to see a higher proportion of male patients, who in turn have poorer survival outcomes.

A KM curve was plotted for both genders included in the dataset (fig. 4a) to compare the effects of this characteristic on survival. The patient cohort was comprised primarily of men (N=176), as expected, with only 18 female patients meeting the inclusion criteria (table 1): the proportion therefore was in line with expected trends (male = 90.7%, female = 9.3%). Median survival was greater for the female group (387.0 days) versus the male group (282.0 days). The LR test did not indicate a difference in survival likelihood between genders (hazard ratio, 0.7743 [95% CI, 0.4995 to 1.200]; p=0.3029) because of the expansive confidence interval, although this is likely an artifact of the disparate sample sizes between groups and the small female sample size.

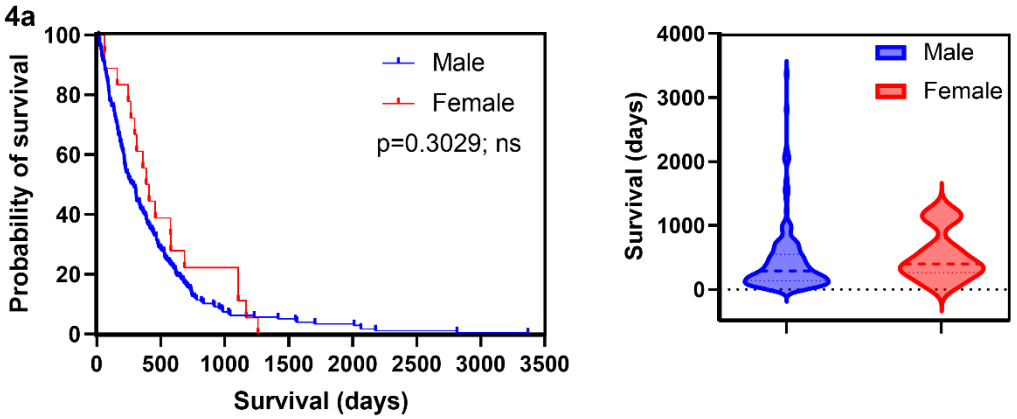

Figure 4a. Figure 4a. mesothelioma patient gender and survival prognosis: A Kaplan-Meier (KM) curve was plotted for male (N=176) and female (N=18) patients. Log-Rank statistics did not find a significant difference between these curves that would indicate gender to be prognostic for this data set (p=0.3029), however sample size differences may have impacted the output.

4.2.2: Histopathology

Histopathology is a strong prognostic indicator in malignant mesothelioma[100], with the epithelioid histology being both the most common and associated with the best prognosis. Conversely, sarcomatoid histology, and its desmoplastic subtype, are the least common but most lethal. Biphasic, which is comprised of both epithelioid and sarcomatoid histologies, has an intermediate prognosis, strongly impacted by the proportion of sarcomatoid content in the tumour. We therefore expected to observe similar trends, with worsening prognosis from epithelioid to biphasic, to sarcomatoid.

Four histological subtypes, epithelioid, biphasic, sarcomatoid, and desmoplastic, were present within the cohort. In the first analysis (fig, 4b), epithelioid, biphasic and sarcomatoid survival was compared. There were only two desmoplastic patients in the dataset, and as a subtype of sarcomatoid histopathology they were included in the larger sarcomatoid pool. The epithelioid pool contained the most patients (N=119) followed by biphasic (N=46), and sarcomatoid (N=29), in line with wider trends.

Median survival was observed to vary by histology (fig. 4b), following the expected trends, and was highest in the epithelioid group (402.0 days). This value was 1.3-fold that for the biphasic group (310.0 days), and 4.1-fold when compared to the sarcomatoid group (97.0 days). The log-rank test generated a significant p-value (p<0.0001), indicating that histology is a prognostic factor.

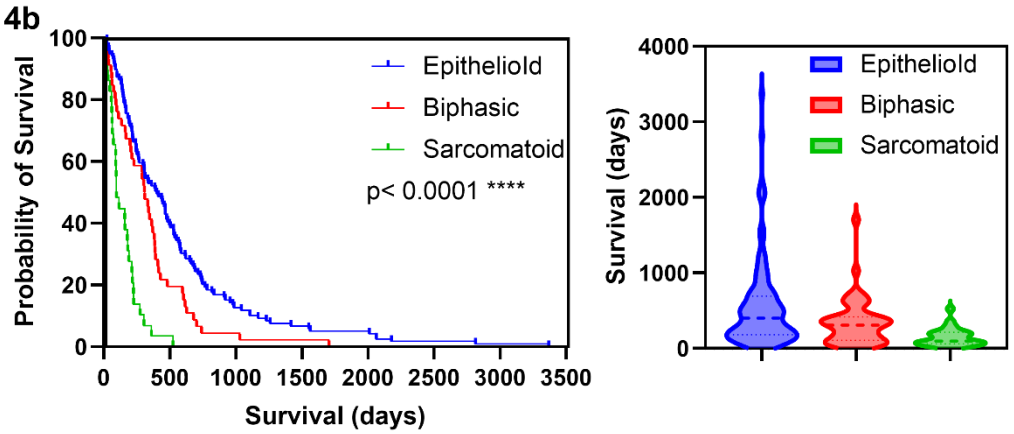

Figure 4b. Mesothelioma histopathology and survival prognosis: KM curves were plotted for each of the histological subtypes included in the patient cohort. As there were only two desmoplastic patients and it is a sarcomatoid subtype, these patients were grouped with sarcomatoid. LR test determined that the curves differed significantly (p<0.0001) and histopathology was prognostic, supported by the distributions of the corresponding violin plots. A box-and-whiskers plot was used to determine whether GCN2 score correlated with histopathology. This was assessed statistically using ANOVA and the Bonferroni post-hoc test, which found no significant difference by score. Acronyms: KM = Kaplan-Meier | LR = Log Rank

Biphasic histopathology is a combination of epithelioid and sarcomatoid, with sarcomatoid content being linked to worse prognoses[100]. A second analysis was carried out to compare survival in epithelioid and non-epithelioid (fig. 4c) tumours to determine whether this affected prognosis, as we would expect any sarcomatoid content to result in poorer prognosis.

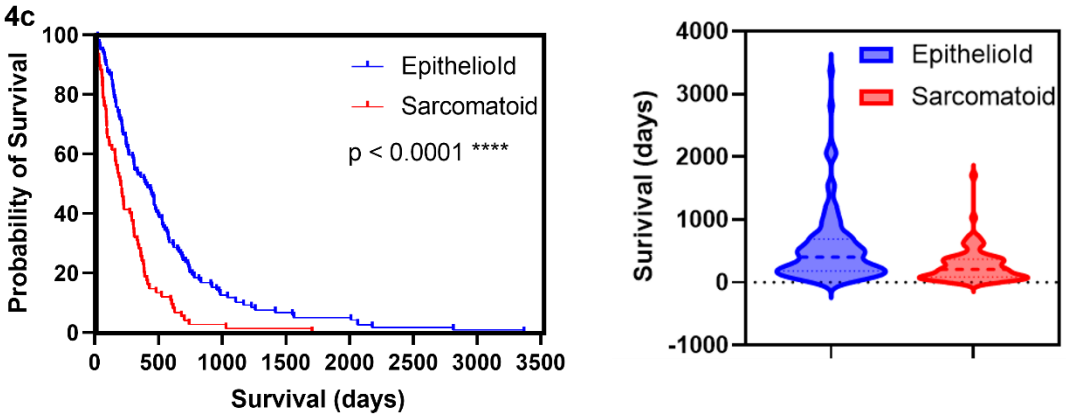

Figure 4c. Sarcomatoid histopathological content and survival prognosis: KM survival curves were plotted for epithelioid and sarcomatoid-containing histopathologies. The latter group comprised sarcomatoid, desmoplastic, and biphasic patients. As for fig.4b, the LR test found histopathology to be prognostic (p<0.0001). The differing survival distributions evidenced in the violin plot also indicates that the sarcomatoid group (red) has a lower survival than the epithelioid group (blue). Acronyms: KM = Kaplan-Meier | LR = Log Rank

The epithelioid group was the same size (N=119) as for the previous analysis, whilst the sarcomatoid group (containing sarcomatoid, desmoplastic, and biphasic patients) had a sample size of 75. The median survival period was 1.95-fold higher in the epithelioid group (402.0 days) versus the sarcomatoid-containing group (206.0 days), as expected. The LR test comparing survival between the two curves (fig. 4c) found that sarcomatoid content was a a prognostic factor (hazard ratio, 1.979 [95% CI, 1.425 to 2.750]; p<0.0001), with an almost two-fold greater probability of death versus epithelioid histology.

4.2.3: TNM Scores

The tumour, node, and metastasis (TNM) classification system are a set of parameters used to classify the size and extent of tumours, including malignant pleural mesothelioma (MPM) tumours, with each component describing an aspect of tumour size or spread, as decided by the International Association for the Study of Lung Cancer[142].

4.2.3.1: Tumour extent (T)

The tumour (T) score component, for other tumours, typically describes spread from a central site of primary metastasis, however, in MPM this central site is replaced by the presence of multiple nodes that can achieve confluence over time[142]. The T score (T0 to T4) describes the areas of the chest cavity involved in metastasis, for example the parietal, mediastinal, diaphragmatic, and visceral pleura, and the degree of invasion into other regions such as the lungs and diaphragm (extensively reviewed in Berzenji *et al*., 2018[142]). T0 indicates no primary tumour, and T4 is used where extensive spread beyond the pleural cavity has occurred, such as to the spine or mediastinal organ(s)[142]. We would therefore expect to observe worse prognosis with higher T scores.

65 patients in our cohort had a T score and could be included in this analysis. As there were five potential subcategories (table 1) with unequal distributions, it was decided that a binary analysis would be most effective, allowing reasonable population of groups used in the analysis. Group one (T0-T2, N=27) patients had tumours that had not progressed to cover the entire pleural surface, whereas group two (T3-T4, N=36) was populated with patients whose tumours had spread to the entire pleural surface or encroached beyond it. We would therefore expect that group one would have a better prognosis than group 2.

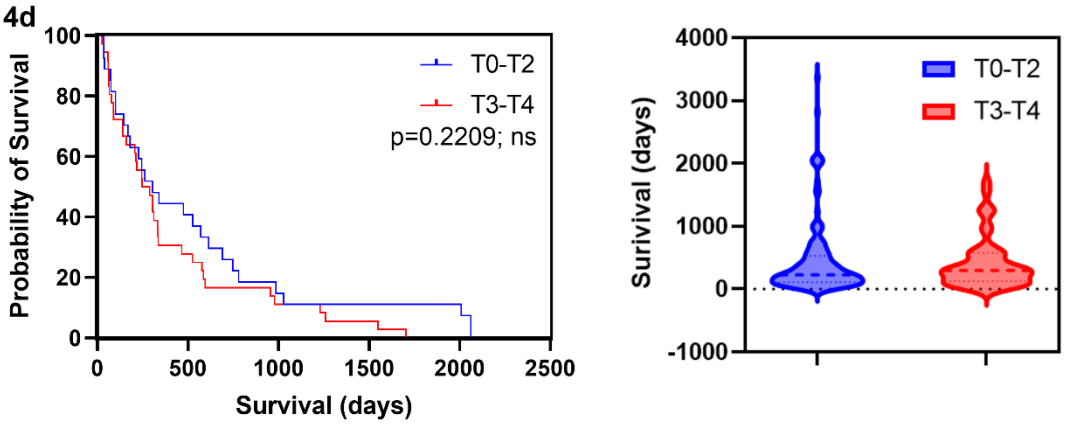

Figure 4d. Tumour T score and survival prognosis: Tumour T scores range from 0-4; these were split into two groups, group one (T0-T2), and group 2 (T3-T4), the latter with more advanced tumours. KM curves were plotted for each group. The log-rank analysis comparing

the two survival curves did not find a significant difference between the two groups (p=0.2209), indicating that T score was not prognostically significant for this cohort. This is further supported by the violin plots, which display similar survival distributions for both groups. Acronyms: KM = Kaplan-Meier

The median survival period for group one was slightly larger than that for group 2 (304.0 days versus 267.0, 1.1-fold difference). However, the T score was not found to be prognostic when comparing the survival curves for each group using the log-rank test (hazard ratio, 0.7408 [95% CI, 0.4360 to 1.212]; p=0.2209), further evidenced by the significant overlap between these two groups (fig. 4d) as well as the hazard ratio confidence interval.

4.2.3.2: Node involvement (N)

Node involvement is an important prognostic factor in MPM patients, with survival rates significantly reduced in patients with nodal metastasis[143]. Four levels of scoring are possible, with N0 denoting a total lack of nodal involvement, and N1-3 covering the involvement of increasingly distal nodes. 61 patients had information on node involvement, distributed unevenly across classifications (table 1). To ensure a reasonable sample size in analysis groups, a binary survival comparison (fig. 4e) was carried out for patients in group one, without node involvement (N0, N=37), and group two, with node involvement (N1-N3, N=24). We expected to observe better survival outcomes in group one when compared to group two.

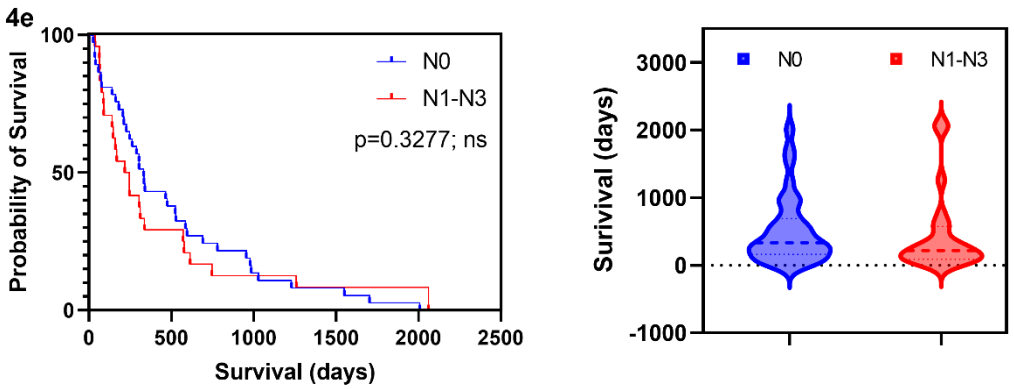

Figure 4e. Node involvement and survival prognosis: Node scores range from 0 to 3, and patients were grouped into two groups depending on whether any node involvement was recorded (group one = N0, no node involvement; group two = N1-3, node involvement. KM survival curves were plotted and LR analysis comparing survival between the two groups, generated a non-significant p-value (p=0.3277), indicating that N score is not prognostic. This is further supported by significant overlap between the two curves and similar survival distributions in the violin plot. Acronyms: KM = Kaplan-Meier | LR = Log Rank

Median survival was 1.4-fold greater in the N0 group (333.0 days) than in the N1-N3 group (231.5 days), however the LR test did not find node involvement to be a prognostic indicator (hazard ratio, 0.9321 [95% CI, 0.5553 to 1.565]; p=0.3277).

4.2.3.3: Metastasis (M)

The M classification is a binary indicator of distant metastasis beyond the ipsilateral hemithorax, where M0 = no metastasis and M1 = metastasis[142]. Previous work has found no survival difference between T4-stage patients with metastasis ('M0', median survival = 10.7 months [95% CI, 5.9-15.6], 3.7% 2-year survival) when compared to those with ('M1', median survival = 13.3 months [95% CI, 2-24.6], 0% 2-year survival)[144]. Although our cohort was populated by patients with T0-4 scores, we did not expect that M score would be found prognostic.

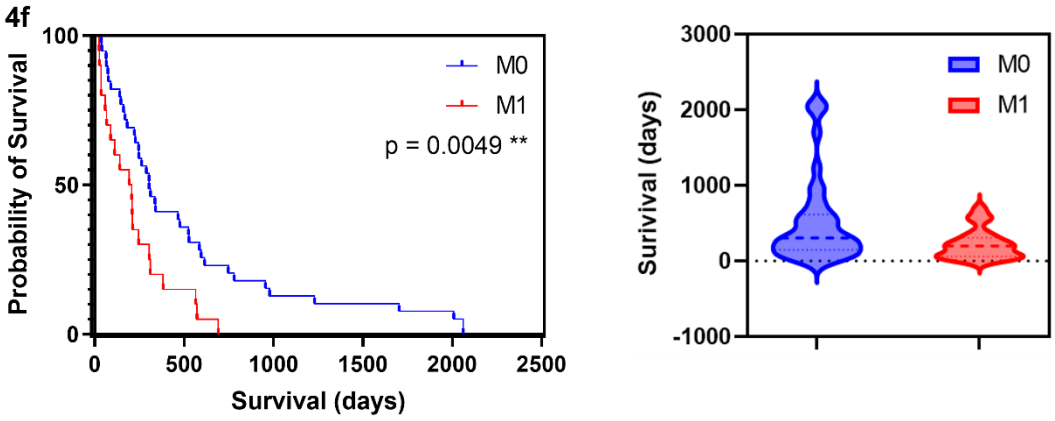

Figure 4f. Metastasis score and survival prognosis: Metastasis is assessed according to a binary assignation that indicates mesothelioma either with (M1) and without (M0) metastasis.

The KM plots showed distinct traces, and LR analysis determined M score to be prognostic (p=0.0049), indicating different survival outcomes between the two groups. This was further supported by the violin plot distribution, with the metastatic (M1, red) group demonstrating poorer survival values when compared to the non-metastatic (M0, blue) group, which has broader, higher values. Acronyms: KM = Kaplan-Meier | LR = Log Rank

Of 62 patients with data on distant metastasis, 59 met inclusion criteria (i.e., dead at time of analysis). Patients were split into two groups based on the absence (M0, N=39) or presence (M1, N=20) and had varying T classifications in both groups ranging from T0 to T4. Median survival was 1.5-fold greater in the M0 group versus the M1 group (304.0 days and 199.0 days, respectively). The KM curve shows distinctive curves for the two groups (fig. 4f) with no overlap beyond the origin, indicating differences in survival outcomes between the two groups. This was further supported by the LR test, which found metastasis status to be a significant prognostic indicator (hazard ratio, 0.4821 [95% CI, 0.2542 to 0.9143; p=0.0049].

Section 4.3. Survival analysis of GCN2 score and histopathology: Kaplan-Meier curves and Log-Rank test

GCN2 scoring was carried out by assigning each TMA section two scores: an intensity score from one to five describing the strength of staining, and a proportion score (1 to 100) describing what proportion of the section was stained (fig. 5a).

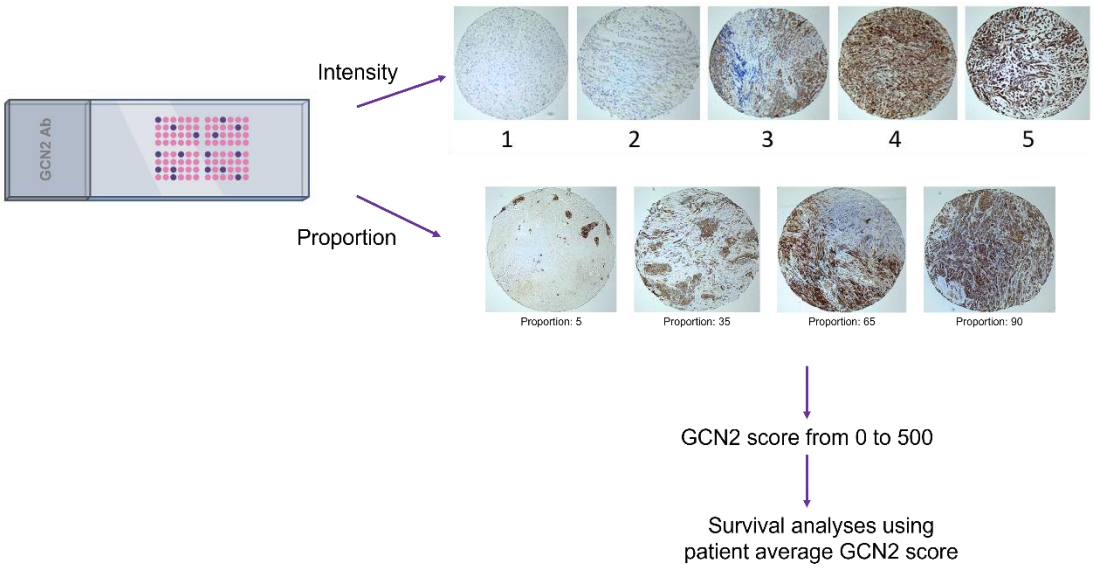

Figure 5a. Tissue microarray (TMA) GCN2 immunohistochemical scoring guide: Each tissue core (section) is approximately 0.6 mm diameter, with between four and five repeats per patient. Each tissue section was assigned two scores to assess staining as a measurement of GCN2 level. Firstly, an intensity score was assigned between 1 and 5, with 1 indicating no staining, and 5 indicating maximal staining intensity. A second proportion score, from 0 to 100, was then assigned, with a lower score indicating more localised staining, and a score of 100 indicating that all cells in the section are stained. These two values were then multiplied to generate a score from 0 to 500 for each section. The average score across sections for each patient was averaged and this value used in subsequent survival analyses

TMA's were populated with sections from patients with epithelioid, biphasic, sarcomatoid, and desmoplastic histopathologies (fig. 5b), with non-diseased tissues regularly interspersed (see methods). Intensity scores were assigned independently by three observers (LG and two undergraduate students) and confirmed to be within 5% of each other by GM. Proportion scores (1-100) were assigned solely by LG due to time constraints.

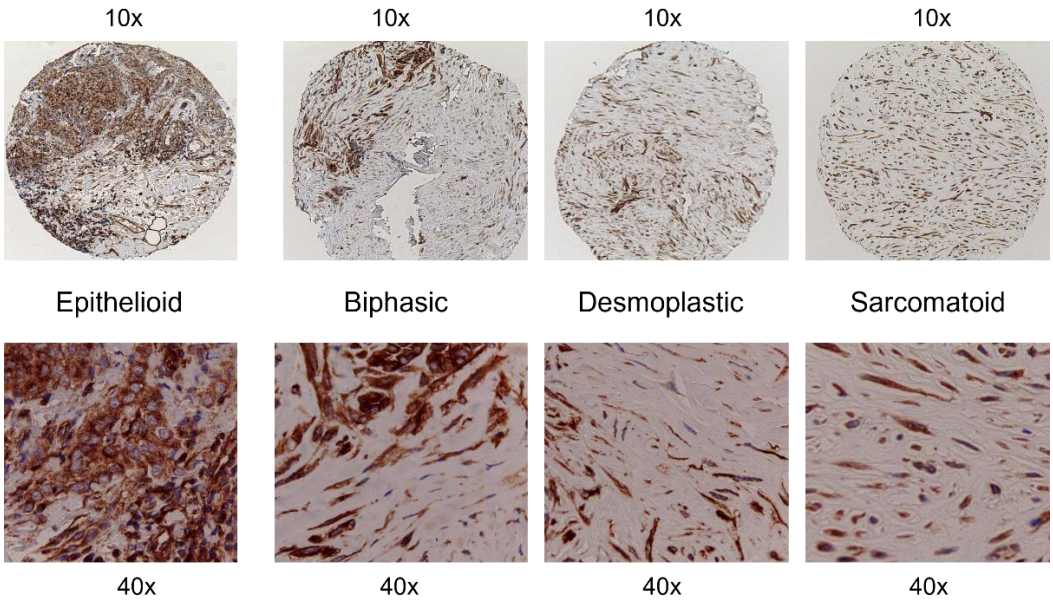

Figure 5b: TMA histopathology at 10x (top) and 40x (bottom) magnification: Example TMA sections for each subtype taken from this dataset, demonstrating the morphological variation present. Epithelioid cells tend to be rounder with a more visible nucleus (counterstained in blue, haematoxylin). Sarcomatoid-type cells are elongated with a spindle appearance, whist biphasic tumours show a combination of the two morphologies.

Final GNC2 staining scores were obtained by multiplying the intensity and proportion scores, giving a score from 0 to 500. Each patient had between four and five sections as functional repeats, located sequentially within the slide. GCN2 staining scores were averaged across replicates for each patient and this value was used for data analysis.

4.3.1: Survival analysis comparing patients with high and low GCN2 scores

If GCN2 score is prognostic in malignant pleural mesothelioma, we would expect to observe a survival difference between patients with high versus low scores. To determine this, patients were ranked by GCN2 score (fig. 5c) and survival analysis was carried out, comparing patients with high (≥300.0, N=54) and low (≤200.0, N=64) GCN2 staining scores.

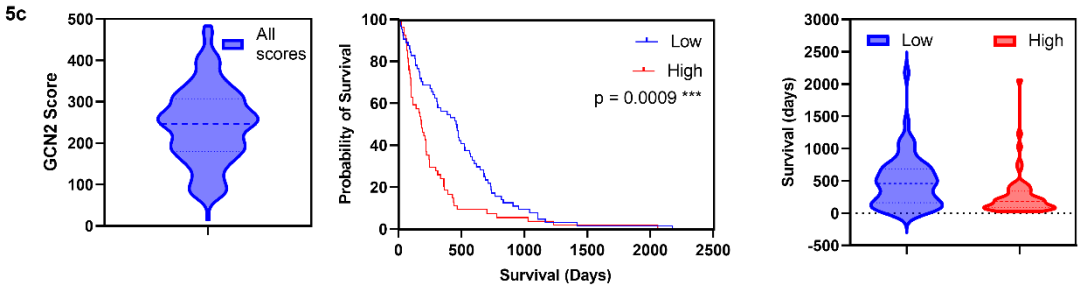

Figure 5c. Distribution of GNC2 scores and survival versus high and low GNC2 score: Violin plot showing the distribution of all GCN2 staining scores for the 194 patients included in the data analysis. KM Survival curves of for high (≥300) and low (≤200) scoring patients showed two distinct tracts with little overlap beyond 100 and 1000 days. LR test comparing the two curves generated a significant p-values (p=0.0009), indicating that the two groups have different survival outcomes and GCN2 score is prognostic. This is further supported by the violin plot of the two group's scores, where the low-scoring group (blue, 461.5 days) has a higher median survival when compared to the high-scoring group (red, 181.5 days). Acronyms: KM = Kaplan-Meier | LR = Log Rank

The low-scoring group has a median survival 2.5-fold that of the high-scoring group (461.5 days and 181.5 days, respectively). The two plots experience very little overlap between 100 and 1000 days, indicating different survival outcomes, which is further supported by the LR test which determined that GCN2 score is prognostic factors, and that high GCN2 score is associated with poorer survival outcomes (hazard ratio, 1.798 [95% CI, 1.221 to 2.648]; p=0.0009) in malignant pleural mesothelioma patients.

4.3.2: Survival analysis comparing patients with high GCN2 scores to all other patients

If the prognostic effect observed in fig. 5c is true, we would expect to observe this trend in the wider cohort. To determine this, a second survival analysis was carried out to compare the high-scoring patient group (≥300.0, N=54) to all other patients (<300, N = 140) in the cohort (fig. 5d).

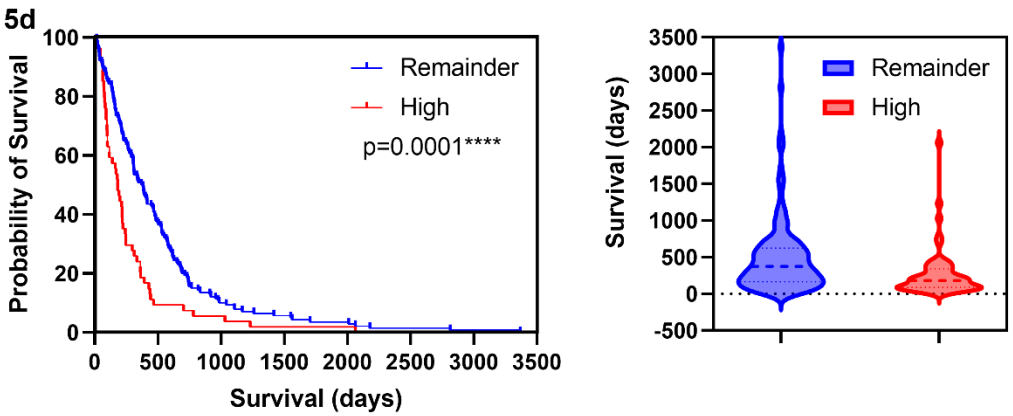

Figure 5d. Distribution of GNC2 scores and survival comparing high-scoring patients to the remainder of the cohort: Survival of high-scoring patients (N=54, score = ≥300) was compared to all other (remainder) patients in the cohort (<300, N = 140) using a KM survival curve and LR statistics. The two curves again show very distinct tracts, and therefore survival trends, with overlap only at the beginning and end of the plot. LR- test comparing the two curves generated a significant p-value (p=0.0001) agreeing with findings in fig. 5c and determining GCN2 score to be prognostic. This is further supported by the violin plot of the two group's scores, where the remainder group (blue, 382.0 days) has a higher median survival when compared to the high-scoring group (red, 181.5 days). Acronyms: KM = Kaplan-Meier | LR = Log Rank

Median survival in the remainder group was 2.1-fold higher than in the high-scoring group (181.5 days versus 382.0 days). The KM curve plotted shows little overlap, and the LR test generated a significant p-value (p=0.0001), finding high GCN2 score again to be prognostic, and an indication of poorer survival outcomes (hazard ratio, 1.815 [95% CI, 1.253 to 2.628]; p=0.0001) even in comparison with the rest of the cohort. Together with fig. 5c, this indicates that GCN2 score is prognostic in malignant pleural mesothelioma patients.

4.3.3: Survival analysis comparing survival in high and low-scoring patients with epithelioid histopathology

Analysis of the relationship between survival and histopathology found this to be a significant prognostic indicator, with sarcomatoid content associated with poorer prognosis. Further analysis was carried out to determine whether the

differential survival observed in high and low-scoring patients is also observed within individual histological subtypes, which could indicate that GCN2's prognostic role is histology-specific. The epithelioid subtype contained 47 low-scoring patients and 31 high-scoring patients.

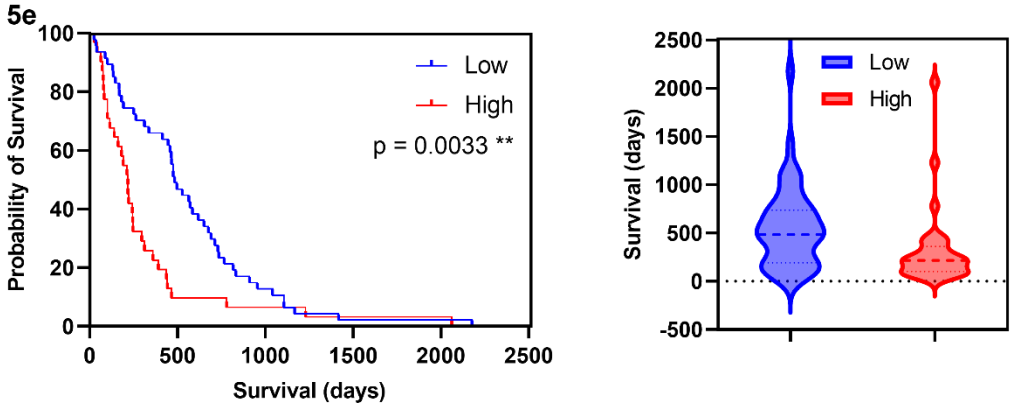

Figure 5e. Survival of high and low-scoring patients with epithelioid histopathology: Epithelioid patients with a high GCN2 score (N=31) and low GCN2 score (N=47) were plotted using a KM survival curve, giving two distinct plots indicating different survival outcomes between the two groups. The LR test comparing the two curves confirmed GCN2 score to be prognostic within the epithelioid histological subgroup (p=0.0033). This is further supported by the violin plots of each group's survival: the low-scoring group has a significantly higher median survival (blue, 484.0 days) than the high-scoring group (red, 217.0 days). Acronyms: KM = Kaplan-Meier | LR = Log Rank

Median survival was 2.2-fold greater in the low-scoring group when compared to the high-scoring group (484.0 and 217.0 days, respectively). KM survival curves showed distinct plots, and therefore survival outcomes, between the two groups, with minimal overlap. The LR-test confirmed this, generating a significant p-value (p=0.0033) and showing that within the epithelioid subgroup, high GCN2 score is significantly prognostic (hazard ratio, 2.203 [95% CI, 1.302 to 3.727]; p=0.0033).

4.3.4: Survival analysis comparing survival in high and low-scoring patients with sarcomatoid histopathology

The previous survival analysis for histopathology determined that sarcomatoid content was also a negative prognostic indicator (fig. 4c). A second analysis was therefore carried out to compare survival between high and low-scoring patients with sarcomatoid histopathology and determine whether GCN2 score is also prognostic within the sarcomatoid subgroup.

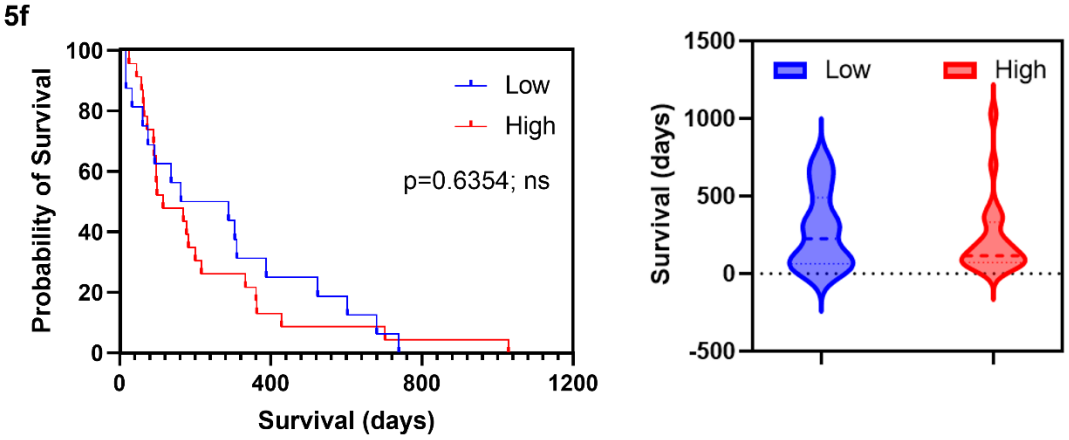

Figure 5f. Survival of high and low-scoring patients with sarcomatoid-containing histopathology: Survival in sarcomatoid patients with high (N=23) and low (N=16) GCN2 scores was assessed by plotting a KM curve and carrying out a LR analysis comparing the two curves. The two plots are less resolved than in fig. 5e, with fewer datapoints in the non-overlapping region. LR test did not find a significant survival difference between the two groups (p=0.6354), indicating that GCN2 score is not prognostic within this subgroup. Violin plots do show different median survival between the high (red, 115.0 days) and low (blue, 225.0 days) groups. Acronyms: KM = Kaplan-Meier | LR = Log Rank

Median survival in the low-scoring sarcomatoid group was 1.95-fold that observed in the high-scoring group (115.0 and 225.0 days, respectively). However, the KM curves plotted were less resolved than in fig. 5e, and LR test comparing survival outcomes between the two groups did not find a significant difference in survival between high and low-scoring patients (fig. 5f) with sarcomatoid-containing histopathology (hazard ratio, 0.5111 [95% CI, 0.270 to 0.9674]; p=0.6354). The violin plot of the two categories indicates that there is far less difference in survival periods for high and low-scoring sarcomatoid patients, in comparison with the epithelioid high versus low analysis (fig. 5e),

or the epithelioid versus sarcomatoid comparison (fig. 4c) which may explain why these two curves do not differ significantly. This result, when taken together with the same analysis for the epithelioid subgroup, could indicate that GCN2 score is prognostic in that histology specifically.

4.3.5. Correlation of GCN2 score and histological subtype

Previous work, and the findings presented here, have found histology to be prognostic in MPM. This previously identified correlation between histological differentiation and prognosis could potentially be responsible for the GCN2 score prognostic effects in this cohort. To determine whether GCN2 score correlated to histological differentiation in MPM, box-and whiskers plots (fig. 5g) for the GCN2 scores of histopathology were plotted. Differences in variance between the three groups were determined using one-way ANOVA, with a Bonferroni post-hoc correction to correct for family-wise error that can arise from multiple comparisons[145]. Significance was determined by a p-value cut-off of p=0.05.

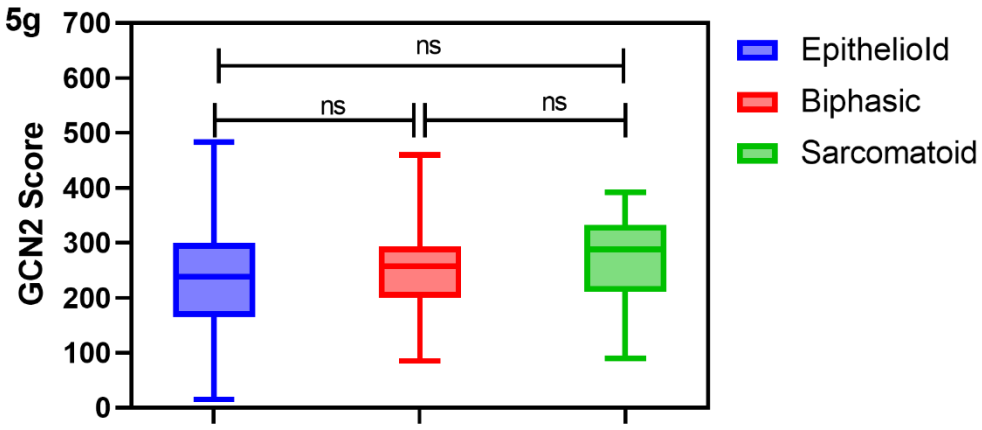

Figure 5g. Correlation of GCN2 score to histological subtype: Box-and-whisker plots were plotted for each subtype's GCN2 scores. Sarcomatoid = sarcomatoid and desmoplastic. One-way ANOVA with Bonferroni post-hoc test used to determine whether the differences between pairs was statistically significant ($p<0.05$). No significant difference was generated for any of the three comparisons.

No significant relationship between GCN2 score and histopathology was found, with all three tests generating a non-significant p-value. This indicates that the prognostic results generated for GCN2 score are independent of histopathology. This also further supports a potential histology-specific relevancy for GCN2 score's prognostic effects, specifically for the epithelioid subgroup, demonstrating that the difference observed is not a result of a shift in score distribution for that subgroup.

Section 4.4. GCN2 score as a prognostic predictor: ROC (receiver operating characteristic) curves

An ROC curve is a classification model that plots the relationship between a binary outcome variable (i.e. whether death has occurred at a certain timepoint or not), and a continuous predictor variable. It determines the ability of the predictor variable to correctly discriminate whether an event has actually occurred at any point along the curve, and this therefore indicates whether there is a predictive relationship between the two variables. The true positive rate, or specificity (i.e., the rate at which the continuous variable correctly predicts the outcome, x-axis) is plotted against the false positive rate, or sensitivity (y-axis)[138]. If the relationship between the two is truly predictive, the true positive rate will exceed the false positive rate. The area under curve (AUC), also referred to as the C-statistic[139], is the output from this analysis, and indicates whether the two variables have a predictive relationship. A perfect, correctly predictive relationship generates an AUC value of 1.0 (blue line, fig. 3b, methods), wherein the entire plot lies under the curve. Conversely, a model that indicates a non-predictive relationship no different from chance would plot a linear line with an AUC value of 0.5 (green line, fig. 3b). Finally, an incorrectly predictive model (purple line, fig. 3b), where the false positive rate exceeds the true positive rate, would generate a plot with an AUC <0.5[138]. Statistical analysis and figures were generated in RStudio.

In the context of medical research, ROC curves are routinely used to determine how effective a biomarker is at discriminating between two binary

options, such as disease onset[146], and therefore its prognostic power. Previous work specifically in malignant mesothelioma used a threshold AUC value of 0.65 (red line, fig. 3b) to determine a biomarker's prognostic significance[133,140], and this will be used in this work to determine whether GCN2 levels are prognostic in malignant pleural mesothelioma.

To test individual variables for prognostic significance, ROC curves were generated using the pROC package in R-studio[136]. Survival was treated as the binary outcome in each comparison, with each variable tested on its ability to predict one-year survival outcomes. To facilitate this, the continuous survival classification was converted to a binary good (<365.0 days) or bad (>365.0 days) classification.

Each of the variables tested were either already continuous, such as for GCN2 score, or were converted into a pseudo-continuous variable, described in more detail for each analysis. ROC plots, a C-statistic and 95% confidence interval were generated for each model, summarised in table 2, fig. 6g, and were used to determine whether the variables were predictive for survival.

4.4.1. ROC curve: GCN2 score

Previous work by Dalton et al. in 2013 found CHOP, a transcription factor strongly linked to the ISR and the GCN2-ATF4 pathway, to be prognostic and also capable of predicting MPM patient outcomes, making it a more powerful biomarker. As GCN2 has already shown prognostic relevance in this work, we wanted to determine whether it was also predictive, and used an ROC curve (fig. 6a) comparing the binary one-year survival and continuous GCN2 score to do so.

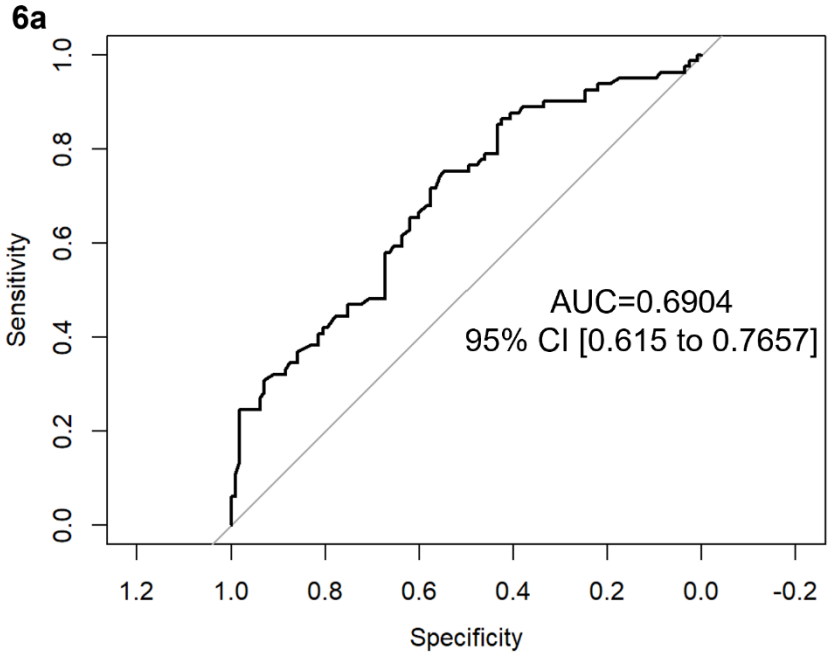

Figure 6a. ROC curve plotting survival against GCN2 score: ROC survival analysis was carried out for 194 patients, comparing survival outcome at the one-year mark (</> one year) to GCN2 score (1 to 500). The AUC is also referred to as the C-statistic: based on previous work, a value >0.65 indicates that GCN2 score is independently predictive for patient survival. AUC/C-statistic=0.6904; 95% CI [0.615 to 0.7657], GCN2 score is therefore predictive as well as prognostic. Acronyms: ROC: receiver operating characteristic | AUC: area under curve.

This generated the plot in fig. 6a with a C-statistic of 0.6904 [95% CI, 0.615 to 0.7657]. Based on thresholds used in previous work (0.65), this value indicates a correctively predictive relationship between the two variables and that GCN2 score is able to discriminate correctly for survival outcome: GCN2 score is therefore a predictor of survival. Taken in combination with the box-and-whiskers plot in fig. 6g, which demonstrates that GCN2 score and histopathology have no significant correlation, GCN2 can therefore be considered a potential biomarker that is *independently* predictive.

4.4.2. ROC curve: histological subtype

Histology was demonstrated to be prognostic, both by this work and in the literature. The next stage was to determine whether histological subtype was capable of predicting one-year survival outcomes, a quality that had not yet

been determined in past work[100]. As histological subtype is a categorical classification and not a continuous variable, the dataset had to be converted prior to ROC analysis. The three histologies were assigned a number (epithelioid=3; biphasic=2; sarcomatoid=1) to produce a pseudo-continuous dataset. The two desmoplastic patients were included in the sarcomatoid group as for the Kaplan-Meier plots/Log-rank test.

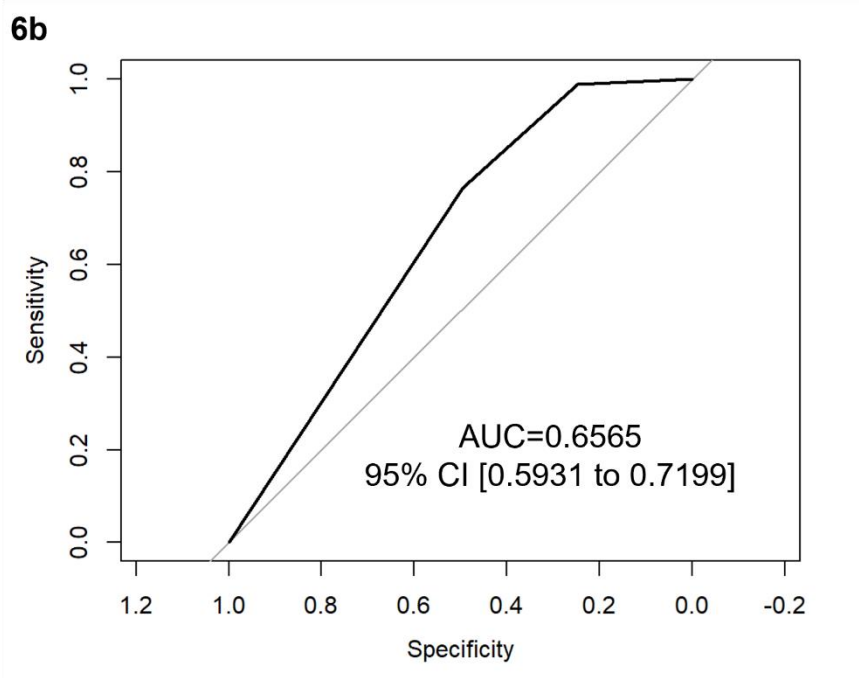

Figure 6b. ROC curve plotting survival against histological subtype. 194 patients were included in this analysis: epithelioid (119), biphasic (46), and sarcomatoid (29). Histological subtype was converted to a pseudo-continuous classification by assigning each histology a number, either 1 (epithelioid), 2 (biphasic), or 3 (sarcomatoid + desmoplastic) in order of increasing sarcomatoid content. AUC/C-statistic=0.6565; 95% CI [0.5931 to 0.7199]. Acronyms: ROC: receiver operating characteristic | AUC: area under curve.

The ROC plotted (fig. 6b) for histological subtype against one-year survival generated a C-statistic of 0.6565 [95% CI, 0.5931 to 0.7199]. This value lies just above the cut-off and suggests a predictive relationship between survival and histology, indicating that histology is capable of correctly predicting the binary survival outcome in the majority of cases.

4.4.3: ROC curve: node score

Node score was not found to be prognostic (fig.4e) from the univariate LR survival analysis. We therefore did not expect to see a predictive effect for this characteristic on one-year survival outcomes. However, unlike the binary LR test, the ROC analysis included all four N scores (0-3) as separate, continuous variables, which could alter the results generated. Node score was available for 61 of 194 patients (table 1). Since values between 0 and 3 were already assigned in the clinical context, no data conversion was required to facilitate analysis.

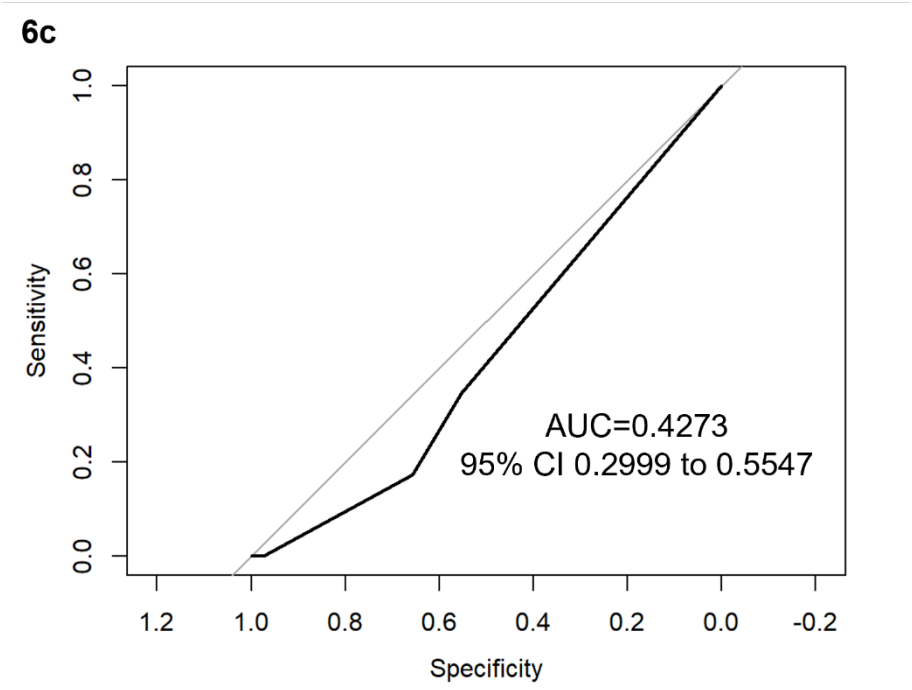

Figure 6c. ROC curve plotting survival against node score. Node scores 61 patients and ranged from 0 to 3 (see table 1 for distribution). AUC/C-statistic=0.4273; 95% CI [0.2999 to 0.5547]. Acronyms: ROC: receiver operating characteristic | AUC: area under curve.

An ROC curve of one-year survival against node score plotted from these data (fig. 6c) produced a C-statistic of 0.4273 [95% CI, 0.2999 to 0.5547]. The majority of the plot lies above the line, which indicates that node score is incorrectly predictive for one-year survival outcome, agreeing with the previous univariate analysis findings.

4.4.4: ROC curve: tumour score

LR survival analysis did not find T score to be prognostic (fig. 4d): we therefore did not expect to generate a positive result (indicating a predictive relationship) under this more stringent survival analysis. Tumour scores (0 and 4) were assigned in the clinical setting prior to this work for 63 of the 194 patients (table 1) and did not require conversion prior to analysis. For one patient, a score of 1b was previously assigned: this was converted to 1 for this analysis.

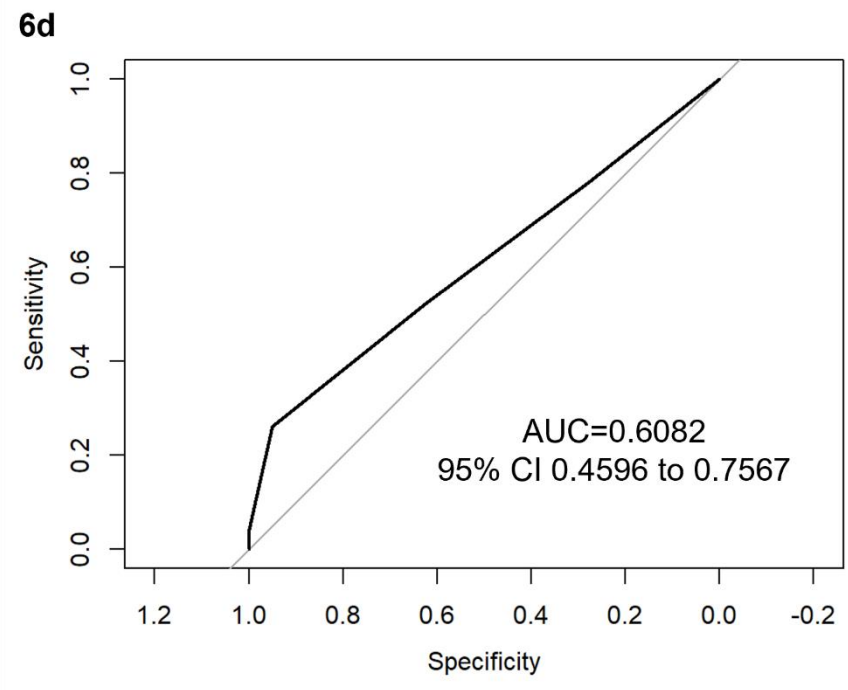

Figure 6d. ROC curve plotting survival against tumour score. Tumour scores were available for 63 patients, with values between 0 and 4 (see table 1 for distribution). AUC/C-statistic=0.6082; 95% CI [0.4596 to 0.7567]. Acronyms: ROC: receiver operating characteristic | AUC: area under curve.

The ROC curve (fig. 6d) plotted had a correctively predictive C-statistic of 0.6082 [95% CI, 0.4596 to 0.7567], indicating that a positively predictive relationship between tumour score and one-year survival is present, although a weak one. However, this value does lie below the cut-off value of 0.65. Taken with the negative prognostic result generated from the LR test, this result may not be accurate.

4.4.5: ROC curve: age

Age did not undergo a LR analysis, however as a continuous variable it is well-suited to the ROC survival analysis against the binary one-year outcome. It would be reasonable to assume that likelihood of a death event increases with age, and therefore age may be predictive. A one-year survival analysis for patient age at diagnosis included all 194 patients. Ages ranged from 47 to 92 years, with a median age of 69 years.

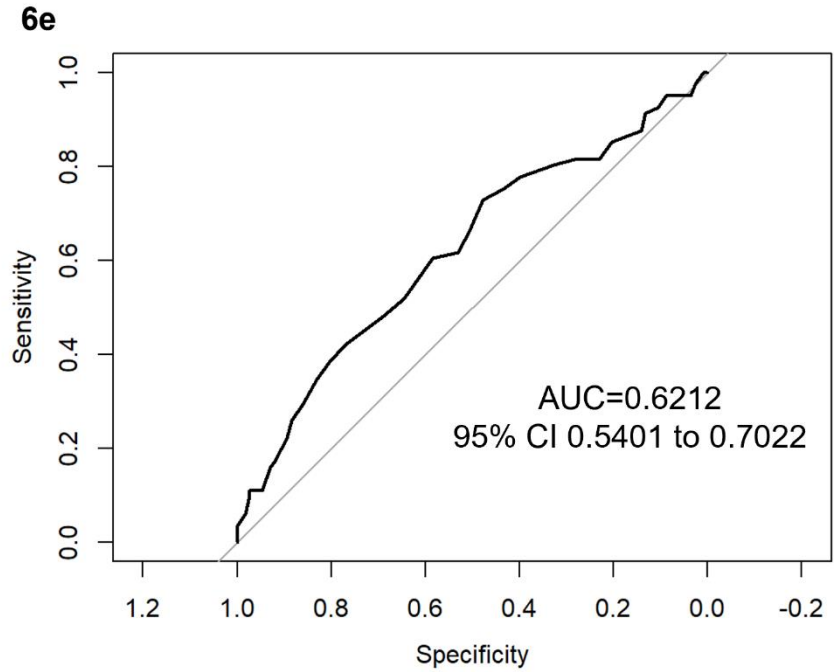

Figure 6e. ROC curve plotting survival against age at diagnosis. 194 patients were included in this analysis, with ages from 47 to 92 years at diagnosis, and a median age on 69. AUC/C-statistic=0.6212; 95% CI [0.5401 to 0.7022]. Acronyms: ROC: receiver operating characteristic | AUC: area under curve.

Age was found to be weakly predictive of one-year survival outcome (fig. 6e), with a C-statistic of 0.6212 [95% CI, 0.5401 to 0.7022], however, given the obvious link between age and mortality, this could be a source of bias in the analysis.

4.4.6: ROC curve: controls

Two control datasets, where the predictive relationship with survival was either (1) completely random, or (2) positively predictive (fig. 6f), were used to validate the results generated using the pROC package.

For the first data set ('random numbers') a string of 194 random numbers between 1 and 1000 was generated. This dataset should have no predictive power towards the binary survival outcome, which was confirmed by the C-statistic of 0.5577 [95% CI, 0.4768 to 0.6386], indicating that the association is governed by chance and that the pROC package was operating correctly.

Patient number (1 to 194) was assigned after patients had been ordered from low to high GCN2 score, therefore, any ROC plot generated using these data should have a correctly predictive relationship for one-year survival comparable to that for GCN2 score (fig. 6a). This was found to be the case, with the plot generating a C-statistic almost identical to that in fig. 6a of 0.6907 [95% CI, 0.6154 to 0.776].

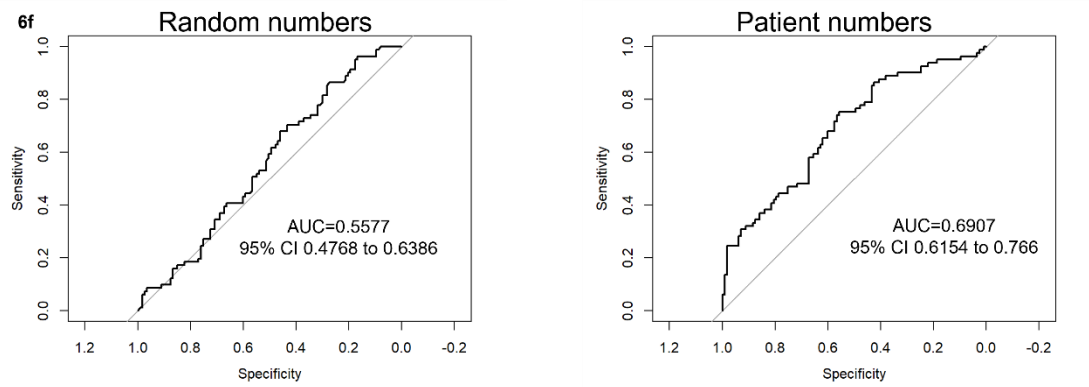

Figure 6f.ROC curves plotting survival against two control datasets. A set of 194 random numbers between 1 and 1000 were generated and this was plotted against survival (first graph, 'random numbers') to act as a negative control – AUC=0.5577; 95% [0.4768 to 0.6386]. Numbers from 1 to 194 were assigned *after* patients had been ranked by GCN2 intensity score to act as a positive control. This ordered data should mimic any correlation to survival observed for the GCN2 score data and this was the case – AUC=0.6907; 95% CI [0.6154 to 0.766]. Acronyms: ROC: receiver operating characteristic | AUC: area under curve.

The C-statistics generated from each ROC curve with 95% confidence interval plotted demonstrate that GCN2 score is the only factor with a correctively predictive relationship to one-year survival above the 0.65 cut-off value (fig. 6g, table 2).

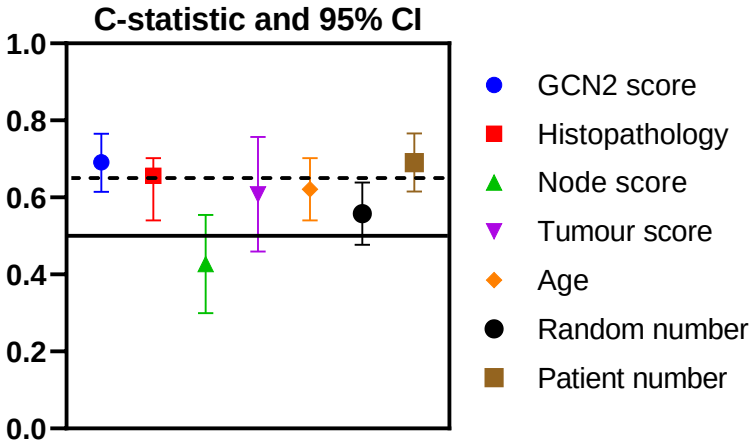

Figure 6g: Summary of C-statistic and 95% CI values generated for each ROC graph, including the two controls. The solid black line demarks the 0.5 'chance' barrier; the dashed line indicates the 0.65 threshold from previous work in MPM.

Table 2: Summary of ROC curve C-statistics (AUC) and confidence intervals

Model	Sample size (N)	C-statistic	95% CI
GCN2 score	194	0.6904	0.615 to 0.7657
Histopathology	194	0.6565	0.5401 to 0.7022
Node score	61	0.4273	0.2999 to 0.5547
Tumour score	63	0.6082	0.4596 to 0.7567
Age	194	0.6212	0.5401 to 0.7022
Random number (control)	194	0.5577	0.4768 to 0.6386
Patient number (control)	194	0.6907	0.6154 to 0.766

Chapter five: Discussion

5.1 Summary

The central aim of this work was to determine whether GCN2 levels correlated with patient survival and therefore its potential as a novel prognostic biomarker and therapeutic target in malignant pleural mesothelioma. To achieve this, tissue microarrays containing malignant pleural mesothelioma tumour sections biopsied from 204 patients were immunohistochemically stained for GCN2 and assigned scores related to GCN2 levels. These scores were then statistically analysed against patient survival data to determine (1) whether GCN2 score was related to prognosis, and (2) whether GCN2 score was a novel predictive biomarker in malignant pleural mesothelioma. The key findings in relation to these aims were that firstly, GCN2 levels are prognostically significant, and secondly, that GCN2 is capable of independently predicting one-year survival outcomes in MPM patients and is also a predictive biomarker. In addition to these findings, this work also identified histological subtype as a potential predictive biomarker in addition to current clinical understanding of its prognostic implications.

5.2 GCN2 results

Kaplan-Meier survival curves and log-rank analysis comparing high and low-scoring patient survival demonstrate that there is a difference in survival between these two groups (p=0.0009) and that high-scoring patients have a 1.8-times greater likelihood of death when compared with low-scoring patients (fig. 5c. Hazard ratio, 1.798 [95% CI, 1.221 to 2.648]). This finding was further validated by a comparison between the high-scoring group and the remainder of the cohort. The log-rank test to compare survival between the two groups generated similar statistics to the high vs. low analysis (hazard ratio, 1.815 [95% CI, 1.253 to 2628]; p=0.0001) with a similar hazard ratio when comparing the high group to the rest of the cohort. GCN2 is therefore prognostically significant not only when comparing the high and low extremes. This result

demonstrates that GCN2 is prognostically significant for the wider MPM cohort.

Patient survival was shown to differ by histological subtype (fig. 4b), specifically by sarcomatoid content (fig. 4c), discussed later in this chapter. A further analysis was carried out to determine whether survival curves differed significantly for high and low GCN2-scoring patients with epithelioid or sarcomatoid histopathology. This analysis demonstrated a significant difference within the epithelioid group (hazard ratio, 2.203 [95% CI, 1.302 to 3.727]; p=0.0033), but not within the sarcomatoid subgroup (hazard ratio, 0.5111 [95% CI, 0.270 to 0.9674]; p=0.6354). There are several explanations for this result. Primarily, the epithelioid subgroup is significantly larger so should more easily mirror the trends observed in the wider group: in a similar vein, the number of sarcomatoid patients falling into the high (N=23) and low (N=16) categories is low compared with the epithelioid groups (high=31, low=47). Additionally, the sarcomatoid group demonstrates a median survival that is 51.2% of that in the epithelioid group (206.0 days versus 402.0 days), therefore this group may lack the variance required to demonstrate a difference between groups. To determine whether GCN2 score correlated with histological subtype, which would suggest that the prognostic relevance of GCN2 score is dependent on histology, a one-way ANOVA to compare the three histological subtypes was carried out (fig. 5g). This analysis determined that there was no correlation, meaning that the differing prognoses observed between the high- and low-GCN2-scoring epithelioid groups is likely mirroring the wider trend observed in the whole group analysis and that GCN2's prognostic potential is independent of histology.

ROC curves were then used to determine the predictive potential of GCN2 score for one-year survival outcomes: the C-statistic of 0.6904 [95% CI, 0.615 to 0.7657] reveals that, for a random patient, GCN2 score can correctly place their survival outcome in 69% of cases. GCN2 score is not only prognostic and independent of histology, but also a novel predictive biomarker in MPM.

These findings make a major contribution to our understanding of GCN2 in cancer, as well as opening a new area for targeted therapy development in

malignant mesothelioma. Although this work does not demonstrate GCN2 activity in MPM, identifying it as a biomarker is an important first step, especially as there are currently no routine prognostic and predictive biomarkers currently available[100]. Given the robust evidence in other cancers of GCN2's role in cancer pathogenesis, this finding lays the foundation for further work, which will be discussed later in this chapter.

Previous work surrounding the role of GCN2 in cancer has shown elevated levels of both the active (phosphorylated) and inactive forms across multiple cancers[12,28,29]. However, only one other work has related GCN2 levels in cancer to patient prognosis. Ge *et al*. demonstrated in 2018 that GCN2 levels in human papillary renal cell carcinoma correlated to worse patient outcomes[30], and suggested that this could be used as a biomarker to tailor treatment strategies. Adjacent to this prognostic relationship, GCN2 reliance has been demonstrated to coincide with more aggressive cancers that require earlier and more prolonged therapeutic interventions[31]. If such reliance is also present in MPM, which the prognostic relationship shown here suggests, this could prove an excellent new option for targeted therapy development.

This is not the first work to implicate the ISR in malignant pleural mesothelioma, the first being work by Dalton *et al*. in 2013[133], which found that levels of ER-stress-related marker CHOP correlate to MPM patient survival. CHOP is a transcription factor that is upregulated by PERK in response to ER stress but is also associated with the GCN2-mediated amino acid response. Understanding what stress response activation looks like in MPM is important as it informs how we target this cancer therapeutically in the future. Of the four ISR kinases, GCN2 and PERK have the most similarity in the stressors they respond to. There is robust evidence that a cooperative relationship exists between the two kinases both in healthy and in cancerous cells. In MEF cells experiencing glucose deprivation, PERK and GCN2 both phosphorylate eIF2α, indicating functional overlap between the two[12]. In human colon cancer cells, combined activation of PERK and GCN2 as a result of MYC oncogenic activity promotes survival by ATF4-mediated transcription of MYC-target genes to relieve proteotoxic stress[147], actively contributing to MYC-driven

cancer, but also demonstrating the potential effectiveness combinatorial therapy targeting both kinases could potentially have.

This cooperativity also contributes to the development of drug resistance. In breast cancer cells treated with the chemotherapeutic paclitaxel, the combined action of GCN2 and PERK via an EIF2AK3/EIF2AK4-eIF2α-ATF4 pathway promotes drug resistance by upregulating several antioxidant genes (HMOX1, SLC7A11, and SHMT2)[148], therefore supressing oxidative stress to ensure survival. Further work in parental MCF-7 breast cancer cell lines by Alasiri *et al*. in 2020[149] identified a reciprocal relationship between the two kinases that aided drug resistance and could be targeted to improve response to paclitaxel and epirubicin. Both kinases were shown to supress the antiproliferative actions of transcription factor FOXO3 (Forkhead box O3) via the JNK/AKT pathway. Silencing/inhibition of GCN2 and PERK respectively, triggers a reciprocal induction of the accompanying kinase to maintain FOXO3 suppression, which Alasiri *et al*. suggest explains why single-agent PERK inhibitors have limited effectiveness[149].

Such crosstalk is only possible due to the overlapping functionalities of these two kinases, and it is crucial to better understand the nuanced differences in how cancer cells hijack the integrated stress response to promote survival or gain drug resistance. This will enable physicians to deploy current therapeutics appropriately and effectively target new ones. For malignant pleural mesothelioma, identifying GCN2 as relevant to tumour survival should inform future drug discovery, but could also offer new perspectives on one of the central impairments to MPM treatment, the low response rate to both single agent (16.7%) and combined chemotherapy (40%). Cisplatin is prescribed as a combination therapy with pemetrexed as the front-line chemotherapeutic treatment in MPM. However, GCN2 has already been shown to facilitate cisplatin resistance in gastric cancer cells by mitigating drug-induced oxidative stress[48]. Although cisplatin is the most effective therapeutic that we currently have against MPM tumours, reliance on GCN2 could explain the low response rate and simultaneously identify a way to sensitise MPM tumours to chemotherapy.

The correlation between high GCN2 levels and worse patient prognoses suggests that GCN2 levels are associated with more aggressive cancers and identifies a potential point of reliance in MPM tumours, whilst simultaneously identifying a weakness that could be exploited therapeutically. This may explain why ADI-PEG20, an arginine deiminase that targets GCN2 activation, is so effective. This compound targets MPM metabolically by artificially triggering arginine starvation[129] to activate GCN2 and induce CHOP-mediated apoptosis[130]. If MPM tumours are already in a state of GCN2 reliance to maintain survival, the additional amino acid stress brought about by this treatment could push GCN2 activity from pro-survival to apoptotic. We already know that prolonged ISR activation is capable of inducing apoptosis[1], and this may explain why activation is an effective mechanism to induce cancer cell apoptosis in this context.

5.3 Other results

In addition to these key findings, this work also evaluated the relationship between other clinical parameters and patient survival. It found histopathology to be prognostically significant (fig. 4b, $p<0.0001$), and specifically, that sarcomatoid content correlates with poorer survival (fig. 4c, $p<0.0001$), in line with previous findings[100]. When taking GCN2 score into account for each histological subtype, it was shown to be prognostically significant within the epithelioid subgroup (fig. 5e, $p=0.0033$), but not within the sarcomatoid subgroup (fig. 5f, $p=0.6354$). This is likely due to the fact that the sarcomatoid group is more lethal (median survival=206.0 days, versus 402.0 days, epithelioid) but has lower sample variation in survival scores (violin plots, fig. 5e and fig. 5f) and has a smaller sample size (N=75) compared with the epithelioid (N=119) group.

Distant metastatic involvement (the ‘M’ classifier of TNM) was also prognostically significant, and median survival time was 45% greater in patients without metastasis (‘M0’, 304.0 days/10.0 months) compared to those with (‘M1’, 199.0 days/6.5 months). This finding contradicts previous work in T4 tumours comparing survival in M0 versus M1 patients, which did not find a

significant difference in survival: M0 median survival was 10.7 months (95% CI, 5.9 months - 15.6 months), M1 median survival was 13.3 months (95% CI, 2 months – 24.6 months)[144]. Most strikingly, the M1 group in our cohort has a significantly lower median survival than observed in the literature. The literature cohort was 622% larger than ours (367 versus 59), and therefore this analysis has far less power.

Other demographic data, namely gender, tumour score, and node score, did not show significant differences in survival between groups and were not prognostically significant.

Finally, ROC curves for demographic data found histopathology to be a predictive factor (C-statistic=0.6565 [95% CI, 0.5931 to 0.7199]), and tumour score (C-statistic=0.6082; 95%, CI, 0.4596 to 0.7567) and age (C-statistic=0.6212; 95% CI, 0.5401 to 0.7022) to be weakly predictive factors.

Histopathology was found to be prognostic and also appears to be predictive of one-year survival outcomes, although the discriminating power is not as strong as for GCN2 score. Current clinical practice utilises histopathology alongside TNM staging as the main assessments of prognosis[150], with epithelioid histology having better prognosis than either biphasic or sarcomatoid and being more likely to receive resective care[100]. The predictive power of histopathology is not as established, so the results presented here are another novel contribution to our understanding of MPM disease progression.

Tumour score, by its design, should correlate negatively with prognosis, and this finding agrees with the International Association for the Study of Lung Cancers (IASLC) most recent parameters for TNM staging, with are also used to decide surgery viability[142]. However, the fact that tumour score is predictive but not prognostic suggests that there is an issue with the analysis. The ROC curve of age versus survival at the one-year mark demonstrated a weak predictive association. However, as this is a survival analysis, this finding introduces an element of bias into the result. Histological subtype and node score were not found to be predictive factors for one-year survival outcomes.

5.4. Limitations and further work

This work is not without limitations, despite the promise and contribution it makes as an initial work linking GCN2 to MPM tumorigenesis. One of the obvious issues with this work is the lack of a validation cohort to complement the discovery cohort in which this initial finding was carried out. The study design itself is robust in that it uses a cohort that is representative of the wider MPM population, utilizes a high throughput screening technique to obtain a sizable dataset, and the population size sampled is large enough to give sufficient power to the analyses answering the main research questions posed. However, to be fully confident in the results found here and their reproducibility, a second 'validation' cohort should be used to confirm the reproducibility of the findings presented here. MPM is a rare cancer subtype and the cohort used here, of 204 patients, is a significant one. Additionally, the cost of TMA's is significant and a potential barrier. An alternative to obtaining a new cohort would be to utilise a resampling method such as bootstrapping to generate successive, smaller, cohorts from within the original cohort, allowing the original findings to be repeatedly re-evaluated[151].

In the analysis portion of this work, patients who were still alive at the time of analysis were excluded from the survival analysis, totalling four patients (table 1), as the true survival time was unknown. Typically, these patients would be included in the survival analysis, and this therefore presents a potential limitation of this study. However, because of the small number of affected patients this is unlikely to have majorly impacted the key findings of this work. In the future, including these patients would increase the weight of this analysis' findings.

In the ROC analysis, patients were ordered from low to high GCN2 score, which demonstrated a predictive relationship with one-year survival outcomes. However, this ordering may also reveal a dose-response relationship with regards to GCN2 patient levels, and this deserves future work.

Another limitation of this work is that only the inactive form of GCN2 was stained for. Whilst this gives us a potential new biomarker, it does not confirm whether GCN2 activity is responsible for the poorer prognosis observed in the

high-scoring patient group. To confirm this, further work should be carried out to investigate levels of active GCN2 and the phosphorylated substrate eIF2α. Initially, this work was to include two further TMA sets to allow for this, so further work should initially utilise this method, However, beyond this, there are experiments that would further validate the initial findings presented here. One such experiment would be a CRISPR-Cas9 competition assay in either MPM cell lines or in organoid models, both of which are available from the Mesobank biobank from which the TMA's used in this work were sourced. Organoids have the added benefit of being a 3D system that is arguably more representative of the heterogeneity and architecture of a tumour environment. The Mesobank currently has 21 fully sequenced cell lines with different histopathologies, which would allow any histological variations in GCN2 activity to be assessed.

A CRISPR-Cas9 competition assay (fig. 7) allows dependency on a certain gene to be verified by silencing the gene of interest with a GFP-expressing guide RNA (gRNA) targeting GCN2[152]. If GCN2 contributes to mesothelioma fitness, then GFP-expressing cells would be expected to be outcompeted over several passages. At each passage, flow cytometry would be used to determine the fraction of fluorescent cells for up to five passages, determining the impact on fitness targeting GCN2 has: if the proportion of GFP cells decreases over time we can infer that GCN2 is contributing to the fitness of these MPM cells. Subjecting these cell lines to different stressors could also inform on how GCN2 is promoting fitness.

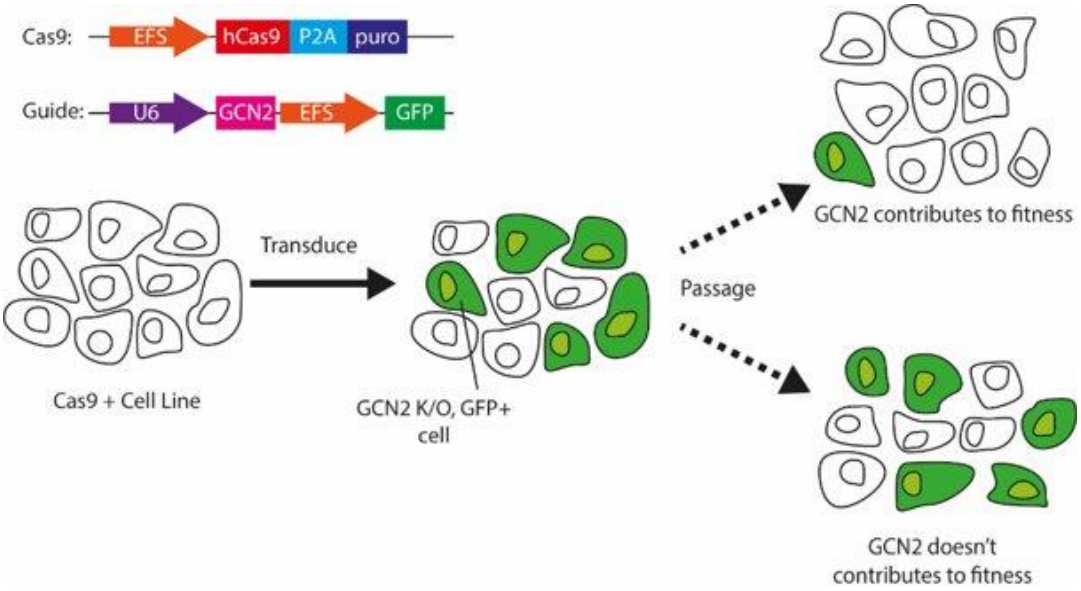

Figure 7. CRISPR-Cas9 competition assay to determine GCN2 dependency in primary mesothelioma cell lines: fluorescent gRNA targeting GCN2 will be used with flow cytometry to determine whether GCN2 KO negatively impacts fitness: if this is the case, non-fluorescent cells would be expected to outcompete fluorescent cells.

Obtaining MPM cell lines or organoids would facilitate single-cell multiomics experiments, which may provide a better understanding of the contribution of GCN2 to MPM fitness. Combined transcriptomic and proteomic profiling would elucidate both changes in the ISR and in the wider MPM cellular context and allow comparison against non-cancerous controls and different stress conditions. The data generated would inform not only on how GCN2 levels and activity respond in these varying conditions, but also provide information on the downstream transcriptional changes mediated by ATF4 to inform explicitly on how GCN2 is benefiting MPM survival, and how this varies between cell lines. Additionally, the potential cross-talk between GCN2 and PERK could be further explored, as understanding if and how this happens is highly important if we are to effectively target the ISR in MPM

With this improved understanding of GCN2's role, and in light of recent work targeting GCN2 with both activating and inhibiting compounds, the next step would be to investigate the effects these different compounds have on specific MPM cell lines using cell or organoid *in vivo* assays. Up- or down-regulating GCN2 may be beneficial in different cell types or stress paradigms, and

combining this with multiomics could also ascertain the mechanisms of these compounds and in what cellular and stress contexts they are most effective.

GCN2 inhibition has been shown to sensitise ALL cancer cells to ASNase treatment, and one of the central issues in MPM chemotherapeutic treatment is the low response rate to even the most effective treatments. It would therefore be of interest to determine whether direct inhibition of GCN2, in a cellular context, has the same sensitising relationship, especially as cisplatin is known to operate by increasing reactive oxygen species, a stress that GCN2 is shown to ameliorate via xCT (SLC7A11) expression. Additionally, although the mechanism by which ADI-PEG20 activates GCN2 to induce CHOP-mediated apoptosis has been demonstrated in bladder cancer cells[130], it would be useful to determine whether its efficacy is the same across cell lines and to confirm whether apoptosis is CHOP-mediated.

GCN2 is still a relatively understudied protein in cancer biology, however its mechanistic role and its therapeutic potential is rapidly becoming more understood. This work hopes to make a contribution to this field that will facilitate more extensive work in the future, and ultimately improve the treatment landscape for a cancer that is both deadly and devastating.

Appendix: Comparison of GCN2 scores for slide one

Interval Diagnosis to Death	SCORE MN	SCORE NH	SCORE LTG	Ratio, LTG vs MN	Ratio, LTG vs NH
739	76.5	80	85	1.111111111	1.0625
680	95	70.25	91.25	0.960526316	1.298932384
136	110	120	123.75	1.125	1.03125
75	135	125	143.75	1.064814815	1.15
288	140	177	150	1.071428571	0.847457627
93	180	177	177	0.983333333	1
388	200	198	180	0.9	0.909090909
162	164	175	182	1.109756098	1.04
603	175	145	188.75	1.078571429	1.301724138
17	230	170	192.5	0.836956522	1.132352941
310	185	156	193.75	1.047297297	1.241987179
616	230	193	203.33	0.884043478	1.053523316
62	250	182	208.75	0.835	1.146978022
228	240	218.4	210	0.875	0.961538462
340	200	265	217.5	1.0875	0.820754717
370	290	240	225	0.775862069	0.9375
409	195	270	230	1.179487179	0.851851852
56	250	240	238	0.952	0.991666667
391	220	280	238	1.081818182	0.85
111	300	280	243.75	0.8125	0.870535714
595	250	190	244	0.976	1.284210526
212	240	280	250	1.041666667	0.892857143
627	290	280	255	0.879310345	0.910714286
34	280	250	259	0.925	1.036
481	260	315	260	1	0.825396825
309	280	255	260	0.928571429	1.019607843
1704	275	283	262.5	0.954545455	0.927561837
37	230	280	265	1.152173913	0.946428571
206	325	250	266.25	0.819230769	1.065
290	266.67	250	266.67	1	1.06668
382	340	330	268	0.788235294	0.812121212
87	310	232	268.75	0.866935484	1.158405172
303	315	311	278	0.882539683	0.893890675
385	250	288	279	1.116	0.96875
416	350	230	292	0.834285714	1.269565217
347	340	295	297	0.873529412	1.006779661
333	360	290	301.67	0.837972222	1.040241379
1029	310	372	308	0.993548387	0.827956989
428	290	320	330	1.137931034	1.03125
169	335	360	332.5	0.992537313	0.923611111
702	380	411	340	0.894736842	0.827250608
200	335	399	380	1.134328358	0.952380952

	363	462	300	385	0.833333333	1.283333333
	99	476	351	390	0.819327731	1.111111111
	63	430	483	403.33	0.937976744	0.83505176
	25	460	473.67	460	1	0.971140245
-						
	276	192.0	194.0	200	1.041666667	1.030927835
	361	371.0	378.0	350	0.943396226	0.925925926
	564	10.0	10.0	15	1.5	1.5
	911	67.0	80.0	67.5	1.007462687	0.84375
	475	60.0	60.0	70	1.166666667	1.166666667
	730	72.0	72.0	75	1.041666667	1.041666667
	572	70.0	80.0	76.25	1.089285714	0.953125
	312	90.0	70.0	78.5	0.872222222	1.121428571
	475	98.0	76.8	80	0.816326531	1.041666667
	466	102.5	92.0	80	0.780487805	0.869565217
	585	95.1	68.3	81.25	0.854363828	1.19047619
	1106	116.1	91.8	90	0.775193798	0.980392157
	497	84.6	107.4	95	1.123595506	0.884955752
	414	96.2	116.4	101.25	1.052631579	0.869565217
	1106	118.7	90.3	105	0.884955752	1.162790698
	817	104.3	106.4	107.5	1.030927835	1.01010101
	955	103.9	83.8	111.67	1.075268817	1.333333333
Alive		123.8	84.4	112.5	0.909090909	1.333333333
	1417	128.1	112.8	117.5	0.917431193	1.041666667
	1041	111.2	117.1	118.33	1.063829787	1.01010101
	736	132.0	126.0	120	0.909090909	0.952380952
	263	115.0	105.0	125	1.086956522	1.19047619
	169	179.2	130.2	140	0.78125	1.075268817
	691	131.6	147.7	146.25	1.111111111	0.99009901
	484	136.9	122.0	148.75	1.086956522	1.219512195
	619	177.0	135.0	150	0.847457627	1.111111111
	458	169.3	144.9	152.5	0.900900901	1.052631579
	527	167.1	138.0	153.33	0.917431193	1.111111111
	192	193.8	130.2	155	0.8	1.19047619
	181	170.5	117.8	155	0.909090909	1.315789474
	1167	138.0	125.6	155	1.123595506	1.234567901
	147	199.7	165.0	165	0.826446281	1
	88	156.8	174.9	165	1.052631579	0.943396226
	36	218.8	191.9	168.33	0.769230769	0.877192982
	675	207.4	137.7	170	0.819672131	1.234567901
	24	188.9	176.8	173.33	0.917431193	0.980392157
	713	188.9	143.9	173.33	0.917431193	1.204819277
	134	198.1	185.9	173.75	0.877192982	0.934579439
	766	201.5	146.2	178.33	0.884955752	1.219512195
	446	184.1	180.5	178.75	0.970873786	0.99009901
	40	176.4	149.4	180	1.020408163	1.204819277
	337	160.2	138.6	180	1.123595506	1.298701299
	131	231.8	149.7	182.5	0.787401575	1.219512195

651	185.0	209.1	185	1	0.884955752
251	226.1	172.9	190	0.840336134	1.098901099
833	174.0	212.3	191.25	1.098901099	0.900900901
465	199.6	203.4	193.75	0.970873786	0.952380952
2177	175.5	185.3	195	1.111111111	1.052631579
100	214.5	220.4	195	0.909090909	0.884955752
168	224.0	220.0	200	0.892857143	0.909090909
661	199.3	168.8	203.33	1.020408163	1.204819277
160	205.4	180.5	207.5	1.01010101	1.149425287
334	262.5	174.3	210	0.8	1.204819277
746	199.5	178.5	210	1.052631579	1.176470588
304	226.5	215.9	211.667	0.934579439	0.980392157
307	242.7	221.0	216.67	0.892857143	0.980392157
985	224.4	220.0	220	0.980392157	1
978	286.0	237.6	220	0.769230769	0.925925926
2062	251.6	196.7	228.75	0.909090909	1.162790698
530	280.6	241.5	230	0.819672131	0.952380952
1550	259.0	212.3	233.33	0.900900901	1.098901099
577	205.9	260.3	236.67	1.149425287	0.909090909
198	244.6	211.4	237.5	0.970873786	1.123595506
2634, Alive	280.3	242.3	237.5	0.847457627	0.980392157
309	309.6	278.4	240	0.775193798	0.862068966
209	288.0	278.4	240	0.833333333	0.862068966
1562	300.7	196.4	242.5	0.806451613	1.234567901
3367	250.6	296.9	243.33	0.970873786	0.819672131
1259	224.3	204.8	243.75	1.086956522	1.19047619
918	215.6	213.2	245	1.136363636	1.149425287
262	226.9	226.9	246.67	1.086956522	1.086956522
530	235.1	212.9	247.5	1.052631579	1.162790698
2009	312.5	300.0	250	0.8	0.833333333
245	317.5	207.5	250	0.787401575	1.204819277
139	310.6	287.9	252.5	0.81300813	0.877192982
579	276.6	213.2	253.75	0.917431193	1.19047619
538	321.3	290.7	255	0.793650794	0.877192982
504	338.0	234.0	260	0.769230769	1.111111111
36	275.6	278.3	262.5	0.952380952	0.943396226
217	282.2	287.5	263.75	0.934579439	0.917431193
152	280.0	234.7	266.67	0.952380952	1.136363636
141	298.3	228.4	268.75	0.900900901	1.176470588
549	237.6	261.9	270	1.136363636	1.030927835
144	350.5	206.5	271.67	0.775193798	1.315789474
615	300.7	319.8	273.33	0.909090909	0.854700855
686	285.6	260.4	280	0.980392157	1.075268817
402	246.4	282.8	280	1.136363636	0.99009901
385	313.6	254.8	280	0.892857143	1.098901099
2813	324.8	229.6	280	0.862068966	1.219512195
150	248.0	339.2	285	1.149425287	0.840336134
742	304.8	241.5	287.5	0.943396226	1.19047619

268	360.4	317.2	288.33	0.8	0.909090909
242	366.0	336.0	300	0.819672131	0.892857143
442	351.0	336.0	300	0.854700855	0.892857143
191	281.3	353.9	302.5	1.075268817	0.854700855
181	261.4	365.9	307.5	1.176470588	0.840336134
63	381.3	272.8	310	0.81300813	1.136363636
222	375.1	344.1	310	0.826446281	0.900900901
245	403.0	279.0	310	0.769230769	1.111111111
312	281.3	293.8	312.5	1.111111111	1.063829787
218	341.5	363.5	313.33	0.917431193	0.862068966
83	270.9	264.6	315	1.162790698	1.19047619
115	383.2	316.7	316.67	0.826446281	1
212	407.5	299.2	318.33	0.78125	1.063829787
391	294.4	304.0	320	1.086956522	1.052631579
466	278.4	355.2	320	1.149425287	0.900900901
2363, Survival	283.8	319.3	322.5	1.136363636	1.01010101
79	331.5	370.5	325	0.980392157	0.877192982
25	359.1	379.1	332.5	0.925925926	0.877192982
217	299.3	380.0	336.25	1.123595506	0.884955752
296	377.4	306.0	340	0.900900901	1.111111111
2681, Survival	411.0	407.5	348.33	0.847457627	0.854700855
71	449.6	291.5	351.25	0.78125	1.204819277
43	304.2	293.6	353.75	1.162790698	1.204819277
139	341.8	341.8	367.5	1.075268817	1.075268817
2062	404.3	308.0	385	0.952380952	1.25
162	340.0	396.0	400	1.176470588	1.01010101
100	507.2	342.1	402.5	0.793650794	1.176470588
361	408.8	343.4	408.75	1	1.19047619
437	370.5	440.5	411.67	1.111111111	0.934579439
77	394.3	332.0	415	1.052631579	1.25
780	463.3	459.0	425	0.917431193	0.925925926
100	524.4	510.6	460	0.877192982	0.900900901
1230	432.3	403.8	475	1.098901099	1.176470588
246	609.0	584.8	483.33	0.793650794	0.826446281

	LTGvsMN	**LTGvsNH**
Average difference:	0.957266364	1.037707144
Percentage difference:	4.273363631	-3.770714359

Bibliography

1. Pakos-Zebrucka, K. *et al.* The integrated stress response. *EMBO Rep* **17**, 1374–1395 (2016).
2. Jousse, C. *et al.* Inhibition of a constitutive translation initiation factor 2α phosphatase, CReP, promotes survival of stressed cells. *Journal of Cell Biology* **163**, 767–775 (2003).
3. Novoa, I., Zeng, H., Harding, H. P. & Ron, D. Feedback Inhibition of the Unfolded Protein Response by GADD34-Mediated Dephosphorylation of eIF2α. *Journal of Cell Biology* **153**, 1011–1022 (2001).
4. Masson, G. R. Towards a model of GCN2 activation. *Biochemical Society Transactions* vol. 47 1481–1488 Preprint at https://doi.org/10.1042/BST20190331 (2019).
5. Somers, J., Pöyry, T. & Willis, A. E. A perspective on mammalian upstream open reading frame function. *Int J Biochem Cell Biol* **45**, 1690–700 (2013).
6. Sokabe, M. & Fraser, C. S. Human eukaryotic initiation factor 2 (eIF2)-GTP-Met-tRNAi ternary complex and eIF3 stabilize the 43 S preinitiation complex. *J Biol Chem* **289**, 31827–31836 (2014).
7. Jackson, R. J., Hellen, C. U. T. & Pestova, T. V. The mechanism of eukaryotic translation initiation and principles of its regulation. *Nat Rev Mol Cell Biol* **11**, 113–27 (2010).
8. Pestova, T., Lorsch, J. R. & Hellen, C. U. *The mechanism of translation initiation in eukaryotes.* (Cold Spring Harbour, 2007).
9. Kedersha, N. *et al.* Evidence that ternary complex (eIF2-GTP-tRNA(i)(Met))-deficient preinitiation complexes are core constituents of mammalian stress granules. *Mol Biol Cell* **13**, 195–210 (2002).
10. Vattem, K. M. & Wek, R. C. *Reinitiation involving upstream ORFs regulates ATF4 mRNA translation in mammalian cells*. www.pnas.orgcgidoi10.1073pnas.0400541101 (2004).
11. Nikonorova, I. A. *et al.* Time-resolved analysis of amino acid stress identifies eIF2 phosphorylation as necessary to inhibit mTORC1 activity in liver. *Journal of Biological Chemistry* **293**, 5005–5015 (2018).
12. Ye, J. *et al.* The GCN2-ATF4 pathway is critical for tumour cell survival and proliferation in response to nutrient deprivation. *EMBO Journal* **29**, 2082–2096 (2010).
13. Costa-Mattioli, M. & Walter, P. The integrated stress response: From mechanism to disease. *Science* **368**, (2020).
14. Young, S. K., Willy, J. A., Wu, C., Sachs, M. S. & Wek, R. C. Ribosome Reinitiation Directs Gene-specific Translation and Regulates the Integrated Stress Response. *J Biol Chem* **290**, 28257–28271 (2015).

15. Hu, H., Tian, M., Ding, C. & Yu, S. The C/EBP Homologous Protein (CHOP) Transcription Factor Functions in Endoplasmic Reticulum Stress-Induced Apoptosis and Microbial Infection. *Front Immunol* **9**, 3083 (2018).

16. Lu, M. *et al.* Opposing unfolded-protein-response signals converge on death receptor 5 to control apoptosis. *Science* **345**, 98–101 (2014).

17. Tian, X. *et al.* Targeting the Integrated Stress Response in Cancer Therapy. *Frontiers in Pharmacology* vol. 12 Preprint at https://doi.org/10.3389/fphar.2021.747837 (2021).

18. Wek, R. C. & Staschke, K. A. How do tumours adapt to nutrient stress. *EMBO Journal* vol. 29 1946–1947 Preprint at https://doi.org/10.1038/emboj.2010.110 (2010).

19. Palam, L. R., Gore, J., Craven, K. E., Wilson, J. L. & Korc, M. Integrated stress response is critical for gemcitabine resistance in pancreatic ductal adenocarcinoma. *Cell Death Dis* **6**, (2015).

20. Wang, S. F. *et al.* Activated integrated stress response induced by salubrinal promotes cisplatin resistance in human gastric cancer cells via enhanced xct expression and glutathione biosynthesis. *Int J Mol Sci* **19**, (2018).

21. Postnikoff, S. D. L., Johnson, J. E. & Tyler, J. K. The integrated stress response in budding yeast lifespan extension. *Microbial Cell* vol. 4 368–375 Preprint at https://doi.org/10.15698/mic2017.11.597 (2017).

22. Romano, P. R. *et al. Autophosphorylation in the Activation Loop Is Required for Full Kinase Activity In Vivo of Human and Yeast Eukaryotic Initiation Factor 2 Kinases PKR and GCN2*. *MOLECULAR AND CELLULAR BIOLOGY* vol. 18 (1998).

23. Coudert, E. *et al.* Annotation of biologically relevant ligands in UniProtKB using ChEBI. *Bioinformatics* **39**, (2023).

24. Lageix, S., Zhang, J., Rothenburg, S. & Hinnebusch, A. G. Interaction between the tRNA-Binding and C-Terminal Domains of Yeast Gcn2 Regulates Kinase Activity In Vivo. *PLoS Genet* **11**, 1–28 (2015).

25. Harding, H. P. *et al.* The ribosomal P-stalk couples amino acid starvation to GCN2 2 activation in mammalian cells. *Elife* **8**, (2019).

26. Inglis, A. J. *et al.* Activation of GCN2 by the ribosomal P-stalk. *Proc Natl Acad Sci U S A* **116**, 4946–4954 (2019).

27. Wu, C. C. C., Peterson, A., Zinshteyn, B., Regot, S. & Green, R. Ribosome Collisions Trigger General Stress Responses to Regulate Cell Fate. *Cell* **182**, 404-416.e14 (2020).

28. Wang, Y. *et al.* Amino acid deprivation promotes tumor angiogenesis through the GCN2/ATF4 pathway. *Neoplasia (United States)* **15**, 989–997 (2013).

29. Furnish, M. *et al.* MIRO2 regulates prostate cancer cell growth via GCN1-dependent stress signaling. *Molecular Cancer Research* molcanres.0374.2021 (2022) doi:10.1158/1541-7786.MCR-21-0374.

30. Ge, L. *et al.* GCN2 is a potential prognostic biomarker for human papillary renal cell carcinoma. *Cancer Biomark* **22**, 395–403 (2018).

31. Saavedra-García, P. *et al.* Systems level profiling of chemotherapy-induced stress resolution in cancer cells reveals druggable trade-offs. *Proc Natl Acad Sci U S A* **118**, (2021).

32. Wei, C. *et al.* Involvement of general control nonderepressible kinase 2 in cancer cell apoptosis by posttranslational mechanisms. *Mol Biol Cell* **26**, 1044–57 (2015).

33. Gold, L. T. & Masson, G. R. GCN2: roles in tumour development and progression. *Biochem Soc Trans* **50**, 737–745 (2022).

34. Jin, L., Alesi, G. N. & Kang, S. Glutaminolysis as a target for cancer therapy. *Oncogene* vol. 35 3619–3625 Preprint at https://doi.org/10.1038/onc.2015.447 (2016).

35. Lehman, S. L., Ryeom, S. & Koumenis, C. Signaling through alternative Integrated Stress Response pathways compensates for GCN2 loss in a mouse model of soft tissue sarcoma. *Sci Rep* **5**, 11781 (2015).

36. Fung, M. K. L. & Chan, G. C.-F. Drug-induced amino acid deprivation as strategy for cancer therapy. *J Hematol Oncol* **10**, 144 (2017).

37. Siu, F., Bain, P. J., Leblanc-Chaffin, R., Chen, H. & Kilberg, M. S. ATF4 is a mediator of the nutrient-sensing response pathway that activates the human asparagine synthetase gene. *Journal of Biological Chemistry* **277**, 24120–24127 (2002).

38. Chiu, M., Taurino, G., Bianchi, M. G., Kilberg, M. S. & Bussolati, O. Asparagine Synthetase in Cancer: Beyond Acute Lymphoblastic Leukemia. *Front Oncol* **9**, (2020).

39. Nakamura, A. *et al.* Inhibition of GCN2 sensitizes ASNS-low cancer cells to asparaginase by disrupting the amino acid response. *Proc Natl Acad Sci U S A* **115**, E7776–E7785 (2018).

40. Qing, G. *et al.* ATF4 regulates MYC-mediated neuroblastoma cell death upon glutamine deprivation. *Cancer Cell* **22**, 631–44 (2012).

41. Longchamp, A. *et al.* Amino Acid Restriction Triggers Angiogenesis via GCN2/ATF4 Regulation of VEGF and H2S Production. *Cell* **173**, 117-129.e14 (2018).

42. Zhang, F. *et al.* Selective and competitive functions of the AAR and UPR pathways in stress-induced angiogenesis. *Cell Discov* **7**, (2021).

43. Arany, Z. *et al.* HIF-independent regulation of VEGF and angiogenesis by the transcriptional coactivator PGC-1α. *Nature* **451**, 1008–1012 (2008).

44. Maher*, P. & Schubert, D. Signaling by reactive oxygen species in the nervous system. *Cellular and Molecular Life Sciences* **57**, 1287–1305 (2000).

45. Chaveroux, C. *et al.* Identification of GCN2 as new redox regulator for oxidative stress prevention in vivo. *Biochem Biophys Res Commun* **415**, 120–124 (2011).

46. Arriazu, E., Pérez de Obanos, M. P., López-Zabalza, M. J., Herraiz, M. T. & Iraburu, M. J. Amino Acid Deprivation Decreases Intracellular Levels of Reactive Oxygen Species in Hepatic Stellate Cells. *Cellular Physiology and Biochemistry* **26**, 281–290 (2010).

47. Chen, M.-S. *et al. CHAC1 degradation of glutathione enhances cystine-starvation-induced necroptosis and ferroptosis in human triple negative breast cancer cells via the GCN2-eIF2α-ATF4 pathway*. vol. 8 www.impactjournals.com/oncotarget (2017).

48. Wang, S.-F. *et al.* Mitochondrial dysfunction enhances cisplatin resistance in human gastric cancer cells via the ROS-activated GCN2-eIF2α-ATF4-xCT pathway. *Oncotarget* **7**, 74132–74151 (2016).

49. Ling, Y.-H., Liebes, L., Zou, Y. & Perez-Soler, R. Reactive Oxygen Species Generation and Mitochondrial Dysfunction in the Apoptotic Response to Bortezomib, a Novel Proteasome Inhibitor, in Human H460 Non-small Cell Lung Cancer Cells. *Journal of Biological Chemistry* **278**, 33714–33723 (2003).

50. Denlinger, C. E., Rundall, B. K. & Jones, D. R. Proteasome inhibition sensitizes non–small cell lung cancer to histone deacetylase inhibitor–induced apoptosis through the generation of reactive oxygen species. *J Thorac Cardiovasc Surg* **128**, 740–748 (2004).

51. Szczepanowska, K. & Trifunovic, A. Tune instead of destroy: How proteolysis keeps OXPHOS in shape. *Biochimica et Biophysica Acta (BBA) - Bioenergetics* **1862**, 148365 (2021).

52. Humpton, T. J. *et al.* Oncogenic KRAS Induces NIX-Mediated Mitophagy to Promote Pancreatic Cancer. *Cancer Discov* **9**, 1268–1287 (2019).

53. Villa, E. *et al.* Parkin-Independent Mitophagy Controls Chemotherapeutic Response in Cancer Cells. *Cell Rep* **20**, 2846–2859 (2017).

54. Ghosh, J. C. *et al.* Ghost mitochondria drive metastasis through adaptive GCN2/Akt therapeutic vulnerability. *Proceedings of the National Academy of Sciences* **119**, (2022).

55. Schmidt, S. *et al.* A MYC–GCN2–eIF2α negative feedback loop limits protein synthesis to prevent MYC-dependent apoptosis in colorectal cancer. *Nat Cell Biol* **21**, 1413–1424 (2019).

56. Dang, C. V. MYC on the Path to Cancer. *Cell* **149**, 22–35 (2012).

57. Liu, G. Y. & Sabatini, D. M. mTOR at the nexus of nutrition, growth, ageing and disease. *Nat Rev Mol Cell Biol* **21**, 183–203 (2020).

58. Fruman, D. A. & Rommel, C. PI3K and cancer: lessons, challenges and opportunities. *Nat Rev Drug Discov* **13**, 140–156 (2014).

59. Guertin, D. A. *et al.* mTOR Complex 2 Is Required for the Development of Prostate Cancer Induced by Pten Loss in Mice. *Cancer Cell* **15**, 148–159 (2009).

60. Kanno, A. *et al.* GCN2 regulates pancreatic β cell mass by sensing intracellular amino acid levels. *JCI Insight* **5**, (2020).

61. Abou Hassan, O. K. *et al.* Novel EIF2AK4 mutations in histologically proven pulmonary capillary hemangiomatosis and hereditary pulmonary arterial hypertension. *BMC Med Genet* **20**, 176 (2019).

62. Eyries, M. *et al.* EIF2AK4 mutations cause pulmonary veno-occlusive disease, a recessive form of pulmonary hypertension. *Nat Genet* **46**, 65–9 (2014).

63. Best, D. H. *et al.* EIF2AK4 mutations in pulmonary capillary hemangiomatosis. *Chest* **145**, 231–236 (2014).

64. Emanuelli, G., Nassehzadeh-Tabriz, N., Morrell, N. W. & Marciniak, S. J. The integrated stress response in pulmonary disease. *Eur Respir Rev* **29**, (2020).

65. Carlson, K. R., Georgiadis, M. M., Tameire, F., Staschke, K. A. & Wek, R. C. Activation of Gcn2 by small molecules designed to be inhibitors. *J Biol Chem* **299**, 104595 (2023).

66. Fujimoto, J. *et al.* Identification of Novel, Potent, and Orally Available GCN2 Inhibitors with Type i Half Binding Mode. *ACS Med Chem Lett* **10**, 1498–1503 (2019).

67. Lee, J. *et al.* The antitumor activity of a novel GCN2 inhibitor in head and neck squamous cell carcinoma cell lines. *Transl Oncol* **27**, 101592 (2023).

68. Tang, C. P. *et al.* GCN2 kinase activation by ATP-competitive kinase inhibitors. *Nat Chem Biol* **18**, 207–215 (2022).

69. Meredith Pelster, M. T. G. S. K. M. A. G. P. M. B. R. N. B. and J. L. I. A multicenter, open-label, phase 1a/b study of HC-7366, a modulator of integrated stress response (ISR) kinase GCN2 in subjects with advanced solid tumors. *Journal of Clinical Oncology* vol. 40 Preprint at (2022).

70. Li, Y. *et al. N* -(3-Ethynyl-2,4-difluorophenyl)sulfonamide Derivatives as Selective Raf Inhibitors. *ACS Med Chem Lett* **6**, 543–547 (2015).

71. Xuhong, J.-C., Qi, X.-W., Zhang, Y. & Jiang, J. Mechanism, safety and efficacy of three tyrosine kinase inhibitors lapatinib, neratinib and pyrotinib in HER2-positive breast cancer. *Am J Cancer Res* **9**, 2103–2119 (2019).

72. Rutkowski, D. T. *et al.* Adaptation to ER Stress Is Mediated by Differential Stabilities of Pro-Survival and Pro-Apoptotic mRNAs and Proteins. *PLoS Biol* **4**, e374 (2006).

73. Rudd, R. M. Malignant mesothelioma. *Br Med Bull* **93**, 105–123 (2010).

74. Senek, M., Robertson, S., Darlison, L., Creech, L. & Tod, A. Malignant pleural mesothelioma patients' experience by gender: findings from a cross-sectional UK-national questionnaire. *BMJ Open Respir Res* **9**, e001050 (2022).

75. Mott, F. E. Mesothelioma: a review. *Ochsner J* **12**, 70–9 (2012).

76. Opitz, I. *et al.* A New Prognostic Score Supporting Treatment Allocation for Multimodality Therapy for Malignant Pleural Mesothelioma. *Journal of Thoracic Oncology* **10**, 1634–1641 (2015).

77. Cancer Research UK. Mesothelioma survival . *Cancer Research UK* https://www.cancerresearchuk.org/about-cancer/mesothelioma/survival (2021).

78. Odgerel, C.-O. *et al.* Estimation of the global burden of mesothelioma deaths from incomplete national mortality data. *Occup Environ Med* **74**, 851–858 (2017).

79. King, D. History of Asbestos. *Asbestos.com* https://www.asbestos.com/asbestos/history/ (2022).

80. Doll, R. Mortality from lung cancer in asbestos workers 1955. *Occup Environ Med* **50**, 485–490 (1993).

81. Selikoff, I. J., Churg, J. & Hammond, E. C. Relation between Exposure to Asbestos and Mesothelioma. *New England Journal of Medicine* **272**, 560–565 (1965).

82. Lin, R.-T., Chien, L.-C., Jimba, M., Furuya, S. & Takahashi, K. Implementation of national policies for a total asbestos ban: a global comparison. *Lancet Planet Health* **3**, e341–e348 (2019).

83. Public Health England. Asbestos: General Information. https://www.gov.uk/government/publications/asbestos-properties-incident-management-and-toxicology/asbestos-general-information (2017).

84. World Health Organisation. Asbestos: Elimination of asbestos-related diseases . https://www.who.int/news-room/fact-sheets/detail/asbestos-elimination-of-asbestos-related-diseases.

85. OBERDÖRSTER, G. MACROPHAGE-ASSOCIATED RESPONSES TO CHRYSOTILE. *Annals of Occupational Hygiene* **38**, 601–615 (1994).

86. Sanchez, V. C., Pietruska, J. R., Miselis, N. R., Hurt, R. H. & Kane, A. B. Biopersistence and potential adverse health impacts of fibrous nanomaterials: what have we learned from asbestos? *Wiley Interdiscip Rev Nanomed Nanobiotechnol* **1**, 511–529 (2009).

87. Kuroda, A. Recent progress and perspectives on the mechanisms underlying Asbestos toxicity. *Genes and Environment* **43**, 46 (2021).

88. Yue, L., Luo, Y., Jiang, L., Sekido, Y. & Toyokuni, S. PCBP2 knockdown promotes ferroptosis in malignant mesothelioma. *Pathol Int* **72**, 242–251 (2022).

89. Oberdörster, G., Ferin, J. & Lehnert, B. E. Correlation between particle size, in vivo particle persistence, and lung injury. *Environ Health Perspect* **102**, 173–179 (1994).

90. Ishida, T. *et al.* Live-cell imaging of macrophage phagocytosis of asbestos fibers under fluorescence microscopy. *Genes and Environment* **41**, 14 (2019).

91. Dostert, C. *et al.* Innate Immune Activation Through Nalp3 Inflammasome Sensing of Asbestos and Silica. *Science (1979)* **320**, 674–677 (2008).

92. Xu, A., Wu, L. J., Santella, R. M. & Hei, T. K. Role of oxyradicals in mutagenicity and DNA damage induced by crocidolite asbestos in mammalian cells. *Cancer Res* **59**, 5922–6 (1999).

93. Jean, D. & Jaurand, M.-C. Mesotheliomas in Genetically Engineered Mice Unravel Mechanism of Mesothelial Carcinogenesis. *Int J Mol Sci* **19**, 2191 (2018).

94. Testa, J. R. *et al.* Germline BAP1 mutations predispose to malignant mesothelioma. *Nat Genet* **43**, 1022–1025 (2011).

95. Pulford, E., Huilgol, K., Moffat, D., Henderson, D. W. & Klebe, S. Malignant Mesothelioma, BAP1 Immunohistochemistry, and VEGFA: Does BAP1 Have Potential for Early Diagnosis and Assessment of Prognosis? *Dis Markers* **2017**, 1–10 (2017).

96. Jensen, D. E. *et al.* BAP1: a novel ubiquitin hydrolase which binds to the BRCA1 RING finger and enhances BRCA1-mediated cell growth suppression. *Oncogene* **16**, 1097–1112 (1998).

97. Dey, A. *et al.* Loss of the Tumor Suppressor BAP1 Causes Myeloid Transformation. *Science (1979)* **337**, 1541–1546 (2012).

98. Yu, H. *et al.* Tumor suppressor and deubiquitinase BAP1 promotes DNA double-strand break repair. *Proceedings of the National Academy of Sciences* **111**, 285–290 (2014).

99. Zhang, Y. *et al.* BAP1 links metabolic regulation of ferroptosis to tumour suppression. *Nat Cell Biol* **20**, 1181–1192 (2018).

100. Brcic, L. & Kern, I. Clinical significance of histologic subtyping of malignant pleural mesothelioma. *Transl Lung Cancer Res* **9**, 924–933 (2020).

101. Edge, S. B. & Compton, C. C. The American Joint Committee on Cancer: the 7th Edition of the AJCC Cancer Staging Manual and the Future of TNM. *Ann Surg Oncol* **17**, 1471–1474 (2010).

102. Betta, P.-G., Magnani, C., Bensi, T., Trincheri, N. F. & Orecchia, S. Immunohistochemistry and Molecular Diagnostics of Pleural Malignant Mesothelioma. *Arch Pathol Lab Med* **136**, 253–261 (2012).

103. Vigneswaran, W. T. *et al.* Amount of Epithelioid Differentiation Is a Predictor of Survival in Malignant Pleural Mesothelioma. *Ann Thorac Surg* **103**, 962–966 (2017).

104. Ricciardi, S. *et al.* Surgery for malignant pleural mesothelioma: an international guidelines review. *J Thorac Dis* **10**, S285–S292 (2018).

105. Su, S. Mesothelioma: Path to Multimodality Treatment. *Semin Thorac Cardiovasc Surg* **21**, 125–131 (2009).

106. Dirix, L. Y. *et al.* A phase II trial of dose-escalated doxorubicin and ifosfamide/mesna in patients with malignant mesothelioma. *Annals of Oncology* **5**, 653–655 (1994).

107. Pennucci, M. C. *et al.* Combined cisplatin, doxorubicin, and mitomycin for the treatment of advanced pleural mesothelioma. *Cancer* **79**, 1897–1902 (1997).

108. Samson, M. K. *et al.* Randomized comparison of cyclophosphamide, imidazole carboxamide, and adriamycin versus cyclophosphamide and adriamycin in patients with advanced stage malignant mesothelioma: a Sarcoma Intergroup Study. *Journal of Clinical Oncology* **5**, 86–91 (1987).

109. Berghmans, T. *et al.* Activity of chemotherapy and immunotherapy on malignant mesothelioma: a systematic review of the literature with meta-analysis. *Lung Cancer* **38**, 111–121 (2002).

110. Vogelzang, N. J. *et al.* Phase III study of pemetrexed in combination with cisplatin versus cisplatin alone in patients with malignant pleural mesothelioma. *J Clin Oncol* **21**, 2636–44 (2003).

111. Kelly, R. J., Sharon, E. & Hassan, R. Chemotherapy and targeted therapies for unresectable malignant mesothelioma. *Lung Cancer* **73**, 256–63 (2011).

112. Nowak, A. K., Brosseau, S., Cook, A. & Zalcman, G. Antiangiogeneic Strategies in Mesothelioma. *Front Oncol* **10**, (2020).

113. Szlosarek, P. W. *et al. In vivo* Loss of Expression of Argininosuccinate Synthetase in Malignant Pleural Mesothelioma Is a Biomarker for Susceptibility to Arginine Depletion. *Clinical Cancer Research* **12**, 7126–7131 (2006).

114. Goel, H. L. & Mercurio, A. M. VEGF targets the tumour cell. *Nat Rev Cancer* **13**, 871–882 (2013).

115. Wilson, W. R. & Hay, M. P. Targeting hypoxia in cancer therapy. *Nat Rev Cancer* **11**, 393–410 (2011).

116. Taiakina, D., Pra, A. D. & Bristow, R. G. Intratumoral Hypoxia as the Genesis of Genetic Instability and Clinical Prognosis in Prostate Cancer. in 189–204 (2014). doi:10.1007/978-1-4614-5915-6_9.

117. Guan, G. *et al.* The HIF-1α/CXCR4 pathway supports hypoxia-induced metastasis of human osteosarcoma cells. *Cancer Lett* **357**, 254–264 (2015).

118. Strizzi, L. *et al.* Vascular endothelial growth factor is an autocrine growth factor in human malignant mesothelioma. *J Pathol* **193**, 468–475 (2001).

119. Masood, R. *et al.* Malignant mesothelioma growth inhibition by agents that target the VEGF and VEGF-C autocrine loops. *Int J Cancer* **104**, 603–610 (2003).

120. Nowak, A. K. *et al.* A phase II clinical trial of the Vascular Disrupting Agent BNC105P as second line chemotherapy for advanced Malignant Pleural Mesothelioma. *Lung Cancer* **81**, 422–427 (2013).

121. Nowak, A. K. *et al.* A Phase II Study of Intermittent Sunitinib Malate as Second-Line Therapy in Progressive Malignant Pleural Mesothelioma. *Journal of Thoracic Oncology* **7**, 1449–1456 (2012).

122. Jahan, T. *et al.* Vatalanib in malignant mesothelioma: A phase II trial by the Cancer and Leukemia Group B (CALGB 30107). *Lung Cancer* **76**, 393–396 (2012).

123. Garland, L. L. *et al.* Phase II Study of Cediranib in Patients with Malignant Pleural Mesothelioma: SWOG S0509. *Journal of Thoracic Oncology* **6**, 1938–1945 (2011).

124. Presta, L. G. *et al.* Humanization of an anti-vascular endothelial growth factor monoclonal antibody for the therapy of solid tumors and other disorders. *Cancer Res* **57**, 4593–9 (1997).

125. Zalcman, G. *et al.* Bevacizumab for newly diagnosed pleural mesothelioma in the Mesothelioma Avastin Cisplatin Pemetrexed Study (MAPS): a randomised, controlled, open-label, phase 3 trial. *The Lancet* **387**, 1405–1414 (2016).

126. Long, Y. *et al.* Argininosuccinate synthetase 1 (ASS1) is a common metabolic marker of chemosensitivity for targeted arginine- and glutamine-starvation therapy. *Cancer Lett* **388**, 54–63 (2017).

127. Cheng, C.-T. *et al.* Arginine starvation kills tumor cells through aspartate exhaustion and mitochondrial dysfunction. *Commun Biol* **1**, 178 (2018).

128. de Santo, C. *et al.* The arginine metabolome in acute lymphoblastic leukemia can be targeted by the pegylated-recombinant arginase I BCT-100. *Int J Cancer* **142**, 1490–1502 (2018).

129. Szlosarek, P. W. *et al.* Arginine Deprivation With Pegylated Arginine Deiminase in Patients With Argininosuccinate Synthetase 1–Deficient Malignant Pleural Mesothelioma. *JAMA Oncol* **3**, 58 (2017).

130. Sahu, D. *et al.* Argininosuccinate Synthetase 1 Loss in Invasive Bladder Cancer Regulates Survival through General Control Nonderepressible 2 Kinase–Mediated Eukaryotic Initiation Factor 2α Activity and Is Targetable by Pegylated Arginine Deiminase. *Am J Pathol* **187**, 200–213 (2017).

131. Chipurupalli, S., Kannan, E., Tergaonkar, V., D'Andrea, R. & Robinson, N. Hypoxia Induced ER Stress Response as an Adaptive Mechanism in Cancer. *Int J Mol Sci* **20**, 749 (2019).

132. Clarke, H. J., Chambers, J. E., Liniker, E. & Marciniak, S. J. Endoplasmic Reticulum Stress in Malignancy. *Cancer Cell* **25**, 563–573 (2014).

133. Dalton, L. E. *et al.* The endoplasmic reticulum stress marker CHOP predicts survival in malignant mesothelioma. *Br J Cancer* **108**, 1340–1347 (2013).

134. Han, J. *et al.* ER-stress-induced transcriptional regulation increases protein synthesis leading to cell death. *Nat Cell Biol* **15**, 481–490 (2013).

135. Rintoul, R. C., Rassl, D. M., Gittins, J., Marciniak, S. J. & MesobanK collaborators. MesobanK UK: an international mesothelioma bioresource. *Thorax* **71**, 380–2 (2016).

136. Allaire, J. RStudio: integrated development for R. *RStudio Team* (2012).

137. Robin, X. *et al.* pROC: an open-source package for R and S+ to analyze and compare ROC curves. *BMC Bioinformatics* **12**, 77 (2011).

138. Carter, J. v., Pan, J., Rai, S. N. & Galandiuk, S. ROC-ing along: Evaluation and interpretation of receiver operating characteristic curves. *Surgery* **159**, 1638–1645 (2016).

139. Austin, P. C. & Steyerberg, E. W. Interpreting the concordance statistic of a logistic regression model: relation to the variance and odds ratio of a continuous explanatory variable. *BMC Med Res Methodol* **12**, 82 (2012).

140. Nowak, A. K. *et al.* A Novel Prognostic Model for Malignant Mesothelioma Incorporating Quantitative FDG-PET Imaging with Clinical Parameters. *Clinical Cancer Research* **16**, 2409–2417 (2010).

141. Kleinbaum DG, K. M. K. D. K. M. *Kaplan-Meier survival curves and the log-rank test. Survival analysis: a self-learning text*. (2012).

142. Berzenji, L., van Schil, P. E. & Carp, L. The eighth TNM classification for malignant pleural mesothelioma. *Transl Lung Cancer Res* **7**, 543–549 (2018).

143. Flores, R. M. *et al.* The impact of lymph node station on survival in 348 patients with surgically resected malignant pleural mesothelioma: Implications for revision of the American Joint Committee on Cancer staging system. *J Thorac Cardiovasc Surg* **136**, 605–610 (2008).

144. Billè, A. *et al.* Analysis of survival of patients with metastatic malignant pleural mesothelioma. *Tumori Journal* **107**, 110–118 (2021).

145. Nicholson, K. J., Sherman, M., Divi, S. N., Bowles, D. R. & Vaccaro, A. R. The Role of Family-wise Error Rate in Determining Statistical Significance. *Clinical Spine Surgery: A Spine Publication* **35**, 222–223 (2022).

146. Kamarudin, A. N., Cox, T. & Kolamunnage-Dona, R. Time-dependent ROC curve analysis in medical research: current methods and applications. *BMC Med Res Methodol* **17**, 53 (2017).

147. Tameire, F. *et al.* ATF4 couples MYC-dependent translational activity to bioenergetic demands during tumour progression. *Nat Cell Biol* **21**, 889–899 (2019).

148. Chen, L. *et al.* EIF2A promotes cell survival during paclitaxel treatment in vitro and in vivo. *J Cell Mol Med* **23**, 6060–6071 (2019).

149. Alasiri, G. *et al.* Reciprocal regulation between GCN2 (eIF2AK4) and PERK (eIF2AK3) through the JNK-FOXO3 axis to modulate cancer drug resistance and clonal survival. *Mol Cell Endocrinol* **515**, 110932 (2020).

150. Rusch, V. W. *et al.* Initial Analysis of the International Association For the Study of Lung Cancer Mesothelioma Database. *Journal of Thoracic Oncology* **7**, 1631–1639 (2012).

151. Efron B, T. RJ. *An introduction to the bootstrap*. (CRC Press, 1994).

152. Girish, V. & Sheltzer, J. M. A CRISPR Competition Assay to Identify Cancer Genetic Dependencies. *Bio Protoc* **10**, e3682 (2020).